Hydrogen-Bonded Layer-by-Layer Assemblies of Poly(2-ethyl-2-oxazoline) and Tannic Acid and Their Biological Applications

by

Saman Hendessi

A Dissertation Submitted to the
Graduate School of Sciences and Engineering
in Partial Fulfillment of the Requirements for
the Degree of

Doctor of Philosophy

in

Materials Science and Engineering

April 2, 2019

Hydrogen-Bonded Layer-by-Layer Assemblies of

Poly(2-ethyl-2-oxazoline) and Tannic Acid and Their

Biological Applications

Koç University

Graduate School of Sciences and Engineering

This is to certify that I have examined this copy of a doctoral dissertation by

Saman Hendessi

and have found that it is complete and satisfactory in all respects,
and that any and all revisions required by the final
examining committee have been made.

Committee: Members

Prof. Levent Demirel (Advisor)

Assoc. Prof. Uğur Ünal

Prof. Füsun Can

Assoc. Prof. Başak Kayıtmazer

Prof. Ahmet Gültek

Date: April 02, 2019

To my beloved family,

ABSTRACT

The biological applications involving antibacterial coatings and controlled release systems require careful design and realization of the material system. Layer-by-layer (LbL) assembly of interacting molecules is a versatile method to prepare functional coatings. The formation of such coatings on sacrificial 3-dimensional templates allows the preparation of hollow capsules which show significant potential as controlled release systems.

In this thesis study, pH-responsive hydrogen-bonded (H-bonded) 2-dimensional (films) and 3-dimensional (hollow capsules) LbL assemblies of poly(2-ethyl-2-oxazoline) (PEOX) and Tannic Acid (TA) have been prepared, investigated and their biological applications as antibacterial coatings and controlled release systems have been demonstrated.

Contact-killing, pH-responsive antibacterial coatings, especially for surgical devices and implants, were realized by H-bonded LbL assembly of PEOX stabilized silver nanoparticles (AgNPs) (~10-20 nm in diameter) as H-acceptor and TA as H-donor. The effect of PEOX molar mass (5,000 to 500,000 g/mol) on the stabilization of AgNPs and the antibacterial efficacy of the resulting coatings has been investigated. The coatings were stable below pH 8.5 and disintegrated above pH 8.5. JIS Z 2801 antibacterial tests demonstrated the antibacterial efficacy of the coatings through contact killing against both gram negative and gram-positive bacteria. The coatings on titanium substrates remained stable and retained their antibacterial efficacy at pH 7.4 in phosphate buffered saline up to 3 months.

Hollow microcapsules (5-8 μm in diameter) formed of 8 bilayers PEOX/TA LbL films were prepared by coating $CaCO_3$ microparticle templates followed by the dissolution of the microparticles. Rhodamine 6G was used as positively charged model cargo to evaluate the loading and release properties of the hollow capsules for potential controlled release applications. Rhodamine 6G loaded capsules exhibited pH-dependent release which increased with pH towards

physiological pH of 7.4. The increase in the amount of released Rhodamine 6G molecules with increasing pH was attributed to the increased permeability of the capsules as a result of the decreasing number of H-bonds due to ionization of TA. Such H-bonded capsules have a high potential to be used as pH-responsive micro-carriers in drug delivery applications.

Keywords: Antibacterial coatings, Hydrogen-bond, Stabilized silver nanoparticles, Hollow microcapsules, Micro-carriers.

ÖZET

Anti-bakteriyel kaplamalar ve kontrollü salım sistemlerini içeren biyolojik uygulamalar malzeme sistemlerinin dikkatli tasarımını ve gerçekleştirilmesini gerektirir. Etkileşen moleküllerin tabaka-tabaka (LbL) yapılandırılması fonksiyonel kaplamaların elde edilebilmesi için çok kullanışlı ve uygun bir yöntemdir. Bu tür kaplamaların ayırılabilen 3-boyutlu şablonlar üzerinde oluşturulması kontrollü salım sistemlerinde önemli bir uygulama potansiyeli olan içi boş kapsüllerin hazırlanmasına olanak verir.

Bu tez çalışmasında, pH duyarlı hidrojen bağlı 2-boyutlu (filmler) ve 3-boyutlu (içi boş kapsüller) tabaka-tabaka poli-2-etil 2-oksazolin (PEOX) ve tanik asit (TA) yapılar hazırlandı, incelendi ve bu yapıların anti-bakteriyel kaplamalar ve kontrollü salım sistemleri olarak biyolojik uygulamaları gösterildi.

Özellikle cerrahi aletler ve implantlar için, temas halinde bakteri öldürme özelliği olan, pH'ya duyarlı anti-bakteriyel kaplamalar, PEOX ile kararlı hale getirilmiş gümüş nanoparçacıkların (AgNP) (~10-20 nm çaplı) hidrojen alıcısı ve TA'nın hidrojen vericisi olarak kullanılmasıyla hidrojen bağlı tabaka-tabaka yapılar şeklinde elde edildi. PEOX molekül ağırlığının (5000 g/mol ile 500 000 g/mol'e aralığında) AgNP kararlılığına ve oluşturulan kaplamaların anti-bakteriyel etkinliğine etkisi incelendi. Kaplamalar pH 8,5 altında kararlı kaldı ve pH 8,5 üzerinde parçalandı. JIS Z 2801 anti-bakteriyel testleri bu kaplamaların temas halinde bakteri öldürme özelliği aracılığıyla, hem gram negatif hem de gram pozitif bakteriler üzerinde etkili olduğunu gösterdi. Titanyum yüzeyler üzerindeki kaplamalar, pH 7,4 fosfat tampon çözeltisi içinde 3 aya kadar kararlı kaldı ve anti-bakteriyel etkinliğini korudu.

8 çift katmanlı PEOX/TA tabaka-tabaka filmlerinden oluşan içi boş mikro kapsüller (5-8 μm çapında), $CaCO_3$ mikroparçacık şablonları üzerine kaplanma sonrası bu mikroparçacıkların çözünmesiyle hazırlandı. Bu içi boş kapsüllerin yükleme ve salınım

özelliklerini potansiyel kontrollü salım uygulamalarında değerlendirmek için, pozitif yüklü Rhodamine 6G model kargo molekülü olarak kullanıldı. Rhodamine 6G yüklenmiş kapsüller fizyolojik pH 7,4'e doğru artan pH-duyarlı bir salım sergiledi. Salınan Rhodamine 6G moleküllerinin miktarının pH ile artması, TA'nın iyonlaşmasına bağlı olarak hidrojen bağı sayısının azalması sonucu kapsül geçirgenliğinin artmasına bağlanmaktadır. Bu hidrojen bağlı kapsüllerin ilaç dağıtım uygulamalarında pH-duyarlı mikrotaşıyıcılar olarak kullanım potansiyeli yüksektir.

Anahtar kelime: Anti-bakteriyel kaplamalar, Hidrojen bağ , Gümüş nanoparçacıklar, pH-duyarlı, Mikrotaşıyıcı.

ACKNOWLEDGMENTS

I would like to take some time to thank all the people without them my Ph.D. would never have been possible. Although it is just my name on the cover, many people have contributed to the research in their own particular way and for that, I want to give them special thanks.

First, my supervisor, Prof. Levent Demirel, you have created an invaluable space for me to do this research and develop myself as a researcher in the best possible way. I greatly appreciate the freedom you have given me to find my own path and the guidance and support you offered when needed. Your heart-warming support has given me great confidence as a researcher, and at the same time made me realize that I am only a beginner in this exciting profession.

Next, some people of outstanding importance for my research, Dr. Annamaria Miko, Dr. Pınar Tatar, and Dr. Hanan Fael. Thank you so much for your knowledge, skills, time and support. You have often been the one for me to turn to, both in times of problems and of victories. You always made me feel at home even I am living away from my home.

I also want to take a moment to thank my groupmates, Aatif Ijaz and Elda Adatoz. Thanks for believing in me and being there for practical support in all those things of life beyond doing a Ph.D. It was great sharing laboratory with you, and my Ph.D. life would be so boring without you two.

I would like to thank my sister by heart, Dr. Zerrin Altıntaş, for your unconditional care and love. I feel so blessed to have you in my life, and I do not have enough words to describe how important you are for me and for my success.

I am also grateful to KUYTAM (Koç University Surface Technologies Research Center) for all AFM, XPS, FESEM and EDX characterization parts of my thesis.

I am extremely thankful to my thesis jury members Dr. Uğur Ünal, Dr. Füsun Can, Dr. Başak Kayıtmazer, and Dr. Ahmet Gültek for evaluating my thesis.

Nobody has been more important to me in the pursuit of this project than the members of my family. I am grateful to my sisters, Setareh and Sima, and my parents, Nader and Soodabeh, whose love and guidance are with me in whatever I pursue. Most importantly, I wish to thank my supportive husband, Dr. Amir Motallebzadeh, and my wonderful son, Arvin, who provide unending inspiration. I could have never accomplished this dissertation without Amir's love, support, and understanding.

The financial support of TÜBİTAK (Project #:214Z165) for the work described in Chapter 3 (Synthesis and Characterization of Stabilized Silver Nanoparticles), Chapter 4 (Hydrogen-Bonded Multilayers of Poly(2-ethyl-2-oxazoline) Stabilized Silver Nanoparticles and Tannic Acid) and Chapter 5 (Antibacterial Properties and Cytotoxicity of Silver Nanoparticle Loaded Multilayers) is acknowledged.

TABLE OF CONTENTS

LIST OF TABLES

LIST OF FIGURES

NOMENCLATURE

AFM:	Atomic force microscopy
AgNPs:	Silver nanoparticles
AMPs:	Antimicrobial peptides
BPEI:	Branched polyethyleneimine
CFU:	Colony-forming unit
CLSM:	Confocal scanning laser microscopy
CVD:	Chemical vapor deposition
DLS:	Dynamic light scattering
E.coli:	Eshrechia coli
EDTA:	Ethylenediaminetetraacetic acid
FESEM:	Field emission scanning electron
HM-PEO:	Hydrophobically modified poly(ethylene oxide)
HPC:	Hydroxypropylcellulose
JIS:	Japanese industrial standard
LB:	Langmuir-Blodgett
LbL:	Layer-by-layer
LCST:	Low critical solution temperature
MF:	Melamine formaldehyde
MIC:	Minimum inhibitory concentration
MPR:	M-methylpheol-fomraldehyde resin
MTT:	3-(4,5-dimethylthiazol-2-yl)-2,5-diphenyltetrazolium bromide
OM:	Optival microscopy
PAA:	Poly(acrylic acid)
PAAM:	Poly(acrylamide)
PAH:	Poly(allylamine hydrochloride)

PAH:	Poly(allylamine hydrochloride)
PANI:	Polyaniline
PAOX:	Poly (2-alkyl-2- oxazoline)s
PBS:	Phosphate buffered saline
PCL:	Poly(caprolactone)
PDA:	Polydopamine
PEA:	Poly(ethylacrylic acid)
PEG:	Poly(ethylene glycol)
PEI:	Poly(ethylene imine)
PEO:	Poly(ethylene oxide)
PEO:	Poly(ethylene oxide)
PEO-*b*-PCL:	PEO-*block*-poly (ε-caprolactone)
PEOX:	Poly(2-ethyl-2-oxazoline)
$PEOX_{SH:}$	Thiol-containing poly(2-ethyl-2-oxazoline)
PHEA:	Poly(2- hydroxyethyl acrylate)
PLAA:	Poly(L-aspartic acid)
PMA:	Poly (methacrylic acid)
$PMA_{C:}$	Poly (methacrylic acid) modified with a cholesterol group
$PMA_{SH:}$	Thiol-modified poly(methacrylic acid)
PMMA:	Poly(methacrylic acid)
PNIPAM:	Poly(N-isopropylacrylamide)
PP:	Polypropylene
PS:	Polystyrene
PSMA:	Poly[styrene-alt-(maleic acid)]
PSS:	Poly(sodium 4-styrene sulfonate)
PVA:	Poly (vinyl alcohol)

PVCL:	Polyvinyl chloride
PVCPL:	poly(*N*-vinylcaprolactam)
PVME:	Poly(N-vinyl methyl ether)
PVP:	Poly-(vinylpyrrolidone)
PVPON:	Poly(vinyl pyrrolidone)
QAC:	Quaternary ammonium chitosan
S. epidermidis:	Staphylococcus epidermidis
SAM:	Self-assembled monolayers
SEM:	Scanning electron microscopy
TA:	Tannic acid
THF:	Tetrahydrofuran
UCST:	Upper critical solution temperature
UV-Vis:	Ultra violet – visible
XPS:	X-ray photoelectron spectroscopy

Chapter 1: Layer-by-Layer Assembly of Multilayer Thin Films

Overview

Surface-mediated layer-by-layer (LbL) assembly results in high control over the properties of the resulting films and allows a wide range of materials to be incorporated within the films. This technique was first established by Decher and co-workers [1, 2], and it has been widely used over the past two decades inspiring the design of novel materials with advanced features. Advantageously, the LbL method can be used to make functional coatings on substrates in almost any shape and also allows the realization of several 3-dimensional structures such as hollow capsules [3] or nanotubes [4].

Pioneering work of Stockton [5] and Wang [6] in 1997 demonstrated that polymer self-assembly can be driven by hydrogen-bonding interactions between adjacent layers. Subsequently, Sukhishvili and Granick demonstrated the pH controlled assembly and degradation of poly (carboxylic acid)-based H-bonded LbL films[7, 8], which was followed by numerous studies involving these multilayers for different applications, for example, to generate self-standing floating films, solid polymer electrolyte films, or for patterned delivery of nucleic acids to cells [9–11]. Since then, hydrogen-bonded LbL films have been receiving growing attention. Today, various applications such as pH- and/or temperature-responsive drug delivery systems, materials with tunable mechanical properties, release films dissolvable under physiological conditions, and proton-exchange membranes for fuel cells [12], have been proposed for hydrogen-bonded films. The possibility to manipulate film properties, such as thickness and permeability by simple changes in solution pH, temperature or ionic strength make hydrogen-bonded films and capsules attractive candidates for controlled release applications. For example, both films and capsules derived from hydrogen-bonded

self-assembly, show an environmental response to pH, and disintegration of the hydrogen-bonds at specific pH value can be used for drug release. Hydrogen-bonded multilayers have been also rendered antibacterial properties after they have been used as matrices for in situ synthesis of silver nanoparticles [13]. When hydrogen-bonded LbL self-assembly was deposited onto particulates, the dissolution of the particulates produces capsules which can be designed to drastically change their size and mechanical properties at neutral pH values. Such capsules present a unique platform for encapsulation and release of a wide range of chemicals based on precise tuning of the capsule wall mesh size triggered by environmental stimuli.

In the present thesis, we present new strategies and functionalities of hydrogen-bonded films and capsules produced by LbL self-assembly of neutral polymer poly(2-ethyl-2-oxazoline) (PEOX) and a polyphenol tannic acid (TA) in aqueous solutions.

The second chapter of this thesis describes the materials and instruments which have been used in this study. The third chapter of this thesis gives details about the synthesis and stabilization of silver nanoparticle (AgNP) with four different molecular weight of PEOX. One aim is to investigate the effect of PEOX on stabilization of AgNP for the first time in literature. Another important aim was to show the effect of PEOX molar mass, PEOX concentration, pH and time on the temporal stability of AgNP dispersions.

In the fourth chapter, the formation of hydrogen-bonded multilayers of PEOX stabilized AgNPs and TA by LbL process is reported. PEOX stabilized AgNPs was used as a hydrogen accepting component and TA as a hydrogen donating component in the preparation of LbL films. This chapter illustrates the growth profiles and the pH-induced disintegration of the multilayers.

Work presented in the fifth chapter explores the potential of PEOX(AgNP)/TA LbL films as antibacterial multilayer films with stabilized AgNPs and examine the antibacterial

properties of multilayer films with different methods to present their non-releasing but effective contact-killing properties. In addition, cytotoxicity of coatings was investigated with *U2OS* cells, which have an extremely high proliferation rate and are very robust in experimental procedures and make them attractive for research that needs cells for in vitro experiments. Also, the long-term stability and contact killing property of the LbL self-assembled coatings on titanium substrates in PBS pH7.4 were also studied.

In the sixth chapter, hydrogen bonded pH-responsive hollow capsules of PEOX and TA are reported for the first time. In this chapter, loading and release properties of hollow capsules are studied by using rhodamine as a model cargo molecule. The formation and disintegration of H-bonds between PEOX and TA can be controlled easily by pH. Therefore, these capsules may have great importance in controlled drug-release systems, since they can be loaded with a large number of functional molecules and release them at physiological pH.

Literature review

1.1 Layer-by-layer self-assembly

Surface engineering can be defined as an enabling technology, and it refers to a broad range of methods that aim to design and modify the surface properties of components. There are two main categories of surface engineering methods that can be used to optimize the surface properties and bulk materials. These are surface coatings and surface modification. Other processes involve surface shape design.

By surface engineering methods we can design the surface of a material with different properties suitable for specific applications. However, in many examples, advances in science and technologies are being limited by surface requirements that cannot be easily satisfied. In this regard, the ability to precisely control and adjust the surface properties of materials using simple means is extremely important.

Recent advances in bio- and nanotechnology have enabled and also demanded the development of functional surfaces and coatings that are potentially useful in advanced fields including energy, biomedical, and microelectronics applications.

Different techniques to modify and functionalize the surface of different materials have been created. Ideally, the method has to be easy and simple to apply onto surfaces with different chemistry and shapes, and also should be reliable and robust. Uniformity and precise control over surface properties are very important but also challenging. Table 1.1 compares the advantages and drawbacks of different surface deposition techniques.

Table 1.1: Comparison of different surface deposition methods.

Methods	Advantages	Disadvantages
Self-assembled monolayers (SAM) [14–16]	• Desired properties can be easily achieved with molecularly thin layers (<2nm)	• Cost is high • Poor thermal stability of thiol compounds on Au surfaces • limited deposition of targeted molecules within the films owing to the unfavorable stability of the films • Need for pre-deposition of specific compounds (e.g., thiols) on the substrate during the preparation of monolayers concurrently restrict its practical applications
Chemical vapor deposition (CVD) [17–19]	• Solvent-less method • Environment-friendly, no pollutants produced	• High-cost vacuum apparatus is required • Difficult to extended to colloidal particles or porous materials
Surface grafting [20–23]	• High molecular weight polymers can be deposited onto surfaces • Covalent attachment of graft chains; excellent adhesion and chemical stability	• Difficult to apply to confined geometrics (e.g., high aspect ration pores) • Usually requires surface functional groups
Langmuir-Blodgett (LB) [24–26]	• High uniformity with low effect density • Films with molecular thickness can be readily deposited	• Limited to macroscopically planer substrates • Cost is high • The requirements for specific molecules to prepare the films and long processing time limit its extensive applications.

In addition to methods mentioned in Table 1.1, there is another method called LbL deposition which is the main method used in this thesis. This method is simple and versatile in the selection of building blocks (e.g., polymers, and particles). Compared to the above mentioned traditional methods, the LbL adsorption technique is a rich, versatile, easy and inexpensive process for fabricating multilayer thin films with controlled architecture and functions. LbL method allows different types of materials to be incorporated in the film structures [1, 27–31]. Therefore, the LbL assembly can be regarded as a versatile bottom-up nanofabrication technique. Singly charged, uncharged, or water-repellent molecules cannot be used directly in conventional LbL assembly. This problem can be solved with unconventional LbL techniques, by using the preassembly of building blocks in solution and use of them for LbL formation at the surface.

An early study by Iler and Kirkland [32, 33] reported multilayer assembly. In both reports, an easy method of surface adsorption-induced multilayer film formation of particles was introduced. Kirkland studied the multilayer formation of inorganic particles concisely and explained the advantages of applied coating technique. Iler added more details about multilayer formation. Indeed, he developed his previous effort [Iler 1964] to build up multilayer films through alternating deposition of charged colloidal particles onto each other in a sequential manner. He also studied the possible adaptation of his method to small molecules and also studied some polymers in particulate form.

Later, in the early 1990s, Decher and coworkers [35–38] developed the LbL technique to the organic materials. They studied the LbL surface deposition of polyelectrolytes on planar surfaces**.** Subsequently, a great number of reports concerning LbL films preparation using various techniques have been published. Many studies were done to improve this method, to extend its applications and to clarify the mechanism behind. Nowadays, polyelectrolytes, nonionic polymers, colloids and nanoparticles, dyes, dendrimers, carbon materials, proteins, DNA, viruses, micelles, and even drug can be assembled as LbL multilayer film [39–53].

As an outline of the technique, LbL assembly is mainly deposition of building blocks on the substrate through intermolecular interactions, as illustrated in Figure 1.1.

Figure 1.1: Formation of layer-by-layer film on the substrate.

One of the most important advantages of the LbL assembly is its simplicity and low cost. To form LbL film beakers and tweezers are the only apparatus required. The variability of the applicable materials is another prominent advantage of this technique. Multilayers may be formed by using LbL assembly techniques that rely on different intermolecular interactions about which more information will be given in the following sections.

1.1.1 LbL techniques:

In the following sections, three main important techniques of LbL film deposition are discussed.

1.1.1.1 Dip coating

LbL assembled multilayer films is generally performed by manually dipping the substrate into solutions of the layering materials followed by rinsing (Figure 1.2). The earliest studies on dip coating LbL assembly actually used charged particles as building blocks, and it was noted that any charged material can be used for LbL assembly as long as deposition takes place at the appropriate pH [54–57].

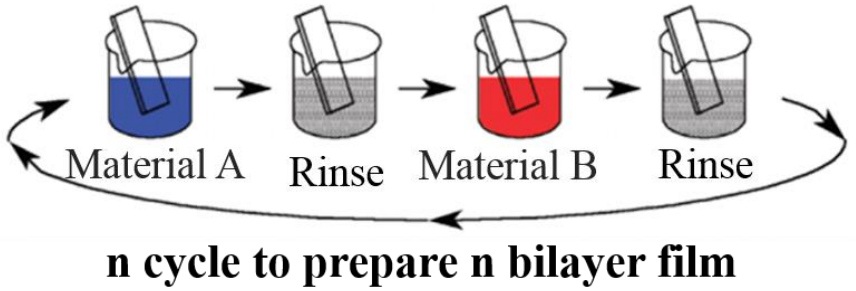

Figure 1.2: Dipping-assisted layer by layer film assembly.

Early studies on dip coating LbL used short material deposition times (1 min per layer) because the large size of the particles and colloids used [55], while it was later determined that, for standard dip coating LbL assembly with polymers, the substrate should be dipped for more than 12 min for optimal deposition [36].

Similarly, particulate substrates can be layered using immersion-based methods; however, the particulate substrates need to be collected between washing and immersion steps, which in most cases needs centrifugation [3, 58–61].

1.1.1.2 Spin coating

Spin coating is another LbL film deposition technique, (Figure 1.3) and it is one of the first technologies used for LbL assembly[62, 63]. Spin coaters are used for this method which facilitates coating and drying. This method is a common method in industry and has not undergone many technological improvements since its introduction to LbL assembly, due to its ease of use and presence in the industry, with associated equipment having been developed over decades.

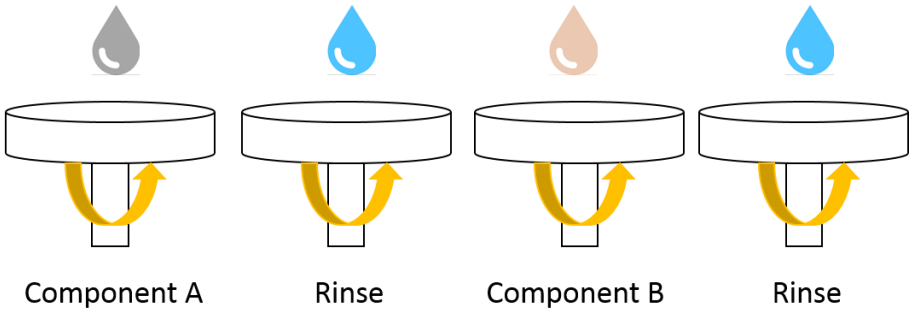

Figure 1.3: Spinning assisted layer by layer film assembly.

In the spin coating method, each spinning step is followed with rinsing and an only well-adhered portion of spin-deposited material stays on the surface. This method is very time-efficient.

Spin coating method can be used for polymers and colloids. In the case of polymers, the spin coating forms thinner films than dip coating[64, 65]; however, for colloids, spin coating deposits thicker films [66]. The reason is that the spin coating results in more homogeneous films because of electrostatic interactions, centrifugal and viscous forces, and air shear. Thus polymer films deposited highly ordered with specific layer interfaces [67, 68]. But in colloids case, these forces lead to a monolayer of colloids, while standard immersive LbL assembly often leads to less than a monolayer, i.e., the substrate is not fully coated by the particles (e.g., <30% coverage has been reported when immersing poly(ethylene imine) (PEI)-modified substrates into dispersions of colloidal gold) [66, 69].

1.1.1.3 Spray coating

The spray coating method is another time-saving alternate method for LbL film fabrication, and it is a common method in industry and research as well. One advantage of this method is the substrate in any type and size can be used. In general, LbL films are

fabricated by spraying polymer solutions onto a substrate and spraying rinse solution on the substrate to remove excess unbounded molecules (Figure 1.4) [70, 71].

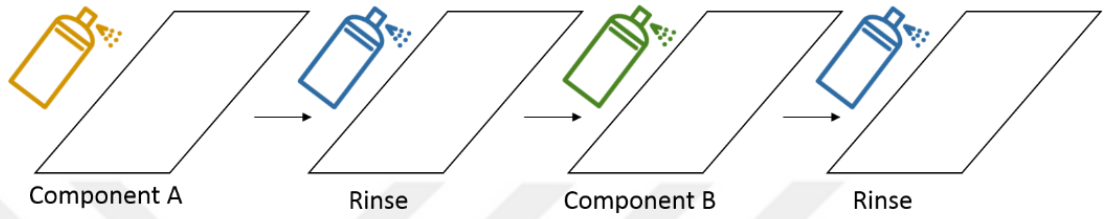

Figure 1.4: Spraying assisted layer by layer film assembly.

The morphology and membrane properties can be tuned based on the polymer concentration, spraying time, flow rate, resting duration, spraying direction, and washing time [70–75]. In some cases, e.g. for 3- dimensional (3D) nonplanar substrates, a vacuum can be used to speed up waiting times between spraying and washing [76]. In addition, sometimes spray assembly can be combined with other techniques to address some of the challenges associated with spraying. For example, a disadvantage of spray LbL assembly is that gravity draining and nozzle shape effects can lead to inhomogeneity in the films [76]. However, this problem can be solved by combining slow rotation with spray assembly [72, 73, 77–80]. Spray assembly can be combined with standard spin assembly to greatly reduce material waste, also allowing for material solution concentrations 10−50 times less than those used in immersive assembly [73, 79].

1.1.2 Molecular interactions used in LbL assembly

LbL assembled multilayer films are driven by different driving forces. They allow for the formation of a large variety of building blocks into multilayer thin films without prior or post-treatment. Different LbL methods are suitable for different building blocks. They have their

advantages as well as disadvantages. In some cases, the advantages and disadvantages are convertible. In contrast with the unconventional LbL methods that involve a two-step assembling process, conventional LbL methods include simply alternating deposition of building blocks with complementary interactions or structures.

LbL films can be fabricated by using assembly techniques that rely on electrostatic interactions, hydrogen bonding, charge transfer, molecular recognition, hydrophobic interactions, van der Waals force, or a combination of these. As a result, such films may be comprised of a diverse range of components.

For many years, electrostatic forces were the main driving forces for layer-by-layer self-assembly. One of the most important molecular interaction for LbL film formation is electrostatic interactions between molecules and surfaces when both molecule and adsorbent surface are electrically charged [81]. This method is basically the formation of multilayers by alternating adsorption of negatively and positively charged molecules on the substrate. LbL assembly based on electrostatic interactions allows us to obtain multilayer films with well-controlled composition, structure, and thickness by simply repeating the alternate immersion of a charged substrate into dilute solutions of oppositely charged molecules [1, 82]. This method, which occurs entirely in aqueous solutions, is well-suited for the fabrication of homogeneous multilayer ultrathin films from combined materials and for several applications, including biomedical applications. Electrostatic attraction based multilayers do not require exact positional matching of the charged groups. Thus we can incorporate more than one molecule into the multilayer, and if necessary, different molecules are incorporated in a designed layer sequence.

Figure 1.5 shows a schematic illustration of the LbL assembly process using polyelectrolytes.

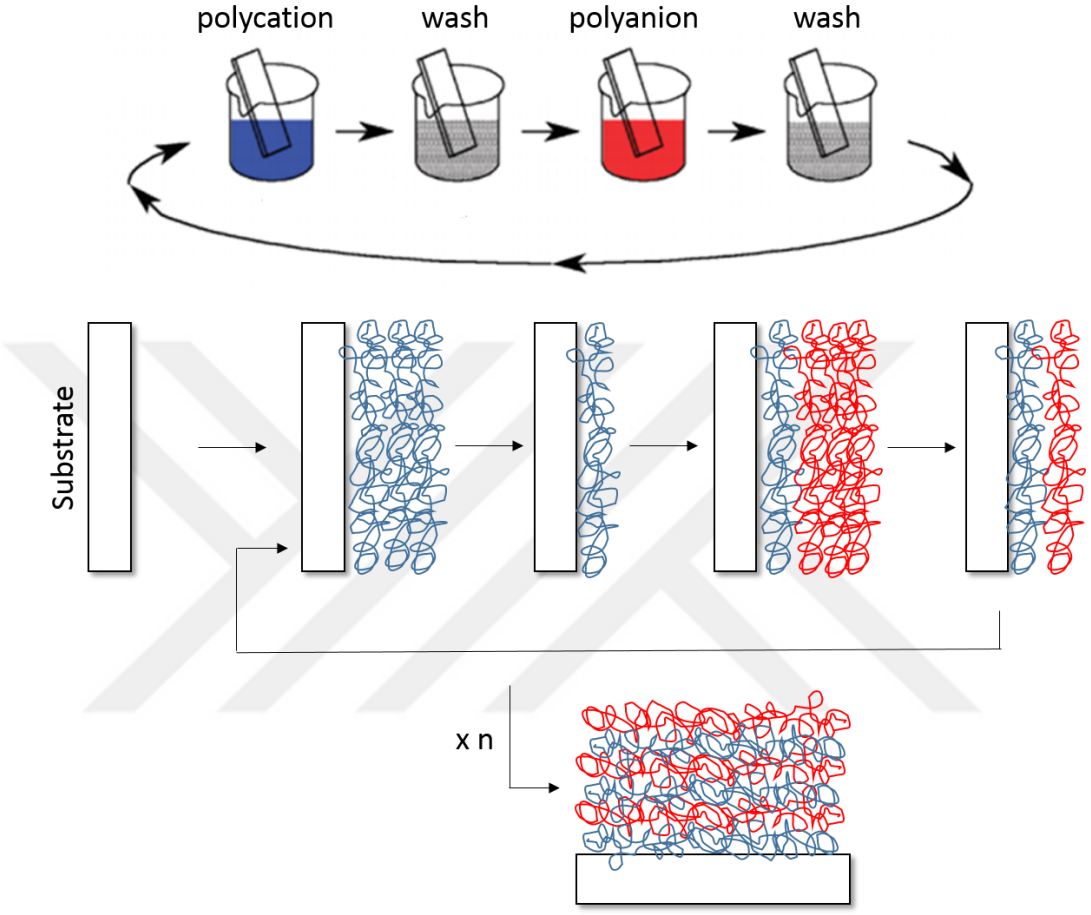

Figure 1. 5: Schematic illustration of electrostatically-driven LbL film.

After Decher and co-workers reports [1, 36, 38, 38, 83], several studies incorporating polyelectrolytes and other building blocks have been reported [84–127]. The mechanisms behind recharging and the driving forces for the buildup of the multilayer films are still not clear enough. In early studies, it was reported that the electrostatic interaction between oppositely charged molecules was the main driving force for the fabrication of the multilayer thin films. The finding that a minimum molecule charge density is needed for the successful

layer growth further supported that theory [128]. In this case, the growth is likely to stop when the coated substrate has a net neutral surface charge. Later on, some studies with weak polyelectrolytes supported this idea [129, 130]. However, in some studies polymers with low charge density have been successfully grown in LbL multilayer films [128, 131, 132] Then, it has been shown that the multilayer film fabrication is not limited is not to charged materials, and so, besides electrostatics, other driving interactions may play a key role in the growth of multilayer films with specific properties, compositions, and structures for the integration of new functionalities [131]. This investigation is important as many materials are uncharged, thus purely electrostatic interactions could not lead to the formation of the films. Moreover, by using electrostatic interactions, changes in the applied external stimuli, e.g. environment change such as pH [133–142], ionic strength[82, 135, 142–149], electrical field[135, 142, 150–158] , light[142, 159–165] , temperature[36, 142, 145, 166] , mechanical stress [1, 32, 35, 142, 167–170] or the addition of specific biological moieties, namely, proteins, [142, 171–175] or ionic surfactants [176] may change the properties of the layers or even cause their desorption, thus making other intermolecular interactions of great importance.

The main focus of this thesis is on H-bonded LbL films, which is explained in details in the next section.

1.2. H-bonded LbL assembly

Although electrostatic interaction has been most widely used to fabricate multilayer thin films, non-electrostatic interactions, such as H-bonding, have also been employed as driving forces for the LbL assembly. This method allows for the combination of different uncharged building blocks into multilayer thin films as long as they can serve as H-bonding donors and acceptors.

Stockton and Rubner [5] and Zhang et al. [6] simultaneously were the pioneer of this method, and they reported the formation of H-bonded LbL multilayer thin films.

H-bonded LbL multilayer assemblies are sensitive to the surrounding environment including pH, ionic strength, temperature, external stress, and electrical field, thus indicating the intrinsic reversible properties [7, 8, 177, 178].

H-bonded systems are pH-responsive. When the pH of the environment increases, the bonds that hold these films together gradually weaken and break as the H-bond donor molecules become deprotonated. The breaking of the bonds within these films causes first to film swelling, as the layers are held weakly together, and finally, if pH conditions are increased beyond the critical pH of the film, the film may disintegrate. The exact value of the critical pH depends on several factors, including the strength of the polymers interaction and the pKa of the H-bonding donor. This allows the dissolution profile of the film to be adjusted to the desired pH. In addition, the pH conditions under which the films are assembled have been shown to have an effect on the resulting film. Just as assembled films will dissolve as the environment becomes more basic, film assembly is hindered and even prevented entirely if the assembly pH is raised to values near the critical pH. If the H-bond donor is deprotonated, no interactions can occur between the two polymers, and no film will be deposited. In contrast, decreasing the pH may also have negative effects on the film assembly. Due to their varied properties, H-bonded LbL films are attractive for a variety of applications. These films are pH-responsive and their ability to absorb large quantities of bio-functional molecules such as dyes or drugs makes them appealing for molecular delivery. Also, this technique allows us to incorporate neutral molecules which is very important in Bio-applications. Tunability and a different number of properties have opened up a variety of opportunities for H-bonded films, and this system is ever growing.

1.2.1 Factors affecting the growth of H-bonded multilayers

Some factors affecting the growth of H-bonded multilayers, such as molecular weight of polymer constituents, and self-assembly conditions (pH, ionic strength, and temperature, and concentration of solutions), LbL deposition method.

1.2.1.1 Polymer Type and Molecular Weight

In H-bonded films a bilayer thickness depends on the number of interpolymer binding point, which is defined by the binding strength. Kharlampieva et al[179] , reported that for neutral polymers of comparable length, films of poly(methacrylic acid) (PMAA) with poly(ethylene oxide) (PEO), poly(N-vinyl methyl ether) (PVME), poly(acrylamide) (PAAM), or poly(2- hydroxyethyl acrylate) (PHEA) demonstrate higher bilayer thicknesses than strongly bound systems, such as PMAA assembled with poly(vinyl pyrrolidone) (PVPON), Poly(N-isopropylacrylamide) (PNIPAM), or Polyvinyl chloride (PVCL). Thicker bilayers is a result of more loopy conformations of the self-assembled polymer chains. The molecular weight dependence of bilayer thickness totally depends on the intrinsic strength of inter-polymer binding. For example, the weakly bound PEO/ poly(acrylic acid) (PAA) system shows about a seven-fold increase in bilayer thickness when the PEO molecular weight is increased from 1.5 to 20 kDa [9]. Likewise, an increase in a bilayer thickness of the deposited layers happened for a relatively weakly bound PAAM/PAA film when the PAAM molecular weight increased from 800 to 5000 kDa [180]. Guan and co-workers[181], reported more strongly bound PVPON/PAA HB films. Their results showed that molecular weight had a significant effect on the film thickness only when the molecular weight of PVPON and/or PAA was lower than 40 kDa. Kharlampieva and Sukhishvili [179] studied even more strongly PVCL/PMAA films. Their results showed the bilayer thickness was the same for polymers of a variety of molecular weights, including PVCL with such a low molecular weight as 1.8 kDa. Such independence of the bilayer thickness from molecular weight is caused by the high density of intermolecular H-bonds in this system.

1.2.1.2 pH of polymer solutions

pH has a great effect on the thickness, content ratio and morphology of the H-bonded LbL films. This effect is a consequence of the ionization degree and conformation change of polymers. The assembly solution pH must be low enough to avoid ionization of the carboxylic acid groups. For both weakly and strongly bound H-bonded films, the bilayer thickness intensely decreases as the deposition pH approach the critical pH. At pH above critical pH, carboxylic acids incorporated into a H-bonded multilayer become ionized and the H-bonds are disrupted and the film dissolves. The critical pH depends on the strength of the H-bonding interactions within the multilayer film, with weaker interactions resulting in lower critical pH values [8, 179]. One of the weakest ones reported so far is PEO/PAA system with critical pH of 3.5 [9]. In order to determine the critical pH of LbL films, films were dipped into a pH-adjusted solution for a specific time, then dried and the film thickness is measured and compared to the original thickness.

The effect of low deposition pH on H-bonded multilayers has been studied by Yang et al [181]. They reported that PAA/PVPON film deposited from solutions of pH 0.2 to 1.0 was very rough and thick, with a bilayer thickness of about 48 nm. This unusual large bilayer thickness was explained by the collapse of PAA chains into denser and less soluble globules at the extreme pH values where PAA becomes completely uncharged [181].

1.2.1.3 Ionic strength of polymer solutions

The effect of salt on the growth of H-bonded LbL films is complex and in different ways. First, ions are capable of electrostatic screening, which causes an increase in ionization of weak polyelectrolytes. In this study, the addition of monovalent and divalent salts in higher concentrations (higher than 0.5 M) during deposition of PEO/ PAA systems resulted in inhibition of film growth, which was probably a result of increased ionization of PAA [9]. the addition of monovalent and divalent salts in higher concentrations (higher than 0.5M)

during assembly of PEO/PAA systems resulted in inhibition of film growth,[30] which was probably a result of increased ionization of PAA. the addition of monovalent and divalent salts in higher concentrations (higher than 0.5 M) during assembly of PEO/PAA systems resulted in inhibition of film growth,[30] which was probably a result of increased ionization of PAA. the addition of monovalent and divalent salts in higher concentrations (higher than 0.5M) during assembly of PEO/PAA systems resulted in inhibition of film growth [30] which was probably a result of increased ionization of PAA. The addition of monovalent and divalent salts in higher concentrations (higher than 0.5M) during assembly of PEO/PAA systems resulted in inhibition of film growth,[30] which was probably a result of increased ionization of PAA.

Second, ions are able to interact with polymers. At the same time, if both polymers remain uncharged, the effects of moderate concentrations of the salts on the growth of HB films involve dehydration and ion-dipole interactions and are usually smaller than that of electrostatically assembled systems. For example, in the case of strongly associated PVPON/PMAA films, the film thickness increased by only ~10% when self-assembly was performed in a 0.5 M NaCl solution [179].

Third, salts can affect the solubility of self-assembled polymers. These three factors affect the bilayer thickness. Quinn and Caruso [182], reported deposition of a relatively hydrophobic poly[styrene-alt-(maleic acid)] (PSMA) from 0.2 M NaCl solutions dramatically increased the thickness and roughness of PEO/PSMA films as compared to when the films were deposited from 0.02 M NaCl solutions [182].

1.2.1.4 Temperature of solutions

Temperature is another important factor in the formation of an H-bonded multilayer. Caruso and coworkers [183], for the first time, demonstrated the effect of temperature on the H-bonded LBL film of temperature-responsive polymer PNIPAAM and PAA [183]**.** The

PNIPAAM/PAA films fabricated at 30 ^{0}C showed higher thickness and much lower roughness compared to films prepared at 10 or 21 ^{0}C [183]**.** The thicker bilayer reason is larger amounts of PNIPAAM were deposited within films when the low critical solution temperature (LCST) of PNIPAAM (32^{0}C) was approached. Sukhishvili's group [184], studied the behavior of another temperature-responsive polymer, PVME (LCST 36^{0}C) and PAA, and found a similar result. The total amount adsorbed within the PAA/PVME film was the same for temperatures 15 and 20^{0}C but increased 1.5 and 2-folds when the temperature was increased to 25 and 30^{0}C, respectively [184].

On the other hand, if H-bonded multilayers contain a polymer pair with an upper critical solution temperature (UCST), thinner layers are deposited within LbL films at higher temperatures [179]**.** One example is the PAAM/PAA system, where the case of PAAM/PAA interpenetrated networks have a UCST of 20–25 ^{0}C [185]**.** As the temperature is raised above the UCST, intermolecular H-bonds between the polyacid and PAAM dissociate, which results in thinner layers.

1.2.1.5 Concentration of solutions

In addition to pH, ionic strength and temperature, the growth of H-bonded multilayers is also affected by the concentration of assembly solutions**.** One example is the work reported by Yang et al [186]. They reported that H-bonded PVPON/PAA films at higher concentrations of assembly solutions resulted in larger amounts of bilayer thickness [186]**.**

1.2.1.6 LbL deposition method

Char and co-workers reported that the surface morphology and surface-wetting behavior of H-bonded LbL films can be controlled using different deposition methods [187]. Specifically, while grainy films were formed using a dip coating method, thinner and smoother films were formed by spin coating deposition. The different surface morphologies were reflected in film-wetting behavior. For the rougher morphology of the dip-assisted

hydrophobically modified poly(ethylene oxide) (HM-PEO) and PAA films, the contact angle increased as the number of layers increased; conversely, it was independent of the film thickness for the more uniform spin-coated films [187].

1.2.2 LbL assembled hollow capsules

The LbL technique has proved to be a simple but versatile method for the preparation of self-assembled films with controlled thickness and composition since it was first introduced by Decher er at al [2]. One advantage of the LbL technique is that there is no restriction on the size and morphology of the substrate on which the film is made, which implies that the LbL method can be extended from 2D to the 3D system (for instance, spherical or other non-planar substrates). Consequently, a large variety of core-shell particles with finely tuned polymer layer thickness and composition have been synthesized [58], and a series of novel hollow microcapsules constructed by subsequent removal of the sacrificial core of the resulting core-shell particles [3, 61, 188]. The LbL assembly of materials on particles and the subsequent formation of capsules [61, 189] are of particular interest, principally because of the promise of these carrier particles in therapeutic delivery applications [190]. In recent years, different techniques have been applied for the fabrication of LbL capsules, including centrifugation, filtration, and electrophoretic approaches. Depending on the type of polymers and templates, the technique has to be chosen carefully to allow for optimal particle coating.

The choice of the template, as well as the polymer system are important factors for the construction of capsules with distinct properties and thus, applications. While the polymer choice directly determines the properties of the capsules, the template determines the size and shape of the final capsules. Suitable templates should be stable during LbL coating and the removal process of the template should not damage the structure and stability of the capsule shell. The most commonly used templates are melamine formaldehyde [61], polystyrene [191], SiO_2 (solid/porous) [192, 193], $CaCO_3$ [194, 195], $MnCO_3$ [195, 196], red blood cell [197, 198], emulsion [199, 200]and bubble[201].

The noteworthy feature of a hollow capsule is that the interior volume can be loaded with functional cargo molecules and serve as a compartment for different applications. Different methods have been reported to load the molecules in LbL capsules. The cargo molecules can be directly loaded during formation of the capsule (pre-loading method), or after capsule formation (post-loading method) [202]. The cargo molecules can be loaded in the hollow capsule, into multilayers or on the external surface of the capsule.

The LbL method for the formation of microcapsules was reported the first time in the late 1990s[60] for oppositely charged polymers. In literature, for the preparation of LbL capsules, various interactions have been reported [203]. These complementary interactions can be categorized into three main strategies: (a) electrostatic interactions between oppositely charged polyelectrolytes [60], (b) H-bonding between H-donor and H-acceptor [12, 204, 205], and (c) covalent bonding for direct multilayer buildup and stabilization of pre-formed films [206], respectively. In addition, other chemical and physical interactions have been implied to assemble and/or stabilize multilayer films, including: (d) DNA hybridization [207–212], (e) stereocomplexation [213, 214], (f) hydrophobic [215], and (g) host-guest interactions [216–218]. The variety of interactions which can be applied for the fabrication of multilayer films further demonstrates the enormous potential of LbL assembly for the fabrication of smart delivery systems.

1.2.2.1 H-bonded LbL capsules

Most common LbL assemblies are based on electrostatic interaction, thus due to cytotoxicity of polycations these systems are not favorable in biological applications. In this paper, the H-bonded LbL coated capsule is studied. H-bonded multilayers offer many different pathways for the development of responsive films and capsules. Firstly, the ability of these materials to disassemble within a mild pH range offers new possibilities for therapeutic delivery applications, as this disassembly pH can be readily tuned by varying the H-bonding pairs or the assembly conditions used. Secondly, stimuli-responsive swelling or cargo release can be achieved

by incorporating polymers such as PNIPAM, which is temperature-responsive, and PMA, which is pH-sensitive. The versatility of H-bonded multilayers has allowed the development of materials with a range of properties tailored to biomedical applications. These include the potential for controllable disassembly, the capability to respond to stimuli such as pH and temperature, and the ability to load and release cargo specifically.

Zhang et al.[219], were first to investigate 3D materials using H-bonding-directed assembly, and they reported H-bond microcapsule of PVP and m-methylpheol-fomraldehyde resin (MPR) on two spherical templates, polystyrene (PS) and SiO_2 particles. They show that intact hollow capsules only can be successfully obtained when SiO_2 used as core and removed by HF. PVP/MPR membrane is not robust enough to allow the penetration of PS molecules with a high molar mass in tetrahydrofuran (THF) which is used to remove PS core [219]. After this work, the field of H-Bonded LbL capsules greatly advanced to achieve a variety of materials with a broad range of chemical compositions, mechanical properties, and permeability characteristics for advanced delivery applications. Feng et al. [220], reported the fabrication hollow H-bonded hollow microcapsules by polymerization of acrylic acid in a solution containing surface-modified silica particles and poly-(vinylpyrrolidone) (PVP) and a subsequent core removal with HF. Their results show that the size of microcapsules increased by increasing pH. This swelling-deswelling process of the microcapsules is completely reversible at high and low pH values, which provides a convenient way to mediate the capsule properties. Rubner and co-workers[221] demonstrated bioinert, H-bonded multilayer coatings of PAA/PAAM on melamine formaldehyde (MF) colloidal particles. The multilayer-coated colloidal particles showed excellent resistance toward mammalian cell adhesion. These bioinert H-bonded multilayer coatings offer the potential for biomedical applications [221]. Guan et al. [222], investigated H-bonded microcapsules of hydroxypropylcellulose (HPC), a cellulose derivative, and PAA onto colloidal SiO_2 particle, and the size change of the hollow capsules in media with various pHs and salt concentrations.

They observed an unexpected slow swelling upon mixing with PBS of higher pH, which is attributed to the semi-rigidity and hydrophobicity of the HPC chains involved in the H-bonded capsule wall [222]. Multilayer capsules of PVPON, PEO, PVME or PNIPAM with PMAA were successfully made on cadmium carbonate and on SiO_2 particles [179, 223]. Kharlampieva et al.[224], demonstrated the feasibility of preparation of hollow capsules based on PMAA/PVME and PMAA/PVCL which they are promising as temperature-responsive containers for controlled delivery applications [224]. Paramasivam et al.,[225] reported the temperature responsive of H-bonded capsules based on tannic acid and poly(2-n-propyl-2-oxazoline) with the ability to capture and release of loaded fluorescent molecules at a physiological temperature of 37^0C. Switching of temperature results in the collapse of the polymer chain and as a result morphological change of the capsules that induces the release of the loaded molecules [225].

In general, the deposition of polymers onto the colloidal substrates occurs in the same way as on planar surfaces; however, to remove the polymer solution a cycle of centrifugation and resuspension steps is typically employed. The film thickness can be controlled by altering the number of layers deposited during LbL assembly. The preparation of LbL hollow capsules using either oppositely charged polyelectrolytes or H-bonded polymers include the same steps. Polymers are sequentially deposited onto a template particle, and after the desired thickness and number of bilayers achieved and a core-shell particle is formed, the sacrificial core is dissolved, leaving behind a hollow capsule. Generally, the sacrificial template is removed by dissolution or calcination [226, 227]. The removal process of the template should not damage the loaded material. Thus, the template and loading method should be chosen based on the molecules that are going to be entrapped into the capsules.

To prepare H-bonded thin film with LbL assembly, a polymer pair, one H-bond donor and the other H-bond acceptor, is needed. H-bonded multilayers based on water-soluble neutral polymers and polycarboxylic acids are mostly prepared at an acidic pH, at which polyacids

are completely protonated [7, 8]. At pH above critical pH, H-bonds disrupted due to ionization of the polyacid, therefore the LbL film is disintegrated [7, 8, 179, 184].

We focus on H-bonded systems because they can be designed to show stimuli-responsive properties under physiologically-relevant conditions, and allow the incorporation of uncharged polymers, which is important for developing stealth materials. Herein to prepare H-bonded LbL capsule, PEOX and TA were used as H-acceptor and H-donor respectively. In the previous chapters, we reported the pH-responsive LbL film of PEOX and TA. Also, we introduced H-bonded LbL film of PEOX stabilized silver nanoparticle/TA as antibacterial coatings. The hollow capsules prepared by PEOX has also been studied. Kempe et al. [228], reported the hollow capsules prepared by the LbL assembly of PEOX and PMMA. Later, they also reported the LbL assembly of Thiol-containing poly(2-ethyl-2-oxazoline) ($PEtOxMA_{SH}$) brushes and PMA multilayers onto silica (SiO_2) particle templates, wherein the layers are stabilized by cross-linking them through disulfide formation [229].

In chapter 6, we report on the formation of pH-responsive hollow capsules of PEOX and TA. H-bonded PEOX/TA capsules have not been reported previously. Rhodamine 6g is used as a model cargo molecule to study the loading and release properties of the PEOX/TA capsule. Since the formation and destruction of H-bonds can be controlled easily by external stimuli, such as pH, PEOX/TA capsules may have great merit when being used in controlled drug-release systems, since they can be loaded with a large number of functional molecules and release them at physiological pH. The instability of this H-bonded capsule is linked with the disassociation of TA when pH approaches its pKa, which is commonly used as H-donor.

1.3 Biomedical applications of H-bonded LbL films

A great deal of researches has focused on the development of H-bond multilayered films as materials with promising properties for biomedical and engineering applications due to special features when compared to conventional electrostatically driven assemblies.

H-bonded systems can be designed to show stimuli-responsive properties under physiologically-relevant conditions, and allow the incorporation of neutral polymers, which is important for the biomedical application. In this section, emphasis will be given to materials engineered for biomedical applications, specifically films/capsules that afford controlled loading/release of therapeutic cargo and films with antibacterial properties.

1.3.1 Encapsulation and release

The LbL films deposited on a surface provide a matrix to load and release functional agents embedded within the film. Moreover, the further release of incorporated molecules can be exactly triggered by changing environmental stimuli and/or through adsorption of polymers. Developing therapeutic molecules loaded LbL systems is fundamental for gene and drug delivery applications [190]. Various molecules have been encapsulated within H-bonded LbL multilayers. Different methods for encapsulation of these molecules are needed due to their different chemical and physical properties. The encapsulation methods divided broadly into three categories: incorporating of cargo molecules within the films/capsules during film deposition; post-loading preformed films/capsules; or pre-loading the cargo onto the template (either planar or colloidal). In following some examples of each is given.

Cargo molecules can be encapsulated into LbL multilayers during LbL deposition. Hammond and coworkers reported that polymeric micelles can be incorporated within H-bonded films to encapsulate the hydrophobic antibacterial and antifungal agent triclosan [230]. Similar loading method has been used to the assembly of films on particles to form microcapsules containing drug-loaded liposomes. For example, liposomes have been incorporated into Thiol-modified poly(methacrylic acid) (PMA_{SH}) / PVPON multilayer films and capsules by using PMA modified with a cholesterol group (PMA_C) as an anchor layer [231]. The cholesterol moiety inserts into the hydrophobic shell of the liposomes, enabling the PMA_C to assemble on top of the liposomes and providing a PMA surface for subsequent film growth. This method has been implied to show that

both enzymes (β-lactamase) [231] and anticancer drugs(thiocoraline) [232] can be encapsulated within PMA_{SH} capsules and retain their activity.

The encapsulation of cargo molecule can be done by adsorbing cargo onto or within a film after it has been assembled. Typically this is achieved using films that are responsive to certain environmental stimuli, causing morphological changes within the film to retain cargo. Wang et al. synthesized pH- and temperature-responsive capsules from PNIPAM and sodium alginate [233]. At low pH (3.5), high molecular weight (2000 kDa) fluorescein-labeled dextran permeates into the capsules, but at close to physiological pH (6.8), the capsule permeability to the dextran is decreased. In a different method, oil-soluble drugs, such as DOX, can be encapsulated in preformed polymer capsules by loading an oil phase into the capsules [234]. Sivakumar et al. incubated dehydrated PMA_{SH} capsules in an oleic acid/DOX mixture. When these capsules were rehydrated in an aqueous buffer, the oleic acid/DOX mixture was retained within the capsules [234].

A recent technique that has been used to encapsulate materials is to preloading. This method has been used to encapsulate DNA within PMA_{SH} films by adsorbing single-stranded oligonucleotides, double-stranded DNA and plasmids onto amine-functionalised (positively charged) silica templates using nano-molar concentrations of DNA [235]. The DNA is electrostatically bound to the surface of the particles and subsequent assembly of PMA_{SH}/PVPON multilayers encapsulates the DNA. Removal of the sacrificial silica particles results in DNA contained within the interior of the PMA_{SH} capsules. A similar method can be used to encapsulate whole proteins [236]. Higher loadings can be achieved by directly layering on cargo that crystallizes into particles (e.g., protein crystals) [233, 237]; however, this technique is limited by the ability to generate a crystalline form of the cargo and the polydispersity of the crystals formed.

Another important aspect of developing of films/capsules for delivery applications is to control the release of the cargo from the LbL system. This ability is fundamental especially

for biomedical applications, where materials need to be engineered to release therapeutics within specific regions (e.g., in cells) and/or in response to specific triggers. There are three main methods used to address this challenge in H-bonded systems: (a) disassembly of LbL film; (b) incorporating responsive components within the film; or (c) using degradable crosslinking agents that result in film disassembly. In this thesis, the focus is on the release of active agents from H-bonded LbL films by disassembly of films or capsules, which more details are given in following.

The ability of H-bonded films to disassemble within a specific pH range has been widely studied for different applications, including drug delivery and biomedical coatings. Ono and Decher reported the construction of free-floating films using a sacrificial film comprised of H-bonded layers [10]. They demonstrated this concept by assembling polyelectrolyte multilayer film of poly(styrene sulfonate) (PSS) and poly(allylamine hydrochloride) (PAH) on top of pH-responsive H-bonded PAA/ poly(ethylene glycol)(PEG) multilayers [10]. By increasing pH to 5.6–6.3, the pH-responsive polymer multilayer segments disintegrate and release self-standing polyelectrolyte multilayer films. Sukhishvili et al. reported a temperature-responsive H-bonded film [184]. They investigated LbL films based on the assembly of PNIPAM/PMA followed by PVPON/PMA multilayers. A detachment of the LbL coating from the substrate was seen when the temperature was decreased to 10^0C at a pH of 5.6 due to the temperature response of the PNIPAM/PMA multilayers. Sukhishvili and Granick also investigated the use of various materials for the tunable disassembly of LbL capsules [8]. In first work PMA assembled with either PEG or PVPON to form responsive polyacid capsules; however, these films were not stable at physiological pH. Next work showed that the pH range where the H-bonded multilayers are stable could be increased significantly by the use of polyacids, such as poly(ethylacrylic acid) (PEA) or tannic acid (TA), due to the higher pKa of both materials [238]. Films were assembled from TA (pKa ~8.5) as H-donor alternately deposited with a series of H- acceptors, and disassembly was

found to occur above pH 8. Sukhishvili and coworkers also showed tuning of the disassembly pH of a weakly interacting H-bonding system, PVCL/poly(L-aspartic acid) (PLAA), by combining this system with a strong H-bonding pair [239]. Mehrotra et al. used similar films to release components from particles, by using PAA/PEG multilayers to release lysozyme over periods greater than two weeks [240]. In another study, Sukhishvili *et al*.[7] used the strategy of adding positively charged dye molecule within LbL film and develop poly-(methacrylic acid) (PMAA)/poly(ethylene oxide) (PEO) dye containing LbL films from a solution with pH = 4, and showing strong retention of dyes at a constant pH. Subsequently, the incorporated dye molecule was released when the pH increased up to 4.6 as a result of film disintegration because of the ionization of the polyacid. Kim *et al*. [241] showed the delivery of biocompatible and biodegradable PEO-*block*-poly (ε-caprolactone) (PEO-*b*-PCL) micelles from the disintegration of PAA/PEO-*b*-PCL multilayers at physiological conditions. The strong capability of micellar core of Poly(caprolactone) (PCL) in loading a large amount of functional compound, triclosan, as well as the biocompatibility of this H-bonding LbL films, offers a new topic to the drug delivery field. Erel et al. [242] reported the fabrication of H-bonded films of micelles of a dually responsive, dicationic block copolymer, poly[2-(N-morpholino)ethyl methacrylate-block-2-(Diisopropylamino)ethyl methacrylate] and tannic acid. At basic pH (pH=8.75), multilayers disintegrated because of ionization of TA and disruption of H-bonding interactions between layers of micelles and TA. H-bonded multilayers of micelles of a dicationic block copolymer are interesting due to the response of both multilayers and micellar cores at different pH paving the way for multiple pH-controlled deliveries of functional molecules from surfaces.

An alternative for loading and releasing cargo is by incorporating components within multilayer films that are responsive to specific environmental stimuli. This allows the release of cargo without degradation of the host film. Ding *et al.* reported this approach for a PAA-based film modified with boronic acid [243]. A model dye, Alizarin Red S, was loaded into the film by

complexation with the boronic acid. When the film was incubated in a glucose solution, the glucose competed with the dye for complexation to the boronic acid, thus releasing the dye.

In another approach, the release of therapeutic cargo can be designed through the responsive characteristics of the H-bonded film, such as temperature or pH-induced swelling, causing an increase in permeability. Zhu and Sukhishvili designed a multilayer system containing PNIPAM-based polymer micelles that swelled reversibly with temperature [244]. It was reported that this structural change could retard cargo release from the micelles by a factor of two.

An alternative method to degraded H-bonded multilayer films is by using cleavable crosslinking moieties. For instance, Becker et al. studied the properties of PMA_{SH} capsules stabilized with different degrees of thiol crosslinking, and found that degradation could be controlled by changing the thiolation degree [245]. Several therapeutics were loaded into these capsules, and the activity of the encapsulated cargo, such as plasmid DNA, was confirmed using PCR.

1.3.2 Antibacterial coatings

Many studies have been done to develop antibacterial surfaces. The antibacterial surfaces aim to eliminate or prevent the initial adhesion of bacteria, and subsequently the formation of a biofilm. Generally, the antibacterial surfaces have to be able to kill (bactericidal) or prevent the adhesion of bacteria (anti-adhesive). Some surfaces may have both functions. A method that has attracted much interest recently to form an antibacterial coating, generally by loading antibacterial agents into the multilayers, is LbL assembly. The functions of the LbL multilayers can be determined by the deposited components.

Jiang et al.,[246] used a hydrophobic polypropylene (PP) membrane, modified the surface by a layer of polydopamine (PDA), and then hydrophilic PVP was immobilized onto the PDA-coated PP membrane via H-bonding interactions. Afterward, they introduced antimicrobial iodine onto the membrane by complexation with the PVP layer. The PP

membranes were endowed with high antimicrobial activity after iodine complexation, being able to suppress the formation of biofilm on the membrane surface during the separation process.

Different bactericidal molecules can kill bacteria based on different mechanisms. Very early studies show that using heavy metals such as silver and copper as bactericidal components were very common. It is well known that metal species participate in spatially localized or discrete reactions that disrupt enzymatic activities, disable membrane function or damage DNA [247]. However heavy metals have bactericidal effects, their potential toxicity for mammalian cells limits their use. Antibiotics only target bacteria, causing bacterial cell death by inhibiting DNA, RNA, cell wall or protein synthesis [248]. Although, the effect of an antibiotic decreases with time because bacteria will develop resistance to the specific antibiotic. Cationic molecules and supramolecular also showed bactericidal properties, and interact with phospholipid components in the cytoplasmic membrane resulting in bacterial cell membrane distortion and protoplast lysis under osmotic stress [249]. LbL assembly allows us to incorporate all the bactericidal components mentioned above into multilayer systems. Due to the different interaction strengths between the bactericidal components and the LbL assemblies, the bactericidal components can be either released into the surrounding environment to kill bacteria or firmly stay on the substrate surface to kill bacteria upon contact.

In general, release-killing capacity is introduced to a surface by incorporating bacteria-killing chemicals such as antibiotics, [250] phenols, [251] and heavy metals [252, 253]. One example of release based bactericidal H-bonded LbL film is a study done by Etienne et al. [254] Silver is one of the most widely used bactericidal agents. Different forms of silver such as ions, metallic nanoparticles and silver halide nanoparticles were incorporated into LbL films and subsequently released to kill bacteria. Silver ions were loaded into H-bonded multilayers (PAA/polyacrylamide) and were reduced in situ into silver nanoparticles

(AgNPs) as a biocidal agent. AgNPs were leached from the assembled multilayer thin films and effectively killed both Gram-positive strain *Staphylococcus epidermidis* (*S. epidermidis*) and Gram-negative strain *Escherichia coli* (*E. coli*) bacteria [254]. The release-based antibacterial coating has its own advantages in certain circumstances but disadvantages in other settings. For instance, when the released antibacterial agent is depleted below the minimum inhibitory concentration (MIC), a chemical-releasing coating will lose its antibacterial efficiency dramatically [255].

Biocidal components in the non-release based bactericidal LbL assemblies are firmly immobilized and will only kill bacteria upon contact. In general, most of the biocidal components used in non-release based LbL systems are similar to those used in a release based LbL films. The main difference is the stability of the biocidal components immobilized in the LbL assemblies. To the best of my knowledge, H-bonded LbL film with contact killing property is not reported. However, there are different studies show electrostatic LbL film with contact killing effect [256–262].

1.4 Materials for H-bonded LbL Systems

H-bonding LbL assembly is based on the alternate deposition of polymers containing an H-acceptor and an H- donor, respectively. Commonly used acceptors include PEG, where the oxygen atoms on the polymer backbone act as H-acceptors, and PVPON where the carbonyl group acts as the H-acceptor. The most commonly used donors include polyacids, such as PMA and PAA, which contain carboxylic acid groups. When protonated, the carboxylic acid groups act as H-donors. Early studies on H-bonded multilayers formed on planar surfaces were reported by the Rubner and Zhang groups [5, 6]. The study by Stockton and Rubner investigated the use of polyaniline (PANI) alternately layered with uncharged polymers, such as PVPON, poly (vinyl alcohol) (PVA), PAAM, and PEG [5]. Zhang *et al.* studied multilayer systems of PAA and poly (vinylpyridine) (PVP) to show H-bonding could be used to facilitate multilayer growth [6]. In 2003, H-bonding assembly was extended to particle templates by using PVPON and *m*-

methylphenol-formaldehyde as the H-acceptor and donor, respectively [219]. Compared to electrostatic interaction based LbL film, the pH range where H-bonding polymers can interact and form stable films is limited. This range is dependent on the pK_a of the components, as well as the strength of the interaction between the H-bonding pairs. For example, PMA/PEG and PMA/PVPON H-bonded multilayer films have different disassembly properties: the former disassemble at pH ≈ 4, while the latter are significantly more stable and disassemble at pH ≈ 6.4 [263]. The strength of the H-bonding interactions also plays an important role in the thickness and morphology of the multilayer films assembled [263].

As it mentioned before, H-bonded allows a range of uncharged materials to be incorporated into the multilayers. Polymers such as PEG, PVPON, and PVA are important because they have well-documented low-fouling properties *in vivo* and thus are attractive polymers for biomedical applications. Another type of component that can be incorporated in H-bonded multilayers is temperature-responsive macromolecules such as PNIPAM, poly(*N*-vinylcaprolactam) (PVCPL) and PVME. These polymers have an LCST, the temperature at which the polymers undergo a dramatic change in solubility [264]. The most common example is PNIPAM, which has an LCST of 32 °C, which can be readily tuned by copolymerization with a hydrophilic or hydrophobic comonomer. Incorporation of these polymers into LbL multilayer films offers the potential to engineer temperature-responsive films and capsules that undergo transitions close to body temperature (37 °C), making them of interest for biomedical applications. The thickness of multilayers based on thermally responsive polymers can be tuned by temperature during polymer deposition [183] or after fabrication of the films [244].

Although H-bonding film assembly has been well demonstrated for a different synthetic polymers such as PAA, PMA, and PVPON, recent interest has also focused on the use of biopolymers. It is well known that DNA forms secondary and tertiary structures based on its capacity to H-bond. These interactions can be used to assemble multilayer films of DNA [212] and PNA (peptide nucleic acids) [190]. For these films, the oligonucleotides are engineered so that

'sticky' single-stranded ends are present on each oligomer, which facilitate multilayer film assembly based on the programmable interactions of specific DNA sequences. DNA films and capsules formed via this process have significantly different shrinking and swelling properties, [207] depending on the type, length and order of the nucleic acid sequences used (e.g., homopolymers, diblock copolymers).

In the present study, we focus on H-bonded multilayers film and capsules produced by LbL self-assembly of TA and PEOX.

1.4.1 PEOX and TA

In this thesis, PEOX and TA were used as H-acceptor and H-donor respectively. TA has a unique functional structure with numerous terminal hydroxyl groups, (Figure 1.6.a) thus it is able to form multiple H-bonding. Moreover, TA has shown high biological activity including antioxidant, antimicrobial, anti-carcinogenic, anti-mutagenic and antibacterial properties [265–267].

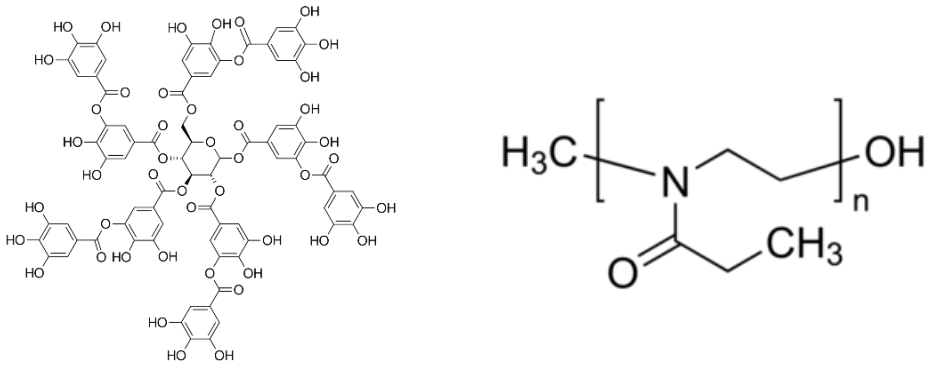

a b

Figure 1.6: Chemical structure of (a) tannic acid, (b) poly (2-ethyl-2-oxazoline).

TA is a polyphenolic molecule consisting of five digallic acid units attached to a glucose core, and its high abundance of hydroxyl groups makes it appealing for inclusion in H-bonded films. In fact, TA has the maximum amount of hydroxyl groups of any tannin derivative [268]**.** Due to its high density of H-donors and relatively high pKa value of 8.5 [269], the inclusion of TA in H-bonded multilayers tends to lead to more stable systems than those fabricated from most other polymers [5]. For these reasons, TA has been assembled with a variety of neutral polymers, including PVPON, PEO, PVCL, and PNIPAM [269, 270].

PEOX is a member of poly (2-alkyl-2- oxazoline)s (PAOX) family and nonionic, non-toxic and biocompatible polymer (Figure 1.6.b) showing LCST of ~60^{0}C [271–274]. H-bonds are primarily formed between the carbonyl groups of PEOX and hydroxyl groups of TA [275].

Previously, H-bonded LbL films based on PEOX and TA were reported by the group of Hoogenbom[276]. Hoogenboom investigated the LbL thin film of TA with poly(2-oxazoline)s with varying hydrophilicity. The results showed the effect of different alkyl side chains of PAOX, and thus hydrophobicity on the thermodynamics of the LbL assembly process[276].

In this thesis, pH-responsive LbL films of PEOX and TA is reported. Also, we introduced H-bonded LbL film of PEOX stabilized AgNP/TA as antibacterial coatings. AgNP loaded LbL films of PEOX and TA have potential biomedical applications as antibacterial coatings which can release Ag^+ ions from stable multilayers below the critical pH and disintegrate by releasing all AgNPs at the critical pH.

1.4.1.1 Antibacterial efficacy of PEOX/TA LbL Films containing AgNPs

Bacterial adhesion on the surface of materials such as medical implant can lead to biofilm formation. This biofilm can spread the infection diseases, and cause critical problems in surgeries [277]. Since the development of effective surface coatings to prevent bacterial

growth has great importance, many studies have been done on antimicrobial coatings. Therefore, new alternative methods are needed for killing or slowing down the growth of bacteria. For an effective antimicrobial surface design, the coating material should delay or prevent bacterial growth either through the release of an antibacterial agent or through the direct contact-killing mechanism. Several types of nanomaterials can be modified and incorporated as antibacterial agents in polymer coating matrices which prohibit harmful microorganisms from growing, therefore, minimize the risk of infection. An often used method to form nanoparticle loaded thin film coating on colloidal particles is via LbL assembly. LbL films provide an alternative method for creating nanoparticle-loaded thin films on different substrates. It is very well known that metal and metal oxide nanoparticles such as silver, copper, gold, titanium, and zinc along with carbon-based nanotubes have antibacterial properties. which they reflect these antibacterial properties on their polymeric nanocomposites [278–283]. Among them, AgNPs are one of the most promising and potential candidate nanomaterials for antibacterial coating. AgNPs have captured wide attention due to their sustained Ag^+ ion release, low-toxicity of the active Ag^+ to a human cell, and great antimicrobial activities against a broad spectrum of bacterial and fungal species [284–286].

Several methodologies are available to synthesize AgNP. The most frequently used method is the chemical reduction of Ag^+ into zero-valent silver (Ag^0) in aqueous solution [287–298]. Commonly, a silver salt (e.g. $AgNO_3$) is mixed together with a reduction agent (e.g. $NaBH_4$) and a coating agent. After having been reduced, Ag^0 atoms aggregate and forming the AgNPs, and the coating agent attaches on their surface, preventing collisions and agglomeration, and adding specific properties to the AgNP. Types of possible coating include organic or inorganic molecules, which can be neutral, positively or negatively charged, and which stabilize the AgNP electrostatically or sterically. Consequently, the AgNP can show both hydrophobic and hydrophilic properties, which will strongly effect their behavior in the

aquatic environment, as well as biological interactions. Examples of coatings that electrostatically stabilize the AgNPs include the negatively charged citrate [290], L-cysteine [298] , gallic acid [287] and thiol [295], as well as positively charged molecules such as branched polyethyleneimine (NH_4^+) [299] As sterically stabilizing coatings, sodium dodecyl sulfate [288, 300], PVP [289] and oleic acid [292, 294] were reported in the literature. In the case of adenine [296], cellulose [289], gelatin [289], and humic acids [293], both negative electrostatic and steric stabilization can be expected.

Antibacterial studies of AgNPs show the effect of AgNP depend on their size [287, 301], shape[302], surface charge and coating composition [303]. For example, an increase in the toxicity of gallic coated AgNP with decreasing particle size was reported for both Gram-negative (*E.coli*) and Gram-positive (*S.aureus*) bacteria [287]. The role of the AgNP coating was studied by [303]. Higher toxicity of positively charged AgNP compared to negatively charged AgNP to a non-specified Gram-positive B*acillus* species was observed, probably because of the higher electrostatic attraction between the negatively charged bacterial cell membrane and the positively charged nanoparticle surface. Additionally, the presence of organic molecules or oxygen in the exposure media can influence the toxicity of AgNP. As reported by [304], effects of citrate-coated AgNP on bacterial biofilms (*Pseudomonas putida*) were lower in the presence of fulvic acids, suggesting the formation of a fulvic acids coating. For *E. coli*, lower AgNP toxicity was seen under anaerobic conditions, which hindered AgNP oxidation and Ag^+ release [305]. *E. coli* biofilms compared to planktonic culture were observed to be less sensitive to PVA-coated AgNP and $AgNO_3$, suggesting a limited diffusion of AgNP and Ag^+ through the biofilm [306].

The exact mechanism which AgNPs employ to cause antimicrobial effect is not clearly known and is a debated topic. However, several mechanisms of action were reported to explain the bactericidal effect of Ag^+ and AgNP, AgNPs are able to physically interact with the cell membrane of different bacteria. This is especially important in the case of Gram-

negative bacteria where several studies have observed the adhesion and accumulation of AgNPs to the bacterial surface. Many studies have reported that AgNPs can damage cell membranes leading to structural changes, which render bacteria more permeable [307, 308]. This effect is highly effected by the nanoparticles' size, shape and concentration [307, 309] and a study using *E.coli* [14] confirmed that AgNPs accumulation on the membrane cell creates gaps in the integrity of the bilayer which predisposes it to a permeability increase and finally bacterial cell death [310]. Various studies reported that AgNP activity is strongly dependent on size [311, 312]. In fact, the bactericidal activity of AgNPs of smaller dimensions (<30nm) was found to be optimal against *S.aureus* and *Klebsiella pneumoniae* [313]. Smaller nanoparticles seem to have a superior ability to penetrate into bacteria. In fact, the interactions with the membranes and any resulting damage, which may lead to cell death, are certainly more evident in the case of nanoparticles with a smaller diameter and positive zeta potential. Electrostatic forces that develop when nanoparticles with a positive zeta potential encounter bacteria with a negative surface charge promote a closer attraction and interaction between the two entities and possibly the penetration in bacterial membranes.

AgNPs have not only been noted to show broad antimicrobial activity but also broad cytotoxicity towards mammalian cells [314, 315]. Cytotoxicity studies of nanoparticles towards mammalian cells have focused on (I) uncapped AgNPs, (II) chemically capped AgNPs and (III) biogenic capped AgNPs [315]. Herein, my focus is on the cytotoxicity of capped AgNPs. AgNPs are often stabilized with reagents such as citrate [316], chitosan [316], polyethylenimine [317], polyvinylpyrrolidone(PVP) [318], polysaccharides [316], carbon , hydrocarbons [318–320], starch [302], peptides [320], and bovine serum albumin [321]. The capping agent could introduce several surface chemistries on AgNPs in solution [321]. Capping agent used to stabilize AgNPs can have an effect on inducing oxidative stress, DNA damage, and apoptosis of mammalian cells. Ahamed et al. compared the performance of uncapped and polysaccharide capped AgNPs of similar sizes and found that polysaccharide-

capped AgNPs was lethal towards mouse embryonic stem cells and fibroblasts and showed extensive genotoxic DNA alterations and apoptotic changes [322]. On the other hand, carbon-coated AgNPs were found to be less lethal than uncoated AgNPs of similar sizes in mouse macrophages[323]. This shows that the capping agent functionality is critical to the cytotoxicity of AgNPs. Further studies are needed to determine the effect of capping agent and surface charge on AgNPs -induced cytotoxicity.

Aggregation of colloidal AgNPs in biological mediums caused the uncontrollable release of Ag^+ ions, an increase in adhesion of bacteria and reduction of the antibacterial effect of AgNPs [324–329]. Also, ecotoxicology studies have shown that silver is highly toxic for some aquatic organisms, accumulate in phytoplankton's and also toxic to zebrafish embryos [330–339]. Therefore the nanoparticles should be embedded to a polymer matrix where the release of silver ions should be controlled. Different nanocomposites containing AgNPs alone or in combination with other nanomaterials have been prepared with natural and biodegradable polymeric matrices[340–345].

Polymers do not only stabilize the nanoparticle dispersions, but also influence their sizes and shapes resulting in different physical properties for various applications. PEG, PVA, and PVP were commonly used in AgNP synthesis for stabilization [346]. Among these, PVP is preferred because of the highly polar cyclic amide group on the side chain which has a strong affinity for silver ions and AgNPs. The mechanism of formation and stabilization of AgNPs in the presence of PVP has previously been reported [323]. However, the stability of poly(N-vinyl-2-pyrolidone-co-vinyl acetate) and PEOX containing AgNP dispersions are significantly better compared to those stabilized by PVP [346].

In this thesis, PEOX was used to encapsulate the AgNP in order to diminish the unwanted aggregation. Then, stabilized AgNPs by PEOX, were used as an H-accepting and TA as H-donating component in the preparation of LbL films. Afterward, antibacterial activity and

cytotoxicity of films were also studied. In Chapter 6 of this thesis, the formation of pH-responsive hollow capsules of PEOX and TA will be reported.

Chapter 2: Materials and Methods

2.1 Chemicals

Silver nitrate ($AgNO_3$), sodium borohydride ($NaBH_4$), tannic acid (TA, Mw = 1701.2 $g.mol^{-1}$), hydrochloric acid (HCl), sodium hydroxide (NaOH), calcium chloride ($CaCl_2$), sodium carbonate (Na_2CO_3), and sodium dihydrogen phosphate ($NaH_2PO_4.2H_2O$) were purchased from Merck. Branched polyethyleneimine (BPEI, Mw ~25,000 $g.mol^{-1}$), poly(sodium 4-styrene sulfonate) (PSS) (Mw = 70,000 $g.mol^{-1}$) and ethylenediaminetetraacetic acid (EDTA) were purchased from Sigma–Aldrich. Poly(2-ethyl-2-oxazoline) having Mw ~50 000 $g.mol^{-1}$ (PEOX50K) and Mw ~500 000 $g.mol^{-1}$ (PEOX500K) were purchased from Aldrich. PEOX having Mw ~ 5000 $g.mol^{-1}$ (PEOX5K) and 200 000 $g.mol^{-1}$ (PEOX200K) were purchased from Alfa Aesar. The polymers used had broad molar mass distributions (PDI ~ 3–4). Prime quality Silicon (100) wafers were purchased from Ultrasil Corporation (USA). Optical grade quartz substrates were purchased from Louwers (Netherlands). All chemicals were used without further purification. Deionized (DI) water (~ 18.0 MΩ cm resistivity) was purified through a Milli-Q system (Millpore).

2.2 Instruments

2.2.1 Dynamic Light Scattering (DLS)

Hydrodynamic size distributions of nanoparticles were determined by dynamic light scattering (DLS) measurements at 25 ^{0}C using Malvern Zetasizer Nano S instrument with 632.8 nm wavelength laser at 173^0 scattering angle.

2.2.2 Ultra Violet – Visible (UV-VIS) spectroscopy

In this work, PG T80 Ultraviolet-visible spectrophotometer was used to monitor AgNP synthesis and dispersion stability, to determine the nanoparticle concentrations, LbL growth and pH-induced disintegration of LbL films on quartz substrates. The spectra were measured in the 200-600 nm range.

2.2.3 Ellipsometry

Thickness of the films after each bilayer deposition was measured by ellipsometry (EL X-01R Ellipsometer, Microphotonics with 632.8 nm HeNe laser at a 70^0 angle).

2.2.4 Field emission scanning electron microscope (FESEM)

The surface morphology of the multilayers at the surface and microcapsules were characterized by Zeiss Ultra Plus FESEM. Secondary electron and in-lense detectors were used for SEM images. The images of multilayers were taken at different magnifications by using accelerating voltage in the range of 3 to 5 kV. To avoid surface charging and improving the imaging of the samples, a 10-15nm gold coating was deposited on the silver nanoparticle loaded multilayers, and carbon coating was deposited on the microcapsules by sputter coater before insertion them in the sample chamber. Sensitive X-ray Spectroscopy (EDX) measurements were performed with the Bruker XFlash 5010 EDX detector at a precision of 123 eV.

2.2.5 Atomic Force Microscopy (AFM)

AFM, a very-high-resolution type of scanning probe microscopy, is used to image surface morphology. In this thesis, AFM was used to study microscopic details and morphology of multilayers. All AFM images in this thesis are recorded by Bruker Dimension AFM in tapping mode with silicon cantilevers at room temperature.

2.2.6 X-ray Photoelectron Spectroscopy (XPS)

Thermo Scientific K-Alpha X-Ray Photoelectron Spectrometer (XPS) was used to determine the amount of AgNP loaded in the multilayers by etching from the top surface down to the substrate. The X-ray source was monochromatized Al-Kα irradiation. During the measurements, the load compensation was controlled with the flood gun at a pressure of ~ 2.0 × 10-7 mbar. The beam size was ~ 400 μm.

2.2.7 Fluorescence spectroscopy

In this thesis, fluorescence spectra were recorded with an Agilent Cary Eclipse Fluorescence Spectrophotometer equipped with a Xenon flash lamp and a slit width of 1.5 nm. Fluorescence spectra were recorded in the range of 535–700 nm upon excitation at 532 nm.

2.2.8 Confocal scanning laser microscopy (CLSM)

Confocal micrographs were taken with a Leica DMI8 Confocal System. Images were acquired using 100X oil immersion objective (HC PL APO CS2 100x/1.40 OIL) with a numerical aperture of 1.4. The excitation wavelength was 553 nm. Confocal micrographs were used to study the loading and the effect of pH on shell permeability and morphology of microcapsules. The release of loaded Rhodamine 6G from the capsules was investigated in phosphate buffer solution (PBS) at pH 1.5, 4.5, and 7.4. For CLSM imaging, 2 mL of the capsule suspension was placed on a microscopic cover glasses and allowed to desiccate gradually. Cover glasses were inverted on glass slides and their edges were immobilized onto the glass slides. Images were processed using Adobe Photoshop cc 2018.

Chapter 3: Synthesis and Characterization of Stabilized Silver Nanoparticles

Overview

In recent years, incorporation of AgNPs in the polymer matrix has attracted great interest because of their broad-spectrum antimicrobial activity in preventing biofouling, optical properties and potential as electron-transfer catalysts [347–349]. For these applications, the selection of the polymer system for surface stabilization is crucial because it can ideally fulfill various functions. For example, the adsorbing polymer can affect the NP sizes and morphologies during the preparation of the metal colloids, or it can also prevent the destabilization and deactivation of the metal colloids during storage and application [346].

One approach for the preparation of AgNP loaded polymeric systems is to synthesize stable AgNPs first for better reproducibility. Among different methods of AgNP synthesis, chemical reduction of Ag^+ ions is the most common used method. In general, different reducing agents have been used for the reduction of Ag^+ ions in aqueous or non-aqueous solutions. One method for aqueous synthesis of AgNPs where $NaBH_4$ is used as a reducing agent is Creighton method [350]. The reducing agent reduces Ag^+ ion and cause the formation of metallic Ag^0 which then grows and forms metallic colloidal AgNPs with possible agglomeration into clusters [351–353]. Using stabilizing agents to coat dispersive NPs during synthesis is important in order to protect the NPs that can be absorbed on or bind onto NP surfaces and avoiding their agglomeration [354]. Types of possible coating include inorganic or organic molecules. These molecules can be positively or negatively charged or neutral and enable to stabilize the AgNP sterically or electrostatically.

For incorporation of AgNPs in polymer systems, stabilization of AgNPs by polymers has also been commonly studied. Polymers do not only stabilize the NP dispersions but also affect their sizes and shapes resulting in different physical properties for different applications. Commonly used polymer stabilizer in AgNP preparation is PEG, PVA, and PVP [346]. PVP is the most preferred one due to highly polar cyclic amide group on the side chain which has a strong affinity for Ag ions and AgNPs. Previously, the formation mechanism and stabilization of AgNPs with PVP has been studied [355]. They prepared silver colloids by photo reduction of $AgNO_3$ with 254 nm UV light in the presence of PVP. Results showed that both UV-vis absorption peak and particle size are strongly dependent on the PVP concentration. In addition, PVP is seen to have a significant effect on the silver reduction and may actually participate in the process [355]. However, the stability of PEOX containing - as presented in this chapter - and poly(N-vinyl-2-pyrolidoneco-vinyl acetate) containing AgNP dispersions are significantly better compared to those stabilized by PVP [346].

In this chapter, the synthesis and characterization of PEOX stabilized AgNP are reported. PEOX is a biocompatible and non-toxic polymer, which has an amide group linked to the backbone and the side chain which is expected to result in better stabilization of AgNPs. The effect of PEOX concentration, PEOX molar mass, pH and time on the stability of AgNP colloidal dispersions have also been investigated.

3.1 Experimental details

3.1.1 Synthesis and characterization of PEOX stabilized AgNPs in aqueous solutions

Among the various known approaches, a chemical reduction method is one of the simple and facile methods for bottom-up synthesis of AgNPs. Reduction of Ag salts to form AgNPs has been achieved by using sodium borohydride and/or citrate. Using $NaBH_4$ (a strong reductant) usually leads to the formation of smaller monodispersed AgNPs while the use of only citrate (a weaker reductant) usually leads to the formation of larger polydispersed

AgNPs because of slower reduction rate [356]. $NaBH_4$ has been used with PVA, PVP, cellulose, Bovine Serum Albumin (BSA), and citrate which are used as stabilizing agents.

In this part of the study, $NaBH_4$ was used as reducing agent. The fundamental method used in the current work is a chemical reduction from $AgNO_3$. AgNPs were synthesized in aqueous solutions using $AgNO_3$ and $NaBH_4$ as a reducing agent in the presence of PEOX as a stabilizer. (Figure 3.1) A large excess of $NaBH_4$ is needed to reduce the ionic silver. Freshly prepared $NaBH_4$ and $AgNO_3$ solutions were cooled down to $3 \pm 1\ ^0C$ and the synthesis was done in an ice-bath while continuous stirring to slow down the rate of reaction and give better control over final particle size/shape. 30 mL of 2×10^{-3} M $NaBH_4$ solution was stirred in an ice bath for about 20 min. 1mL of 2 mg/mL PEOX solution was mixed with 5mL of 2×10^{-3} M $AgNO_3$ solution at room temperature and cooled in ice bath. PEOX containing $AgNO_3$ solution was added into the stirring cooled $NaBH_4$ solution at approximately 1 drop per second. Stirring was stopped as soon as all of the $AgNO_3$-PEOX mixed solutions was added. By adding both solutions ($NaBH_4$ and $AgNO_3$-PEOX), Ag^+ ions were reduced and clustered to form monodispersed AgNPs in the aqueous medium.

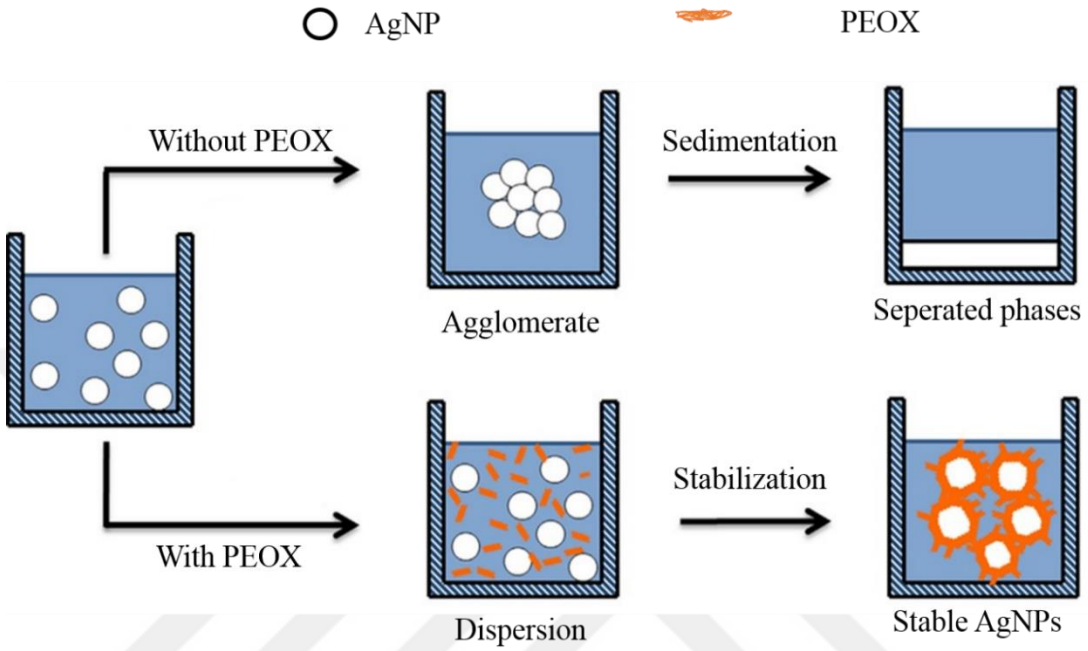

Figure 3.1: Schematic presentation of AgNP stability, with and without PEOX.

Four different molar mass PEOX (5K, 50K, 200K and 500K) were used to synthesize PEOX stabilized AgNPs (PEOX-AgNP). At the end of the reaction, yellow suspensions were observed confirming the formation of AgNPs. The AgNP dispersions were then stored in dark bottles or bottles covered with aluminum foil at 4^0C for further studies. Hydrodynamic size distributions of AgNPs were determined by DLS measurements at 25 ^{0}C. UV–visible spectra of dispersions were measured by UV–vis Spectrometer between 300 and 600 nm to monitor dispersion stability and to determine the nanoparticle concentrations.

3.2 Results and discussion

3.2.1 Synthesis of PEOX stabilized AgNPs

To synthesize stable AgNPs by chemical reduction method, it is important to select a suitable reducing agent and stabilizer. In this study, a water-soluble stabilizer (PEOX) and a strong reducing agent ($NaBH_4$) were used. $AgNO_3$ was reduced by $NaBH_4$ in the presence of PEOX and resulting in formation of AgNPs, according to the following equation.

$$AgNO_3 + NaBH_4 \xrightarrow{PEOX} Ag^0\,(PEOX) + 1/2\ H_2 + 1/1\ B_2H_6 + NaNO_3 \qquad (3.1)$$

The freshly synthesized AgNP dispersions had initially light yellow color indicating the presence of colloidal AgNPs. (Figure 3.11) AgNPs with no PEOX was also synthesized as the control sample. The color change from yellow to brownish yellow in about 2 days was observed for control samples. This change was either because of an increase in NP size, agglomeration of NPs or both. To investigate more in detail, the stability of AgNP dispersion in time was monitored by DLS and UV–visible spectroscopy. Figure 3.2a shows the change of UV–visible spectrum of the control sample in 2 weeks after preparation. The peak wavelength stayed nearly constant at 390–396 nm, but the peak intensity decreased sharply 2 days after synthesis and continued to decrease later at a slower pace by as much as 25% in 2 weeks. UV–visible spectra also showed a slight increase in absorbance at larger wavelengths (~450–500 nm) in time. Both the appearance of the shoulder at a larger wavelength and the decrease in peak intensity demonstrated that the AgNPs were not stable in time and agglomerated [357, 358]. This result also has been confirmed by DLS analysis as shown in Figure 3.2b. Just after synthesis, a bimodal distribution of NP sizes at 2 nm and 45 nm was seen. Both sizes increased sharply to 30 nm and 230 nm, respectively, within 2 days after synthesis. The sizes continued to increase at much slower rate after the 2nd day indicating both growth and agglomeration.

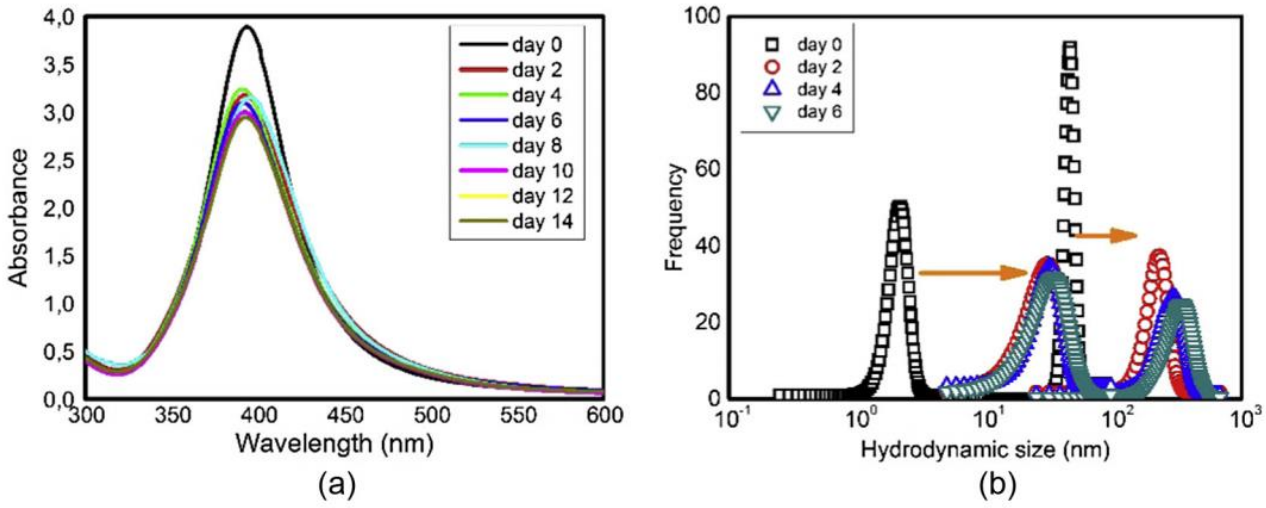

Figure 3.2: a) The change of UV–visible spectra of control AgNPs (no PEOX) in time, b) the change of hydrodynamic size of control AgNPs (no PEOX) in time [359].

The effect of PEOX molar mass, PEOX concentration, pH and time on the stability of AgNP colloidal dispersions has been studied.

3.2.1.1 Effect of PEOX molar mass

The addition of PEOX during synthesis cause steric stabilization of nucleated AgNPs significantly. The duration of stability depended on the PEOX molar mass. Four different PEOX molecular weight have been studied (5K, 50K, 200K, and 500K). Figure 3.3 shows the UV–visible spectra of AgNPs stabilized by different molecular weight PEOX 6 days after synthesis. UV–visible spectrum of freshly prepared dispersions all showed an intense absorbance peak at 394 ± 2 nm. In time, the absorbance peak position stayed nearly constant at ~394 nm, but the peak intensity decreased. In contrast to the ~20% decrease in peak absorbance of control samples in 6 days, the peak absorbance of PEOX(AgNPs) decreased

maximum by ~10%. The absorbance at larger wavelengths (~450–500 nm) also increased slightly but depended on the molar mass of PEOX as shown in Figure 3.3. The shoulder at a larger wavelength was more apparent for PEOX5K and decreased with increasing PEOX molar mass. These results are in consistence with the color change of dispersions. The change in color of the AgNP dispersions from yellow to brownish yellow was more dominant for the control sample and decreased with the PEOX molar mass. The color change of dispersions and the corresponding shoulder appearance shows an increase in the NP size and agglomeration in time [357, 358].

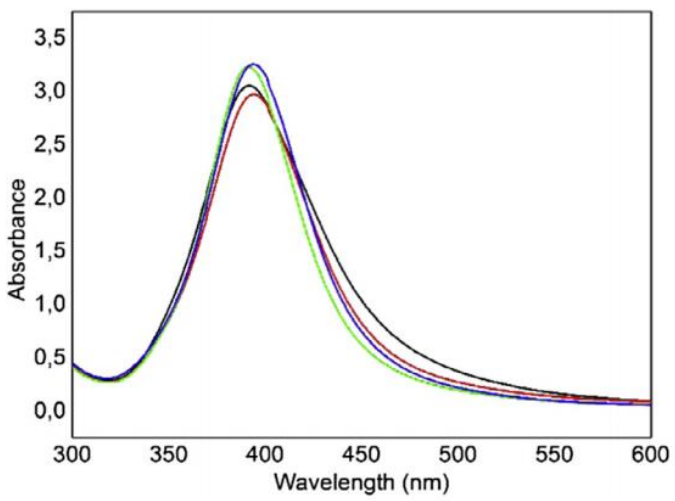

Figure 3.3: UV-visible spectra of AgNPs stabilized by different molar mass PEOX 6 days after synthesis: PEOX5K(black), PEOX50K(red), PEOX200K(green), PEOX500K(blue) [359].

Surface plasmon band of AgNPs smaller than 10 nm in size is known to peak at 394 nm [357, 358, 360]. The absorbance peak exhibited a red shift and significant broadening at larger wavelengths with increasing NP size. Larger wavelength broadening can be because

of an increase in size, agglomeration of particles and formation of different shape particles [361].

The change of AgNP size in time was determined by a DLS analyzer. A bimodal distribution of NP sizes was observed for all AgNP dispersions. Figure 3.4a shows the size distributions of the control sample 2 days after synthesis, for PEOX200K and PEOX500K stabilized AgNPs. For the control sample, both small and large size particles agglomerated initially fast and at later stages slower as shown in Figure 3.4b. The AgNP sizes were measured as 2 and 45 nm just after synthesis which after 2days increased to 30 and 230 nm respectively. Small particles of PEOX200K-AgNPs showed significantly smaller size change from ~6 nm to ~9 nm in 10 days, but agglomerated particles size was observed nearly constant at 71 ± 8 nm. For PEOX5K-AgNPs and PEOX50K-AgNPs, similar size distributions were seen initially, but the dispersions were only stable up to 6 days. After 6 days the AgNP dispersions showed more agglomeration and their size increased above 200 nm. In the case of PEOX500K-AgNPs, the size of both small and agglomerated particles stayed constant at 10 ± 2 nm and 90 ± 11 nm, respectively. The DLS measurement at 6–10 nm corresponds to individual PEOX stabilized AgNPs in the dispersion, and the peaks larger than 70 nm correspond to individual AgNP agglomerates in the mesh of bridging PEOX chains. Microscopic analysis also confirms these assignments as shown below.

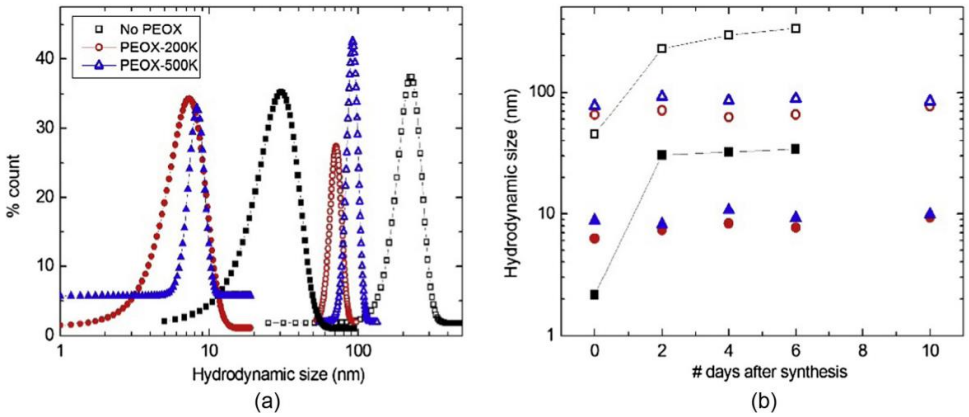

Figure 3.4: a) Hydrodynamic size distribution of AgNPs 2 days after synthesis, b) the change in the size of AgNPs in days: Control sample (black squares), PEOX200K stabilized (red circles), PEOX500K stabilized (blue triangles). The filled symbols correspond to the small size individual particles and the open symbols to large size agglomerates for the bimodal distribution seen in (a) [359].

The difference between the initial size of control AgNP and PEOX-AgNP clearly shows that PEOX adsorbs on the nanoparticle surface and sterically stabilizes them in dispersions. Amide dipole of PEOX monomer is expected to interact strongly with the Ag surface [362–364]. This interaction is significantly enhanced in PEOX chains by the connectivity of the monomers and results in stronger adsorption of PEOX chains on AgNP surfaces with increasing PEOX molar mass. Therefore, the stability of AgNP dispersions increased with increasing molar mass of PEOX chains from ~2 days for the control sample to ~6 days for PEOX5K and PEOX50K to more than 2 weeks for PEOX200K and PEOX500K. While UV–visible spectra of PEOX200K and PEOX500K stabilized AgNP dispersions did not show significant agglomeration in time, agglomerates were observed by DLS in these dispersions as well. The agglomerate size was slightly larger for PEOX500Kcompared to PEOX-200K. We ascribe these agglomerates to bridging capability of larger molar mass chains. In these

agglomerates, ~10 nm diameter individual AgNPs (Figure 3.5a) are expected to be well-separated but held together by bridging polymer chains as shown in Figure 3.5b. Therefore, the surface plasmon band of individual AgNPs stabilized by PEOX200K and PEOX500K was clearly seen in UV–visible spectra without any significant shoulder at larger wavelengths. The flexibility of the bridging PEOX chains is expected to result in rather flattened conformations of these agglomerates when adsorbed on the substrate during LbL film preparation which is depicted in Fig. 5c. This is discussed below in relation to the observation of rather smooth surface morphology in PEOX(AgNP)/TA LbL films.

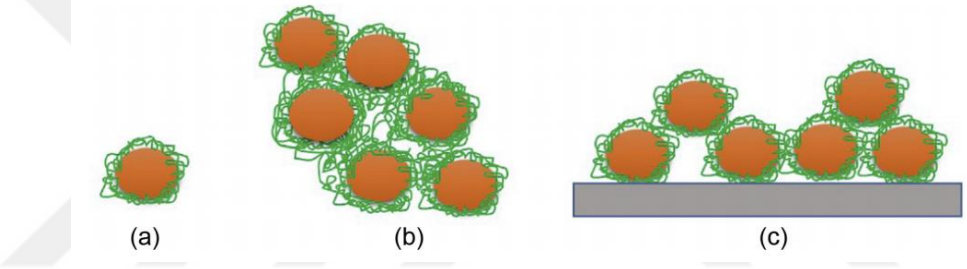

Figure 3.5: Illustrations of: a) individual PEOX stabilized AgNP, b) agglomerate of AgNPs in dispersion formed by bridging PEOX chains, c) rather flattened conformation of the agglomerate adsorbed on a solid substrate [359].

3.2.1.2 Effect of polymer concentration

The effect of PEOX concentration on the stability of NPs was investigated for PEOX500K, which was the most effective in stabilizing AgNPs. AgNPs with four different PEOX500K concentrations (0.005 mg/mL, 0.010 mg/mL, 0.030 mg/mL and 0.055 mg/mL) were synthesized. AgNPs without PEOX was synthesized as a control sample. All PEOX coated AgNPs showed stability up to 2 weeks after synthesis. The peak wavelength in the UV–visible spectrum increased by ~2 nm, while the peak absorbance decreased slightly (Figure 3.6).

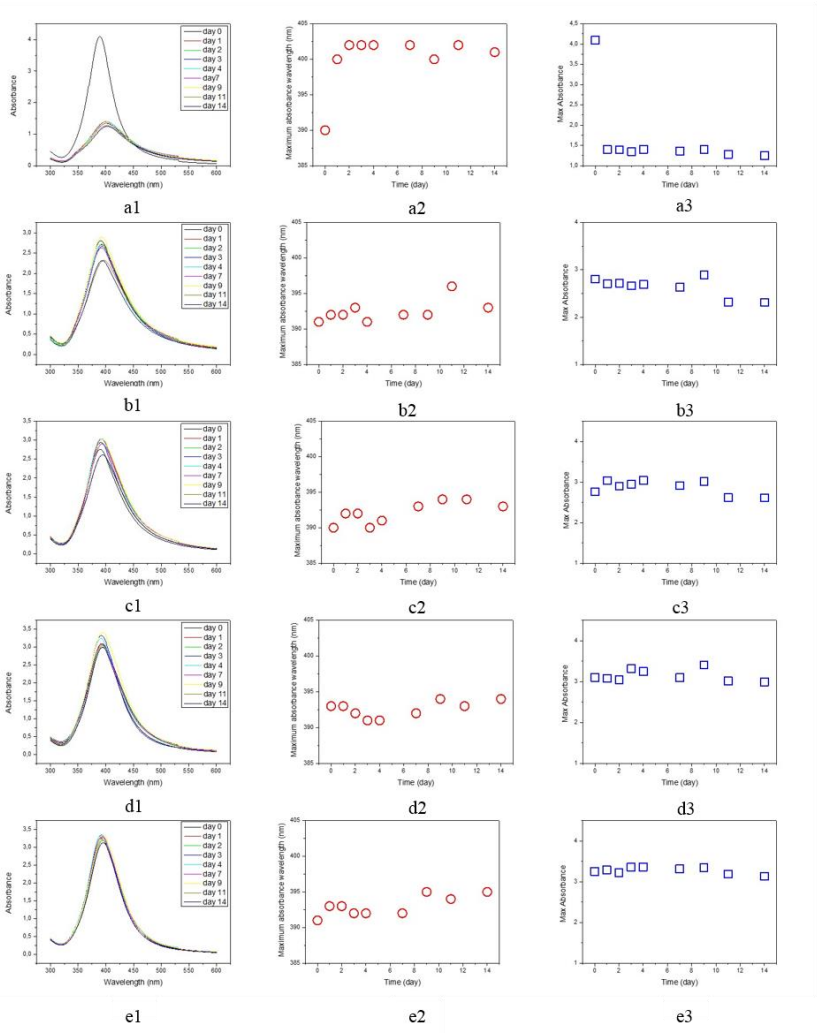

Figure 3.6: UV-visible spectra of: a) control sample of control AgNP dispersion in time, b) PEOX500K(AgNP) dispersion at PEOX-500K concentration of 0.005 mg/mL in time, c) concentration of 0.010 mg/mL in time, d) concentration of 0.030 mg/mL in time, e) concentration of 0.055 mg/mL in time. All middle figures show the change in peak wavelength in time, and all right figures show the change of peak absorbance in time[359].

The lowest decrease in absorbance was observed for the highest concentration of PEOX500K 0.055 mg/mL. The individual AgNP sizes stayed constant at ~8±2 nm and the agglomerate sizes at ~85 ± 15 nm. In contrast, in the control AgNP sample, the peak wavelength increased by ~12 nm within 2 days after synthesis with no significant change afterward. The peak absorbance decreased by more than 50% within a day after synthesis and continued to decrease slightly afterward. The main difference with changing PEOX concentration was seen in the UV–visible peak absorbance. The absorbance peak increased with increasing PEOX concentration (Figure 3.7).

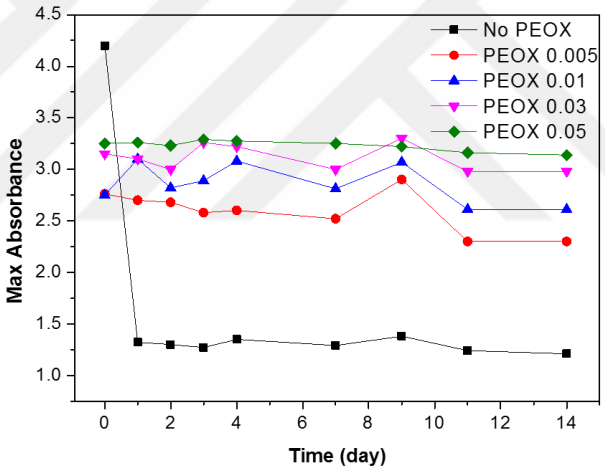

Figure 3.7: The change of peak absorbance in time in the UV-visible spectra of PEOX500K(AgNP) dispersions at different PEOX-500K concentrations (Figures 3.6 a-e) [359].

These results demonstrate that the concentration of AgNPs increased with PEOX concentration and show the effect of PEOX chains in the stabilization of nucleated AgNPs.

3.2.1.3 Effect of pH

LbL films of PEOX-AgNPs/TA were assembled at pH 4.5, therefore the effect of pH on the stability of different molar mass PEOX stabilized AgNPs at a concentration of 0.055 mg/mL was also investigated. The pH of the as-prepared AgNP dispersions was measured as ~9.9, and adjusted to 4.5 by adding HNO_3. By the addition of HNO_3, an increase in peak absorbance wavelength from ~5–6 nm to 396–397 nm was observed for all PEOX molar masses and stayed constant in the range of pH 7 to pH 4 (Figure 3.8).

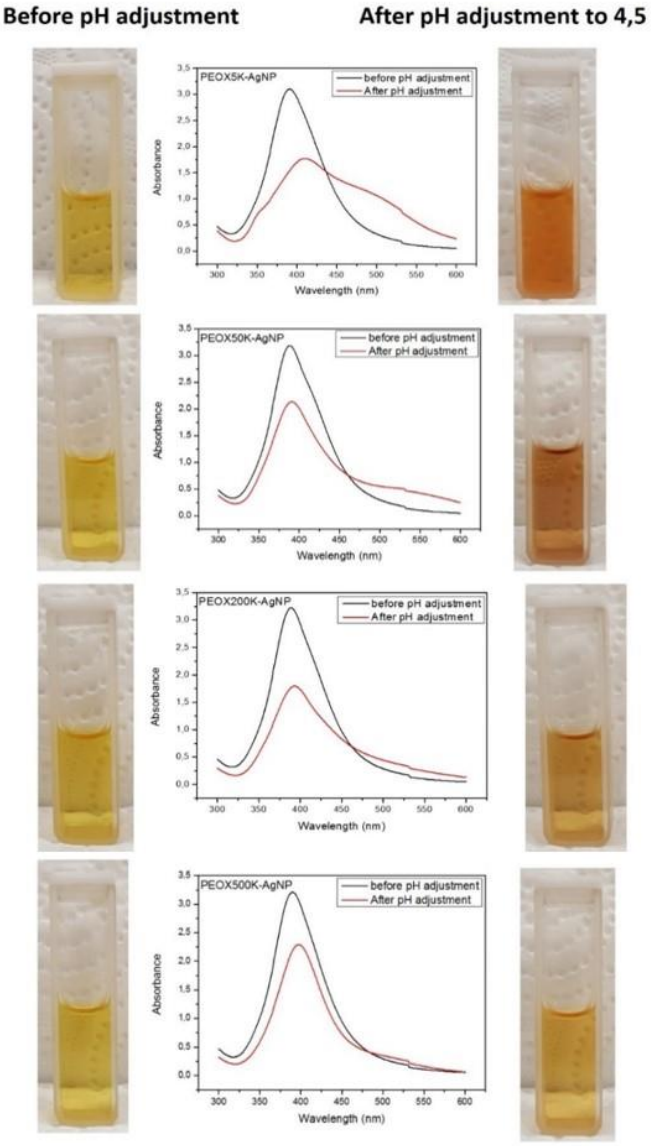

Figure 3.8: The effect of changing the pH of dispersion from 9.9 to 4.5 on the UV-visible spectrum and on the dispersion color of: a) PEOX5K(AgNP) dispersion, b) PEOX50K(AgNP) dispersion All PEOX stabilized AgNP dispersions are at PEOX concentration of 0.055 mg/mL, c) PEOX200K(AgNP) dispersion, d) PEOX500K(AgNP) dispersion [359].

The individual NP size was measured to increase from ~10 nm to ~15 ± 1 nm (Figure 3.9).

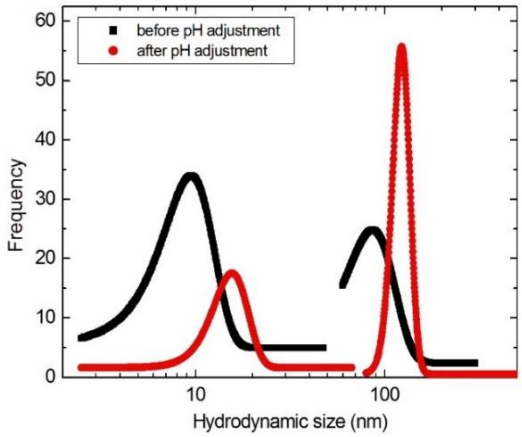

Figure 3.9: AgNP dispersion stabilized by PEOX-500K at concentration of 0.055 mg/mL. The effect of changing the pH of dispersion from 9.9 (black squares) to 4.5 (red circles) on the hydrodynamic sizes as measured by DLS [359].

The agglomerate size also increased slightly with decreasing pH from ~85 nm to ~120 nm and stayed constant in the pH 7 to pH 4 range. All PEOX stabilized dispersions at a concentration of 0.055 mg/mL were stable at pH < 9.9 during the observation period up to 8 days (Figure 3.10).

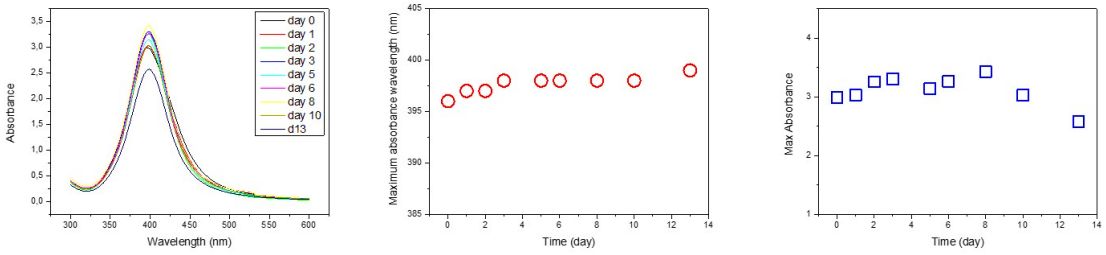

Figure 3.10: Temporal stability of the Ag-NP dispersion stabilized by PEOX-500K at a concentration of 0.055 mg/mL at pH4.5: UV-visible spectra in time (left); peak wavelength in time (middle); peak absorbance in time (right) [359].

By changing pH from 9.9 to 4.5, the change in color of PEOX-AgNP dispersion was observed as seen in Figure 3.6. The color of all AgNP dispersions changed from yellow to brownish yellow as expected from the increase in peak wavelength and the appearance of shoulder in larger wavelength in UV–visible spectra (Figure 3.8). The better stabilization of AgNPs by higher molar mass PEOX is clearly visible at pH 4.5 in Figure 3.11.

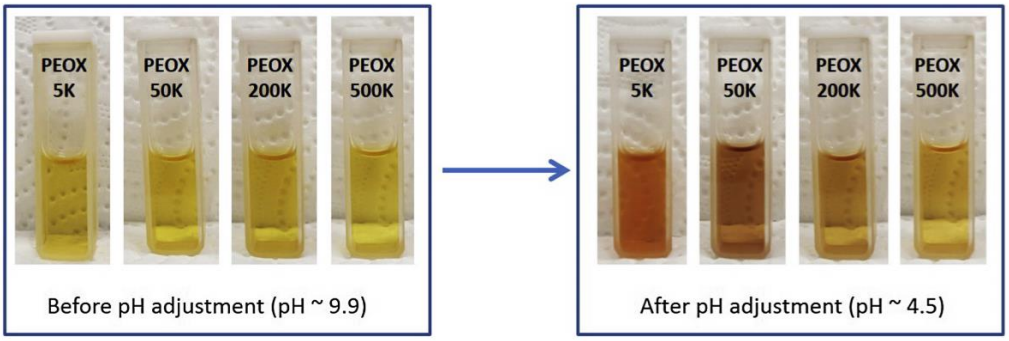

Figure 3.11: The effect of changing the pH of dispersion from 9.9 to 4.5 on the dispersion color for AgNP dispersions stabilized by different molar mass PEOX at a concentration of 0.055 mg/mL [359].

For PEOX stabilized AgNP dispersions, darker brownish yellow color was observed with decreasing molar mass. All dispersions were stable during the observation period up to 8 days. Figure 3.12a shows the dispersions and Figure 3.12b shows their UV–visible spectra at pH 4.5 after 8 days. The peak absorbance wavelength increased slightly to 402 nm and a broad shoulder appeared at larger wavelengths. The intensity of this shoulder was largest for the control sample which showed the most intense color change to brownish yellow. The shoulder decreased with increasing PEOX molar mass and was not apparent for the dispersion stabilized by PEOX-500K.

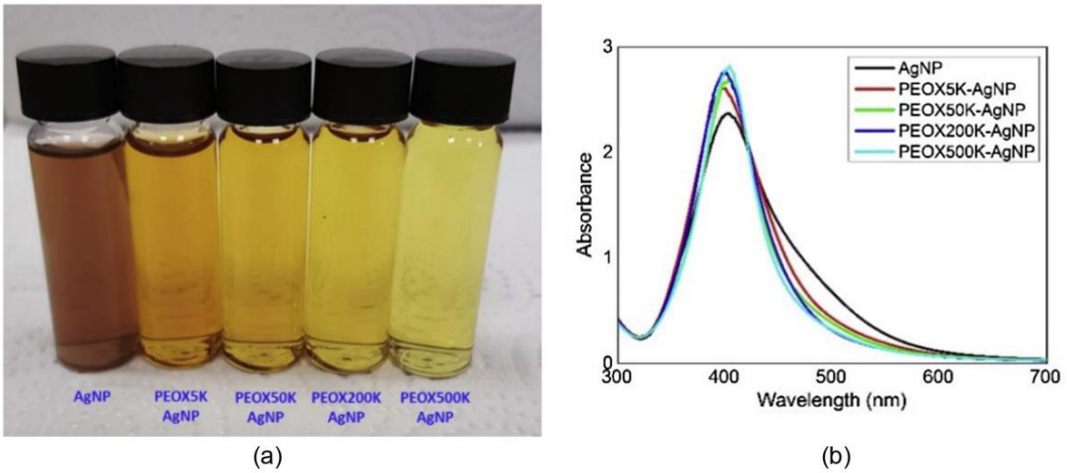

Figure 3.12: a) AgNP dispersions at pH 4.5 after 8 days. No PEOX, PEOX-5K, PEOX-50K, PEOX-200K, PEOX500Kstabilized dispersions are seen from left to right. b) UV–Visible absorption spectra of AgNP dispersions seen in (a) [359].

PNIPAM (molar mass ~22,000 g/mol) and TA were also investigated as stabilizing agents during AgNP synthesis. TA was slow in stabilizing the AgNP dispersions and required ~2–3 days for stable dispersions. PNIPAM stabilized AgNPs in ~1 day similar to PEOX. While

both TA and PNIPAM were observed to stabilize AgNPs initially, the resulting AgNP dispersions did not show long term temporal stability as good as those stabilized by PEOX chains. We attribute the effectiveness of PEOX chains in stabilizing AgNPs to better interaction of its amide dipoles with Ag^+ ions (less steric hindrance compared to PNIPAM) and stronger adsorption of the chains on the AgNP surface.

3.3 Conclusions

AgNPs were prepared by a chemical reduction process in aqueous solution in the presence of PEOX as a stabilizing agent. Four different molar mass PEOX (5K, 50K, 200K, 500K) was used to stabilize the AgNPs in the dispersion. The effect of PEOX molar mass, PEOX concentration, pH and time on the temporal stability of AgNP dispersions was studied. All dispersions showed a bimodal size distribution. Individual PEOX stabilized AgNPs had sizes less than 10 nm. The size of agglomerates depended on the PEOX molar mass and was larger than 50 nm. The agglomerates consisted of individual AgNPs held together by bridging polymer chains. DLS and UV-vis spectrum show that the particle size and the kinetic stability of the dispersions depended on PEOX molar mass. The effect of the molar mass study showed that PEOX5K and PEOX50K stabilized AgNP dispersions were stable for 6 days, while PEOX200K and PEOX500K stabilized dispersions remained stable during the observation period up to 2 weeks. The effect of PEOX concentration study showed that the amount of AgNPs in the dispersion increased with PEOX concentration. Control samples (no PEOX) were not stable. The effect of pH on stabilization of AgNP study showed that by decreasing pH from 9.9 in as prepared dispersion to 4.5 the individual AgNP size increased slightly from 10 nm to 16 nm. All PEOX stabilized dispersions were stable up to 8 days at pH < 9.9.

Chapter 4: Hydrogen Bonded Multilayers of Poly(2-ethyl-2-oxazoline) Stabilized Silver Nanoparticles and Tannic Acid

Overview

LbL assembly is a simple, versatile and pervasive method for formation of functional coatings on solid substrates with interacting macromolecules [365]. Recently, incorporation of nanoparticles in LbL multilayer films has attracted scientific interest due to formation of composite films with enhanced antibacterial, optical and mechanical properties [366–370]. Regarding metal nanoparticles, compared to the in-situ synthesis of them in multilayers [371–373], the external synthesis has the advantage of controlling the particle size, surface chemistry, and shape better prior to using them as one of the LbL process component [287, 361, 374, 375].

In Chapter 3, synthesis and stabilization of AgNPs by chemical reduction of Ag^+ ions by $NaBH_4$ in presence of PEOX has been reported. In the first part of this chapter, the construction of H-bonded LbL films of PEOX stabilized AgNPs and TA, and their stability at different pH is reported. H-bonded LbL film deposition is quite well-established technique and has the advantage of being pH-responsive [6, 7, 238, 376]. H-bonded LbL films of different poly(2-alkyl-2-oxazoline)s have already been studied [275, 377, 378] and their applications as pH-responsive controlled release systems in the biomedical field has been shown [379]. Using TA as the H-donor in H-bonded LbL coatings has the advantage of being stable up to pH ~8.5 [6, 238, 275, 376]. In this chapter, for preparation of H-bonded LbL film, TA was used as H-donating and PEOX stabilized AgNPs were used as H-accepting component. The growth behavior and the pH stability of LbL films demonstrate that all of them grow linearly and were stable up to pH 8.5 as measured by ellipsometry and UV–visible

spectroscopy. Also UV–visible spectroscopy was used to calculate the AgNP concentration in multilayers formed on quartz substrates.

4.1 Experimental details

4.1.1 Preparation and characterization of PEOX(AgNP)/TA multilayers

TA multilayers with PEOX stabilized AgNP were deposited on silicon wafer and quartz. Before film deposition, substrates were kept in UV-Ozone Cleaner (Model 42-220 Jelight Company, Inc.) for 30 min to remove organic impurities from the surface. UV-irradiated substrates were immersed 30 min in 5.0 mg/mL BPEI solution to deposit a pioneer layer for LbL self-assembly initiation and enhance the adhesion of multilayer films to the substrate. Then the substrate was washed with DI water to remove excess BPEI. After rinsing, the substrate was dried by nitrogen gas. TA solution with a concentration of 0.2 mg/mL was prepared and the pH was measured as 4.5. Thus, the pH of PEOX stabilized AgNP dispersions were adjusted to pH 4.5 by addition of HNO_3. The following process was used for deposition of PEOX(AgNP)/TA bilayers on a substrate: first, the substrate was dipped into the PEOX(AgNP) solution then into TA solution for 15 min at each step. After each layer formation, coatings were rinsed by dipping it in pH 4.5 aqueous solutions and dried gently with nitrogen gas. This process was repeated to obtain 12 bilayers. All solutions were refreshed after each bilayer formation to prevent any possible contaminations. After each bilayer deposition, the thickness of the coatings was measured by ellipsometry. The measured data were collected and averaged from three different spots. UV–vis Spectrometer was used to study film growth and pH-induced disintegration of multilayers on quartz substrates. The pH stability of the multilayers was determined by measuring the thicknesses of the multilayers and by running UV–visible spectrum after immersing them in solutions at different pH (in the order of increasing pH) for 20 min. For pH stability study, aqueous solutions at pH range of 4 to 9 were prepared by using HNO_3 and NaOH. The initial and final

thickness of multilayers after sequential exposure to solutions in the order of increasing pH were plotted to measure the critical dissolution pH. FESEM and AFM were used to check the surface morphology of multilayers and distribution of AgNPs at the surface. Two different detectors were used in FESEM characterization: secondary electron and in-lens detectors. The elemental analysis was done by Energy Dispersive X-ray Spectroscopy (EDX; Bruker XFlash 5010) detector with 123 eV resolution. XPS was used to measure the amount of AgNPs loaded in the LbL films.

4.1.2 Determination of the amount of AgNP loaded in multilayers

To measure the loaded amount of AgNPs in the LbL films, 12 bilayers of PEOX500K(AgNP)/TA films on quartz substrates were prepared by dip coating technique. After each bilayer substrate was dried and UV-vis spectrophotometer was used to measure the absorption. The Beer-Lambert law (Eq. 2.4) was used to calculate the AgNP concentration in films.

Moreover, XPS was used to measure the amount of loaded AgNPs in the LbL films by etching from the top of the surface down to the silicon substrate. The X-ray source was monochromatized Al-K_α radiation while the charge compensation during the measurements was controlled by flood gun at a vacuum chamber pressure ~2.0×10^{-7} mbar. The beam size was ~400 μm.

4.2 Results and discussion

4.2.1 LbL Films of PEOX and TA

12 bilayer (BL) films of PEOX/TA were prepared by using four different molar mass of PEOX. Growth profile of all different molar masses shows that all multilayers grew linearly as shown in Figure 4.1a. Growth profile showed molar mass dependence. A BL thickness of PEOX5K was measured by linear fits to be 3.5 nm. Thickness was increased with increasing

molar mass to 5.0 nm for PEOX500K. As expected, the growth profile of films with different molar masses shows that by increasing molar mass, the PEOX chains are deposited on the surface by larger loops and tails. Another possibility is that the polymer chains deposited on the surface rather flat during assembly and then relaxed to equilibrium conformations reflecting the molar mass dependent sizes [376].

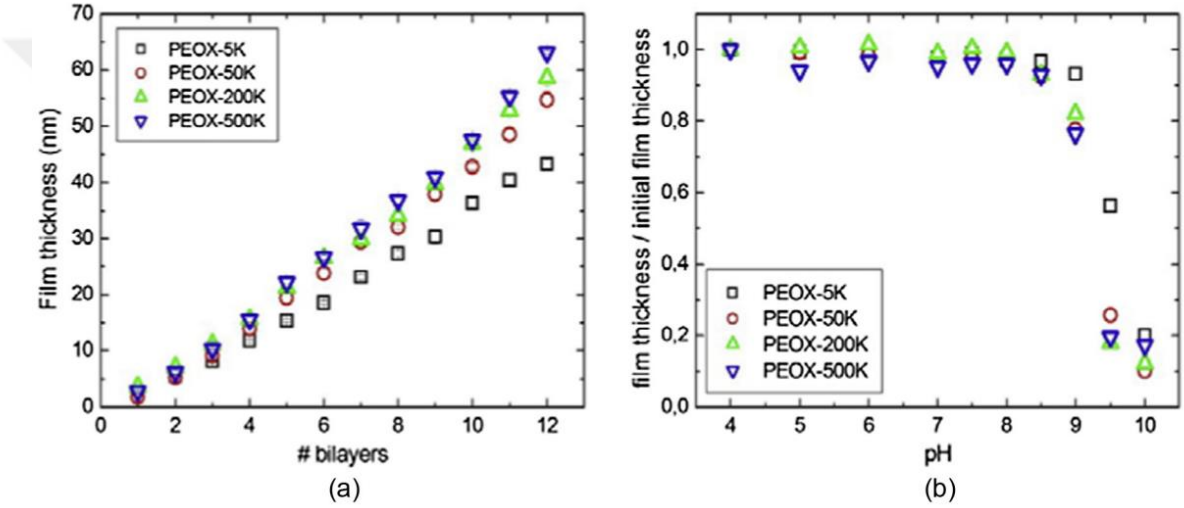

Figure 4.1: a) The growth profiles of PEOX/TA LbL films with different PEOX molar mass, b) pH-induced disintegration profiles of the multilayers in (a) [359].

The pH stability experiments show that all multilayers were stable up to pH 8.5 as demonstrated in Figure 4.1b. The disintegration of LbL films was observed at pH 9 because of deprotonation of TA and breakage of H-bonds between TA and PEOX. Previously, similar results were reported for the critical pH values of PVP/TA and poly(2-isopropyl-2-oxazoline)/TA [238, 275].

4.2.2 LbL Films of PEOX(AgNP) and TA: Growth, Characterization and Disintegration

The H-bonded multilayers of PEOX(AgNPs)/TA were also assembled at pH 4.5 similar to PEOX/TA film. As shown in Figure 4.7a, by adjusting pH, the color of solutions changed and a broad shoulder at larger wavelengths observed in UV–visible spectrum showing an increase in the size of AgNPs due to agglomeration. The AgNP sizes were measured by DLS as ~19 nm, ~18 nm, ~18 nm and ~15 for PEOX5K, PEOX50K, PEOX200K, and PEOX500K, respectively. These sizes are consistent with the color changes observed. The agglomerate size also increased to ~114 nm for PEOX5K and ~120 nm for PEOX50K, PEOX200K, and PEOX500K. The most significant size changes were observed for PEOX5K and PEOX50K confirming that lower molar mass PEOX cannot stabilize the AgNP dispersions kinetically as good as higher molar mass PEOX. The growth profiles of 12 BL PEOX(AgNP)/TA LbL films prepared by using AgNPs (Figure 3.12a) are shown in Figure 4.2a. Similar to PEOX/TA multilayers, PEOX(AgNP)/TA films also grew linearly but with larger BL thickness of 4.6–6.8 nm as measured by linear fits to the data. These larger BL thicknesses of PEOX(AgNP)/TA films show the presence of NPs in the adsorbed layers.

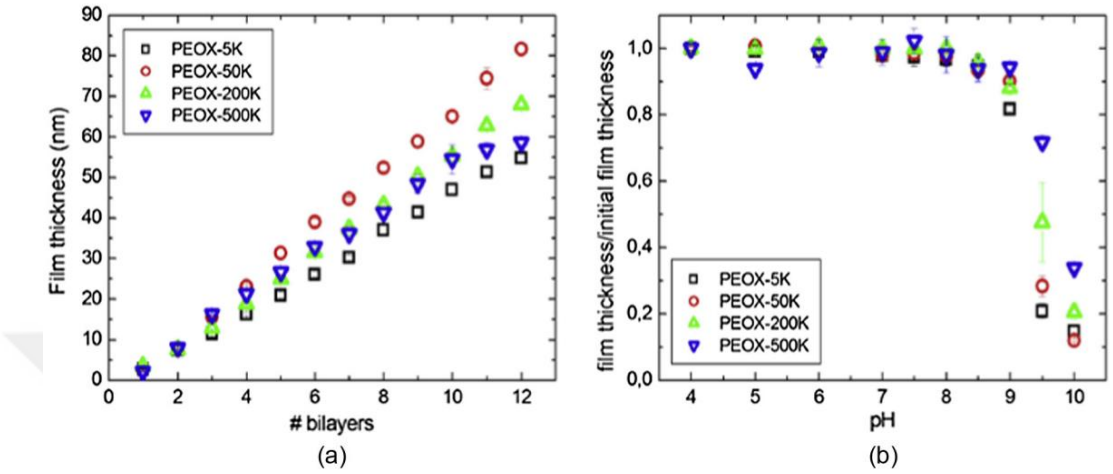

Figure 4.2: a) The growth profiles of PEOX(AgNP)/TA LbL films with different PEOX molar mass, b) pH-induced disintegration profiles of the multilayers in (a) [359].

The BL thickness of PEOX5K(AgNP)/TA film was measured as 4.6 nm and the BL thickness of PEOX-50K(AgNP)/TA films was measured as 6.8 nm. The larger thickness measured for the film with larger PEOX molar mass shows that the adsorption of AgNP agglomerates during film deposition affected the BL thickness. PEOX5K(AgNP) and PEOX50K(AgNP) had a similar individual particle size of 18–19 nm, but the agglomerate size was larger for PEOX50K(AgNP). Agglomerates (114–124 nm in size) are expected to consist of individual AgNPs (15–19 nm in size) in a mesh of bridging PEOX chains (Figure 3.5b). The bridging polymer chain is expected to relax during adsorption on to the substrate and form flatter conformations (Figure 3.5c). The individual AgNP size was measured as 16–19 nm, however BL thicknesses of films was measured as 4.6–6.8 nm. This shows that only a certain fraction of each layer is covered by AgNPs which was also confirmed by microscopies. PEOX(AgNP)/TA multilayers were also stable up to pH 8.5 and disintegration started at pH 9, as shown in Figure 4.2b. Previously, the incorporation of Ag^{+} ions into H-bonded multilayers of poly(vinyl pyrolidone)/poly(acrylic acid) films was reported to

improve pH-stability [380]. No significant increase was observed in critical pH value of PEOX(AgNP)/TA multilayers compared to PEOX/TA multilayers.

The surface morphology of 12 BL PEOX(AgNP)/TA LbL films were characterized by SEM shown in Figure 4.3. The lighter spots in the images are AgNPs which was confirmed by EDX analysis. In Figure 4.3a, an aggregate was chosen on the surface for EDX analysis. The detected EDX signal from the marked regions is also shown in Figure 4.3. Two major peaks were observed, one at 1.75 keV corresponding to Si coming from the substrate and one at 3.00 keV corresponding to Ag. The intensity of the Ag peak from individual AgNPs in Figures of 4.3b-d was rather low compared to AgNP aggregate peak in Figure 4.3a, but still, peak position is at 3.00 keV and the intensity is above the background noise level. This clearly confirms the lighter color regions are AgNPs.

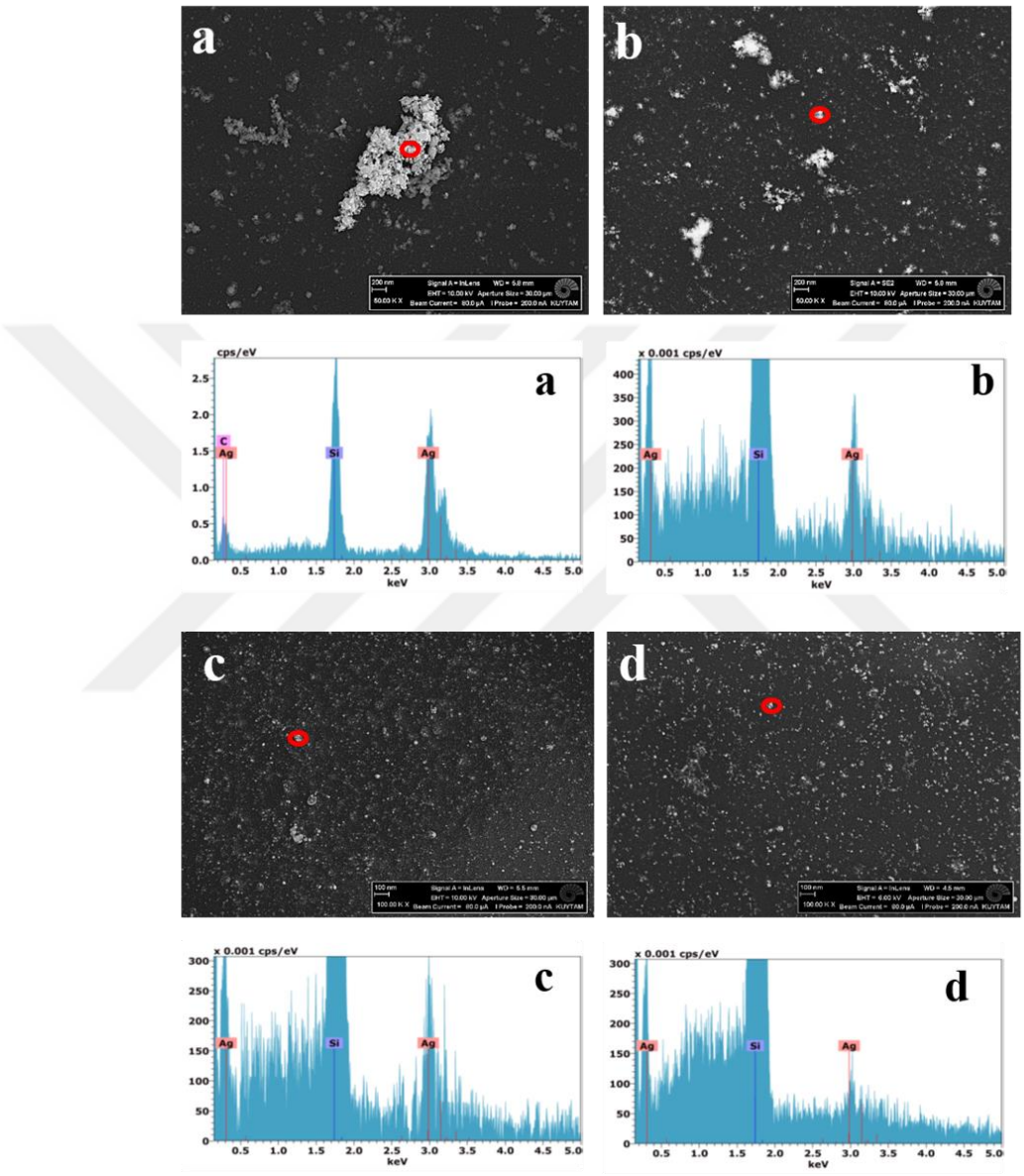

Figure 4.3: SEM pictures of 12 BL PEOX(Ag-NP)/TA LbL films and EDX results. (a) PEOX-5K(Ag-NP)/TA: Ag-NP aggregate chosen for detection of enhanced Ag signal in EDX, (b) PEOX-5K(Ag-NP)/TA, (c) PEOX-200K(Ag-NP)/TA, (d) PEOX-500K(Ag-NP)/TA. Below images are related EDX results [359].

The distribution of AgNPs was more uniform for PEOX200K and PEOX500K compared to PEOX5K films. PEOX5K films had larger particles and agglomerates on the surface which is consistent with the observed stability of AgNP dispersions. The individual NP size measured by SEM as ~15 nm for both PEOX200K and PEOX500K stabilized AgNPs, which is in agreement with DLS size measurement of individual NPs.

4.2.2.1 Determination of the amount of AgNPs loaded in multilayers

To determine the amount of AgNPs loaded in the films by UV-Vis Spectroscopy, we have prepared PEOX500K(AgNP)/TA LbL films on quartz substrates by dip-coating. Figure 4.4a shows the UV–visible spectra of the deposited films after each bilayer up to 12 bilayers. A clear AgNP peak was observed at 419 nm and a TA peak at 277 nm. The red-shift of the AgNP absorbance peak from 397 nm in dispersions to 419 nm in LbL multilayers is due to the absence of H_2O molecules in multilayers. In dispersions, peak absorbance at 419 nm corresponds to a AgNP size of 48 nm [357, 358]. In LbL films, individual AgNP sizes were measured as ~15 nm (Figure 4.3d). Therefore, we do not attribute the red shift in absorbance to an increase in the AgNP size during LbL film formation. As shown in Figure 4.4b, the absorbance at 419 nm increased linearly with the number of bilayers. Considering the linear growth profiles (Figures 4.2a and 4.4b), this illustrates that the same amount of AgNPs was incorporated into the film after each bilayer. Assuming that Beer's law is valid, an enhancement of AgNP concentration in the film by a factor of ~10^4 compared to that in the dispersion is estimated. Using the molar absorptivity values for spherical citrate-capped AgNPs [358] at 398 nm (14–16 nm diameter particles), the number density of AgNPs was found to be 9.0×10^{14} L^{-1} in the dispersion and 9.6×10^{18} L^{-1} in LbL films.

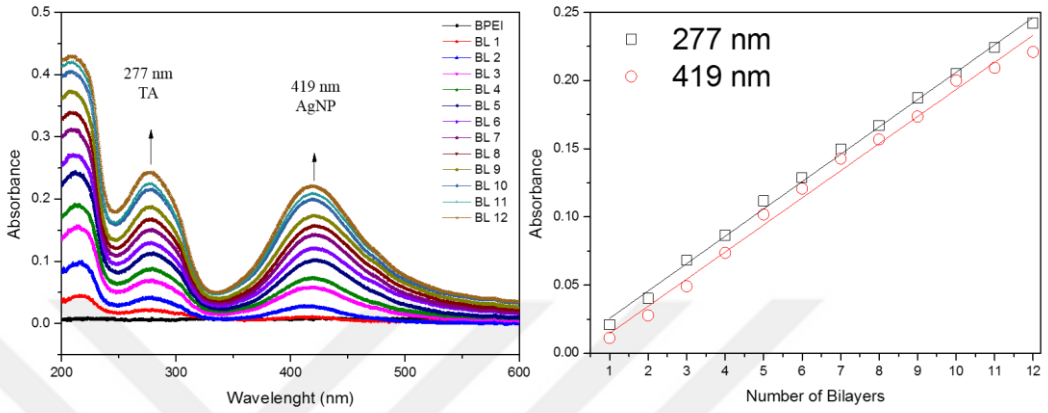

Figure 4.4: (a) The change of UV–visible spectra by bilayer deposition of PEOX-500K(Ag-NP)/TA LbL films prepared by dip-coating on quartz substrates, (b) the change of absorbance at 419 nm with the number of bilayers[359].

The loading capacity of AgNPs in the multilayers was determined by XPS. XPS investigations were done as a function of depth for C, N, O, and Ag by etching down from the top surface. The XPS shows the depth profile of silver in 12 BL of PEOX-AgNP /TA films with different PEOX molecular weights in Figure 4.5. Small PEOX molecular weights (5K and 50K) appear to be more Ag-doped (~ 7-9 atom percentage) into multilayers. For 200K and 500K PEOX coated AgNPs the peak value of atomic % Ag is found in ~ 3-4 atomic% in 12 BL films. The reason that the ability of smaller molecular weight polymer chains to involve more AgNP in the assembly process is the lower possibility of small polymer chains to bridge these NPs and assemble them together. While PEOX coated single Ag-NPs are able to adhere better to the surfaces coated with TA, these NPs in a large PEOX chain cannot adhere strongly to the TA coated surface.

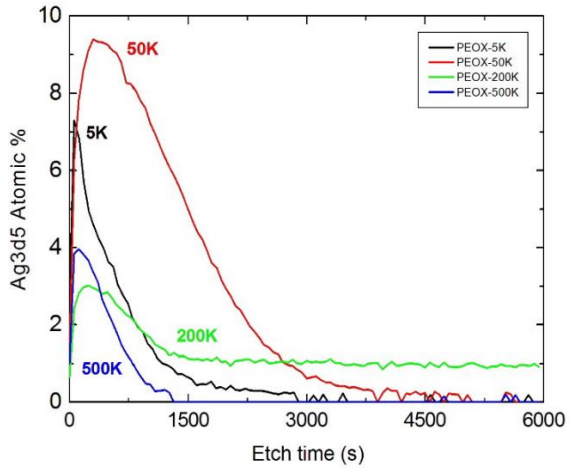

Figure 4.5: XPS depth profile of silver in PEOX-AgNP/ TA films with different PEOX molecular weights. (Films were stripped at a speed of 0.07 nm / s, calibrated with the Ta_2O_5 standard.)

4.2.2.2 pH-induced film disintegration

pH-induced disintegration of PEOX-500K(AgNP)/TA LbL films was also followed by UV–visible spectroscopy. Figure 4.6.a shows the UV–visible spectra of 12 BL PEOX-500K(AgNP)/TA film after 20 min exposure to aqueous solutions at different pH sequentially from pH 6 to pH 10 in the order of increasing pH. The change of absorbance at 277 nm (TA peak) and 419 nm (AgNP peak) was plotted in Figure 4.6b as a function of pH. In agreement with the ellipsometric results (Figure 4.2b), the absorbance values stayed rather constant below pH 9 indicating that the film was stable. UV–visible spectroscopic measurements clearly showed that the release of TA at the critical disintegration pH was much faster than the release of PEOX500Kstabilized AgNPs.

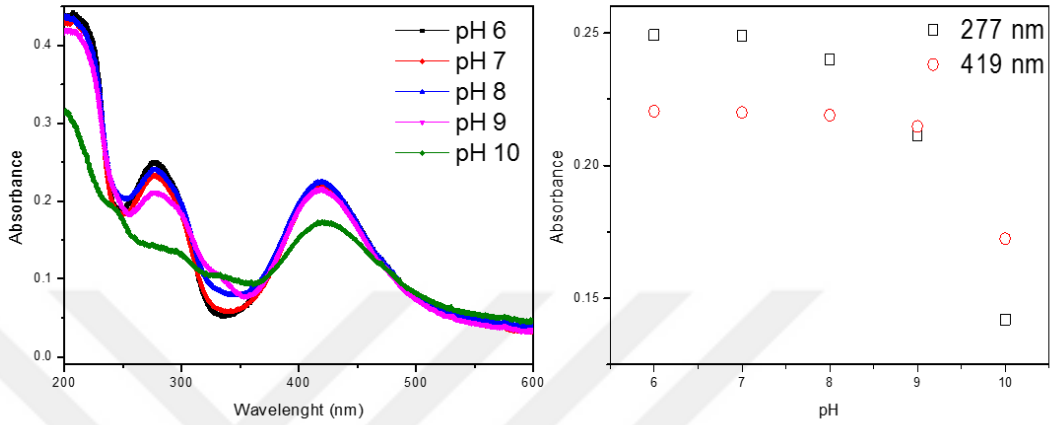

Figure 4.6: (a) UV–visible spectra of 12 BL PEOX-500K(Ag-NP)/TA LbL films on quartz substrates after 20 min exposure to aqueous solutions at different pH sequentially from pH 6 to pH 10 in the order of increasing pH, (b) the change of absorbance at 277 nm (TA peak) and 419 nm (Ag-NP peak) with pH [359].

The surface morphology of the 12 BL PEOX-500K(AgNP)/TA after each pH exposure was also investigated by AFM and SEM. Figure 4.7 shows the 2 µm × 2 µm area AFM height and phase pictures of the as-prepared film (Figure 4.7a and d), after pH 8 exposure (Figure 4.7b and e) and after pH 10 exposure (Figure 4.7c and f). The surface of as-prepared films had peak-to-peak roughness of ~20 nm. Any sign of ~120 nm size agglomerates was not observed in AFM images. This might be due to the relaxation of the bridging polymer chains forming the agglomerate upon adsorption and resulting in flatter conformations for the agglomerates in the LbL films (Figure 4.7c). After pH 8 exposure, the surface morphology of the film was similar to that of the as-prepared film and had the same peak-to-peak roughness of ~20 nm which indicates that the films were stable at pH 8. The bright regions in the phase pictures correspond to the AgNPs. After pH 8 exposure, AgNPs were more

apparent in the phase picture (Figure 4.7e). This might be due to the release of some loosely bound PEOX chains from the surface. After pH 10 exposure, large area patches of the film were seen to be removed from the substrate (the center part of Figure 4.6c and f). Some AgNPs with much less surface density were still present at the upper and lower part of Figure 4.6c and f. This is consistent with the observation of faster release of TA from LbL films above pH 9 compared to AgNPs (Figure 4.6).

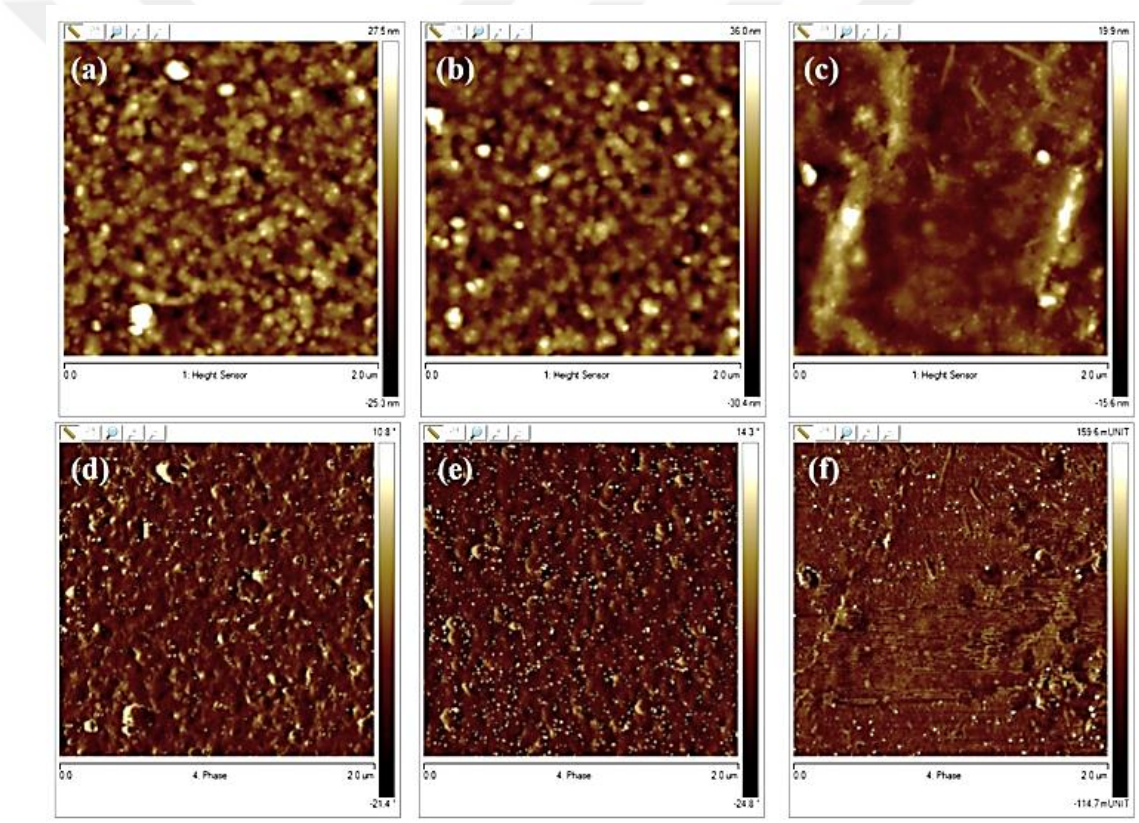

Figure 4.7: AFM images of 12 BL PEOX-500K(Ag-NP)/TA film: (a) height image of as-prepared film, (b) height image after exposure to pH 8, (c) height image after exposure to pH 10, (d) phase image of (a), (e) phase image of (b), phase image of (c) [359].

4.3 Conclusions

In this chapter, we reported on the incorporation of stabilized AgNP in H-bonded multilayers of PEOX and TA by LbL technique. After successfully synthesizing PEOX stabilized AgNP, PEOX(AgNP) were used as H-accepting component and TA as H-donating component in the formation of LbL films. The growth profiles and the pH-induced disintegration of the multilayers were similar to those of PEOX/TA multilayers. All multilayers showed linear growth profiles and were stable up to pH 8.5 as determined by ellipsometry and UV–visible spectroscopy. The pH-induced disintegration of PEOX(AgNP)/TA LbL films was monitored by UV–visible spectroscopy, and showed the faster release of TA at the critical disintegration pH compared to PEOX stabilized AgNPs. The SEM images of the surface of 12 BL PEOX(AgNP)/TA LbL films showed the homogeneous distribution of AgNPs in the films. The lower limit of PEOX-500K stabilized AgNP concentration in multilayers prepared on quartz substrates was measured by UV–visible spectroscopy to be 9.6×10^{18} L^{-1} in 12 bilayer films. The loading capacity of AgNPs in the multilayers was determined by XPS to be 7-9 atomic% for small PEOX molecular weights (5K and 50K), and 3-4 atomic % for 200K and 500K PEOX coated AgNPs in 12 BL films. The understanding of the effect of different molar mass PEOX in stabilizing AgNPs in dispersions and in forming uniform AgNP loaded pH-responsive LbL films are important in controlling the size and loading capacity of AgNPs in multilayers. As shown above, XPS data indicate that films contain silver at 3-9 atomic%. These amounts are more than sufficient to form Ag^+ formation and measurable inhibition sites in aqueous solutions in suitable environments (such as acidic solution).

Chapter 5: Antibacterial Properties and Cytotoxicity of Silver Nanoparticle Loaded Multilayers

Overview

The main reason of infection-related problems after medical implant surgeries is the attachment of bacteria within the body or externally during the surgery on the implant surfaces which grow and lead to biofilm formation and ultimately results in implant rejection [277]. Implant infection is difficult to treat and may eventually cause the removal of the implant. Thus, it is crucial to develop surface coatings that prevent or reduce the adhesion and colonization of bacteria. In spite of the large use of antibacterial coatings, there are many challenges, which need to be evaluated. The ability to control biomolecule accumulation, concentration, bioactivity, coating uniformity and thickness, and the release rate is the significant investigations which need to be considered [381].

For an effective antibacterial coating design, the coating material should inhibit the initial adhesion of bacteria, and consequently the formation of a biofilm. Because of the large variety of fabrication components, substrates and assembly methods, the LbL assembly technology provide a wide amount of choices to assemble antibacterial coatings. LbL technique is a versatile method which is able to incorporate all the bactericidal components (heavy metals [247], antibiotics [248], cationic molecules [249]) into multilayer systems. There are three main strategies for designing antibacterial coatings: release-based coatings, contact-killing, and anti-adhesion/bacteria-repelling coatings.

Release-based antibacterial coatings exert their antibacterial activity by releasing loaded active antibacterial agents from the surface. For instance, the active antibacterial agent in AgNP based coatings is silver ion released from surface [382]. In most of the current silver-

based antibacterial coatings, AgNPs are either deposited directly on the surface of device or present inside the polymeric surface coatings. Antibacterial coatings based on release has its own advantages in certain circumstances but in other settings it has some disadvantages. For these applications slower release of active antibacterial agents has been even considered as a disadvantage due to the possibility of developing resistant bacteria. Also, when the released antibacterial agent is decreased below the minimum inhibitory concentration (MIC), a chemical-releasing coating will lose its antibacterial efficiency dramatically [383].

Contact-killing coatings have been developed to prevent the reservoir exhaustion issue of release-based antibacterial coatings [384]. In this approach, antimicrobial compounds are covalently anchored to the material surface by flexible, hydrophobic polymeric chains. Contact killing based antibacterial coatings utilize the interactions of microbial cells with the surface and subsequent inhibition. Adhered bacteria are believed to be killed because of the disruption of their cell membrane by the attached compounds, reaching across the microbial envelope due to the long tethering chains [385]. Because the main mechanisms of action are based on membrane interactions, such as physical lysing or charge disruption, the most effective compounds for contact-killing coatings have been either cationic compounds (quaternary ammonium chitosan (QACs), chitosan, antimicrobial peptides (AMPs), etc.) or enzymes [386].

Anti-adhesion coatings prevent biofilm formation at the earliest stage by using non-cytotoxic mechanisms. At biomaterial surfaces, bacterial adhesion is generally defined by using a two-step model: a rapid, initial and reversible step (stage 1) which is mediated by non-specific physicochemical interactions, followed by a secondary step (stage 2) involving, among others, species-specific bacterial adhesion proteins [387]. Surface immobilization of molecules that can prevent protein adsorption, such as zwitterion and PEG and, have shown great anti-adhesion properties in vitro and, despite stability issues, are generally regarded as the standard approach for anti-adhesion coatings. However, the use of physical surface

modifications (especially surface topography) as non-specific methods to modulate bacterial adhesion is most likely more complex than previously thought [388–390].

In general, most of the biocidal components used in non-release based LbL systems are similar to those used in a release based LbL films. The main difference is the stability of the biocidal components immobilized in the LbL assemblies. Different design for contact-killing based antibacterial coatings has been studied. For instance, having positively charged surface by immobilizing the cationic molecules [256, 257, 391], antibacterial peptides [254, 260], antibiotics [259, 261, 262].

Different type of nanomaterials can be modified and incorporated as antibacterial agents in polymer coating matrices which prevent the growth of harmful microorganisms, and as a result, minimize the risk of infection. As we discussed in the previous chapter, among metal nanoparticles, AgNPs are one of the most promising and potentially effective candidate nanomaterials for antibacterial coatings. AgNPs have captured wide attention due to their sustained Ag^+ ion release, low-toxicity of the active Ag^+ to a human cell, and great antimicrobial activities against a broad spectrum of bacterial and fungal species [284–286]. On the other hand, aggregation of colloidal AgNPs in biological mediums caused the uncontrollable release of Ag^+ ions, an increase in adhesion of bacteria and reduction of the antibacterial effect of AgNPs [324–329]. Also, ecotoxicology studies have shown that silver is highly toxic for some aquatic organisms, accumulate in phytoplanktons and also toxic to zebrafish embryos [330–339]. Therefore, the nanoparticles should be embedded in a polymer matrix where the release of silver ions should be controlled. Different nanocomposites containing AgNPs alone or in combination with other nanomaterials have been prepared with natural and biodegradable polymeric matrices [340–345].

In Chapter 3, PEOX was used to stabilize AgNP in order to diminish unwanted aggregation. In Chapter 4, PEOX stabilized AgNPs, were used as an H-accepting and TA as H-donating component in the preparation of LbL films. Both TA and AgNPs exhibit

antibacterial activities. The antibacterial properties of AgNP is already discussed in Chapter 1 in detail. In general, the antibacterial effect of AgNPs is attributed to the release of silver ions, which may rupture the cell wall, cause protein denaturation, block cell respiration, and finally cause bacteria death [392, 393]. A few researchers have hypothesized that the contact killing mechanism also contributes to their enhanced antimicrobial effect, although killing is mainly governed by the silver release mechanism [301, 394, 395]. In contrast, the antimicrobial nature of a few silver-containing nanomaterials is believed to be only through the contact killing mechanism, which contributes an even greater potential lethality when bacteria come in contact with them [396, 397]. On the other hand, TA is an effective reducing and stabilizing agent [398] and it is reported that TA show effective antimicrobial activity against bacteria, viruses, fungi and yeasts [399].

In this chapter, antibacterial properties of multilayers have been discussed. Two different release based antibacterial assays (agar diffusion and soft agar assay) have been used to test the antibacterial activity of the coatings. In addition, to show that the films have effective contact-killing properties, JIS Z 2801 tests were carried out against gram-negative *E.Coli* and gram-positive *S.epidermidis*. Results indicate that the coatings are effective in contact killing mechanism. To confirm our results, electrochemical methods have been used to measure the release amount of silver ions from the surface. As we expected, no measurable Ag^+ ion release was observed from multilayers at pH 7.4. Furthermore, cytotoxicity of coatings was studied with *U2OS* cells which have an extremely high proliferation rate and are very robust in experimental procedures making them attractive for research that needs cells for in vitro experiments.

In the last part of this chapter, the stability of coatings prepared on titanium substrates in phosphate buffered saline solution at pH7.4, which was used as simulated body fluid, was studied. This study was done for a period of up to 4 months to determine their stability and

antibacterial activity. All coatings were shown to remain stable for 3 months on titanium surfaces and retain their antibacterial activity

5.1. Experimental

5.1.1 Antibacterial efficacy measurement of coatings based on the release

Several methods have been used to study the in vitro antimicrobial activity of coatings and it is important to develop a better understanding of the current methods. In this chapter, different methods were used for evaluating the in vitro antimicrobial activity of H-bonded multilayers containing AgNPs.

5.1.1.1 Agar disk-diffusion method

Agar disk-diffusion is the method used in many clinical microbiology laboratories for routine antimicrobial susceptibility testing. In this test, the antibacterial agent released from the coating into the agar medium containing standardized inoculum of microorganism and forms a region where no visible colonies are formed. The concentration of the antibacterial agent is the highest on the coated surface and decreases as it moves away from the surface. After a certain point, the concentration is too low to no longer prevent the growth of bacteria. Therefore, a clean area is formed around the coating against the intense growth of the surrounding bacteria and is defined as the inhibition zone. The diameter of the inhibition zone is used to identify antibacterial activity.

In this study, agar diffusion test was applied to determine the release and antibacterial activity of silver ions from the PEOX(AgNP)/TA multilayers by analyzing the zone of inhibitions. Lysogeny broth (LB) was prepared and sterilized under autoclave conditions. Then agar solution was spread evenly on sterile plastic petri dishes with a diameter of 90mm. Overnight suspension of *E. coli* in LB medium was swabbed uniformly across a culture plate containing LB medium. Then agar plates were allowed to cool down and solidify for 5-10 min after inoculation. 1 cm × 1 cm silicon wafer coated with PEOX(AgNP) / TA films were

cut and sterilized under UV-lamp for 30 min. Samples were placed onto the prepared growth plates with the 1% Penicillin-Streptomycin loaded filter paper piece as a control sample and incubated overnight at 37°C. The antibacterial activity of the coatings was determined by the width of an inhibition zone around the samples where larger width value displays better antibacterial property.

5.1.1.2 Soft agar assay

The primary method of monitoring surface-independent growth is the detection of soft agar colony formation or zone formation which measures proliferation by manual counting of colonies and zone measurements in semisolid culture media.

In this test, 1 colony of *E. coli* from streak plate culture is suspended in 3 ml LB medium and incubated overnight at 37°C. 300 ml of LB-agar was prepared and autoclaved for sterilization (75 min) and LB-agar medium was placed on magnetic stirrer to cool it homogeneously by mixing until the temperature reaches around 45°C. 300 µl *E. coli* overnight suspension was added on warm LB-agar medium and mixed with a magnetic stirrer to disperse bacteria homogeneously. H-bonded multilayers on silicon surfaces were sterilized under UV-lamp for 30 min and were placed onto the base LB-agar medium. Then, warm top agar was poured onto samples on agar plates. All plates were incubated overnight at 37°C. Similar to the agar diffusion test, the antibacterial activity of the coatings were determined by the width of inhibition zones around the samples.

5.1.2 Antibacterial efficacy measurement of coatings based on contact-killing

The antimicrobial properties of multilayers were evaluated by using Japanese Industrial Standard method, JIS Z 2801 against gram-negative *E.Coli* and gram-positive *S.epidermidis* bacteria. In this method, 1 colony of *E. coli or S. epidermidis* from streak plate culture is suspended in 3 ml LB medium and incubated o/n at 37°C overnight. Samples were pre-sterilized under UV-lamp for 30 min and placed onto the LB-agar medium. overnight

suspension of *E. coli (or S. epidermidis)* is diluted to 1 to 1000 by LB liquid medium and 30 µl portions of diluted *E. coli (or S. epidermidis)* suspension were placed on samples (around 1 x 1 cm). 500 µl LB solution was dropped around the substrates on agar to keep the medium humid and samples were placed into the oven at 37°C for 3 hours incubation. All samples with their *E. coli (or S. epidermidis)* solutions were dropped into the 10 ml LB mediums in pre-sterilized test tubes and solutions were mixed vigorously with vortex for 10 sec. 100 µl of these solutions were swapped on LB-agar mediums and kept undisturbed for 10 min. All plates were placed upside down into the oven at 37°C and were incubated overnight at 37°C. Surviving microorganisms are counted to evaluate the antimicrobial activity of the test material and the log of the difference between the 2 counts is determined to give a measurement of antimicrobial activity.

To confirm our results, electrochemical measurements were carried out to measure the amount of silver ion release from surfaces [Demirel 2017].

5.1.3 Biocompatibility experiment, MTT Assay

Biocompatibility of coated surfaces was investigated by assessing the metabolic activity of U2OS cells grown on the films, with 3-(4,5-dimethylthiazol-2-yl)-2,5-diphenyltetrazolium bromide (MTT). MTT assay is a calorimetric assay that is used to measure cell viability by assessing the cellular metabolic activity. Yellow colored tetrazolium salt MTT is converted into purple formazan salts by cellular oxidoreductases. Formazan concentration can be determined by optical density at 600 nm (OD) and reflects the relative number of viable cells in the population.

U2OS cells were cultured in Dulbecco's Modified Eagle's Medium (DMEM, Gibco 21969-035) supplied with 10% heat-inactivated fetal bovine serum (FBS, Gibco 10500), 1% L-Glutamine (Gibco, 25030-081), and 1% Penicillin-Streptomycin (Gibco 15240-062). Cultures were maintained at 37°C in a 5% CO_2, 85% humidified incubator.

Films were cut into square pieces with a size of 0.50 x 0.50 cm and then sterilized by 30 min UV-lamp exposure. Sterilized films were placed in a sterile 24-well plate. U20S cells were detached from the culture plate by trypsinization and seeded onto substrates (0.4x105 cells per well) in DMEM containing 10% FBS (500 µL). To observe cytotoxic effects of the substrates, samples were incubated at 37 °C in a 5% CO2 incubator for 48 hours. Then growth medium was replaced with DMEM containing 1 mg/mL MTT and further incubated for 4 hours at 37 °C to allow formazan formation. Then, MTT solution was removed and substrates were transferred to a clean 24-well plate. Formazan salt on the samples was dissolved in EtOH:DMSO (250 µL) and transferred to a microplate. The optical density (OD) was measured at 600 nm with a microplate reader (Synergy H1, BioTek). The relative cell viability was calculated as viability = ($OD_{sample}/_{control}$) × 100. The OD_{sample} was obtained from coated films and $_{control}$ was obtained from silicon control.

5.1.4 Determination of the durability of coatings

In addition to the short-term pH stability of multilayers, the long-term stability of the LbL self-assembled coatings on titanium substrates in PBS pH7.4 was also studied. The composition of the test solution is shown in Table 5.1.

Table 5.1: Preparation of the durability test solution at pH7.4.

Salt	Concentration (mmol/L)	Concentration (g/L)
NaCl	137	8.0
KCl	2.7	0.2
Na_2HPO_4	10	1.42
KH_2PO_4	1.8	0.24

PBS solution was prepared by dissolving the chemicals shown in table 5.1 in DI water at the stated concentrations. Chemicals were added one by one and after each chemical was completely dissolved, the pH of the final solution was measured as 7.4. Titanium substrates were cut into rectangular pieces (1 × 2 cm). Then, they were cleaned with ethanol and kept in UV-Ozone Cleaner for 30 min. Then the substrates immersed in 5.0 mg/mL BPEI solution for 30 min to increase the adhesion of multilayers to the surface of the substrate. After that, PEOX500K(Ag-NP)/TA film were formed on titanium substrates and soaked in 30 mL of PBS at pH 7.4 for 4 months. PEOX500K/TA film on titanium substrates were also prepared and studied as a control sample. Each month one sample was taken out, rinsed in DI water and then dried by nitrogen gas before FESEM characterization and antibacterial analysis. Japanese Industrial Standard (JIS Z 2801) test was done to study the contact killing property of coated substrates.

5.2 Results & discussion

5.2.1 Investigation of release-based antimicrobial activity of coated surfaces

5.2.1.1 Agar disk-diffusion method

The antimicrobial activity of the PEOX-AgNP/TA films was performed against *E.coli.* The antibacterial activity was indicated by a clear zone of inhibition around the samples on the agar plate. As shown in Figure 5.1, the zone of inhibition was not observed for both PEOX-AgNP/TA and PEOX/TA multilayer films independent of the molecular weight of PEOX used to stabilize AgNPs.

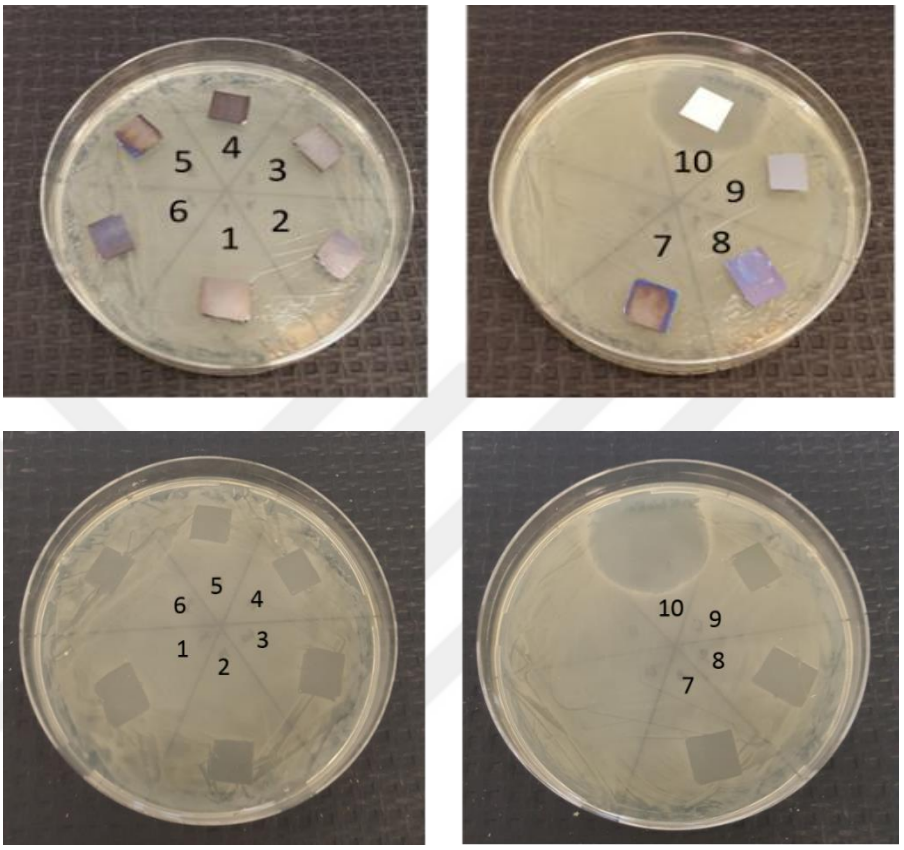

Figure 5. 1: Agar diffusion test using 12BL multilayer coatings. *E.coli* culture was spread on the agar plate and grown for 24h. 1: PEOX5K-AgNP/TA, 2: PEOX5K/TA, 3: PEOX50K-AgNP/TA, 4: PEOX50K/TA, 5: PEOX200K-AgNP /TA, 6: PEOX200K/TA, 7: PEOX500K-AgNP/TA, 8: PEOX500K /TA, 9: Silicon wafer (negative control), 10: Ampicillin impregnated filter paper (1µg/µl, positive control).

In Figure 5.1, an inhibition zone was observed only for antibiotic filter paper, which is used only as a positive control. None of the AgNP doped coatings, which were subjected to the agar diffusion test, formed the inhibition zone. Possible reasons for this are the low concentration of AgNP in the coatings, the inability of AgNPs to form silver ions or the

prevention of the release of silver ions into the environment. As indicated above (section 4.3.2.1), XPS data indicate that films contain silver at 3-9 atomic%. These amounts are more than sufficient to form Ag^+ formation and measurable inhibition zone in suitable environments. The fact that the inhibition zone is not observed is due to TA's being silver ion-binding and silver ions acting as a reducing agent. This is consistent with the above-mentioned Ag^+ ion release results. The ions formed on the nanoparticle surfaces do not spread out from the surface due to the reducing effect of TA and prevent the formation of an inhibition zone in agar diffusion tests.

5.2.1.2 Soft agar assay

Another method that has been used for measurement of the release-based antibacterial activity of coatings is soft agar assay. In this method, the films were embedded in between base agar and soft agar. Soft agar assay allowed us to produce a more homogeneous lawn of bacteria within a thin layer of agar across the surface of a plate compared the agar diffusion test, which is used in vitro indication of cell viability. As shown in Figure 5.2, the coatings did not result in any inhibition zone despite the diffusion of silver ions into the agar medium was favored.

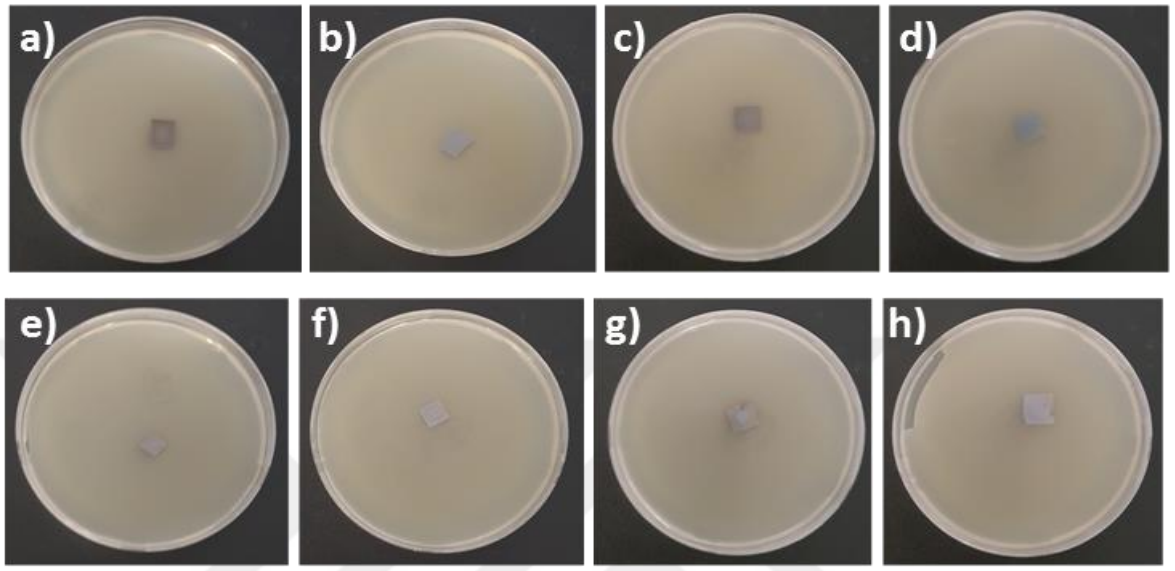

Figure 5.2: Soft Agar assay. 12BL multilayer coatings were embedded into agars with E.coli. a) PEOX5K-AgNP/TA, b) PEOX5K/TA, c) PEOX50K-AgNP/TA, d) PEOX50K/TA, e) PEOX200K-AgNP/TA, f) PEOX200K/TA, g) PEOX500K-AgNP/TA, h) PEOX500K/TA.

Although the diffusion of the silver ions from the coating surfaces to the agar medium was facilitated, no zone of inhibition was observed for any of the coatings. It was concluded that the silver ions could not be released from the prepared coatings because the inhibition zone could not be created in both of the diffusion tests. This result is consistent with the Ag^+ release assays performed by electrochemical methods in the presence of TA in aqueous solutions and confirms that TA influences Ag^+ diffusion.

An ideal antimicrobial coating should prevent the microorganisms from dividing and multiplying by either the release of an antimicrobial agent or by the direct contact killing mechanism. Upon determining that the coatings did not kill the bacteria by diffusion, the bacterial killing mechanism in contact was tested using a different method.

5.2.2 Study of the contact-killing property of coatings

"Japanese Industrial Standard (JIS Z 2801)" assay was used to evaluate contact inhibition effect of the coated material surface against both gram-positive and gram-negative bacteria. In this test, the quantitative value of the antibacterial activity expressed by the difference in the logarithmic value of live cell counts between the antimicrobial coatings and control samples after inoculation and incubation of the bacteria. The bare silicon substrate was used as a control to assess the effect of 12BL multilayer coatings. As shown in Figure 5.3, PEOX5K-AgNP/TA coated surfaces showed significantly higher antimicrobial activity against both gram positive and gram negative bacteria when compared with PEOX5K/TA coated surfaces (Table 5.1).

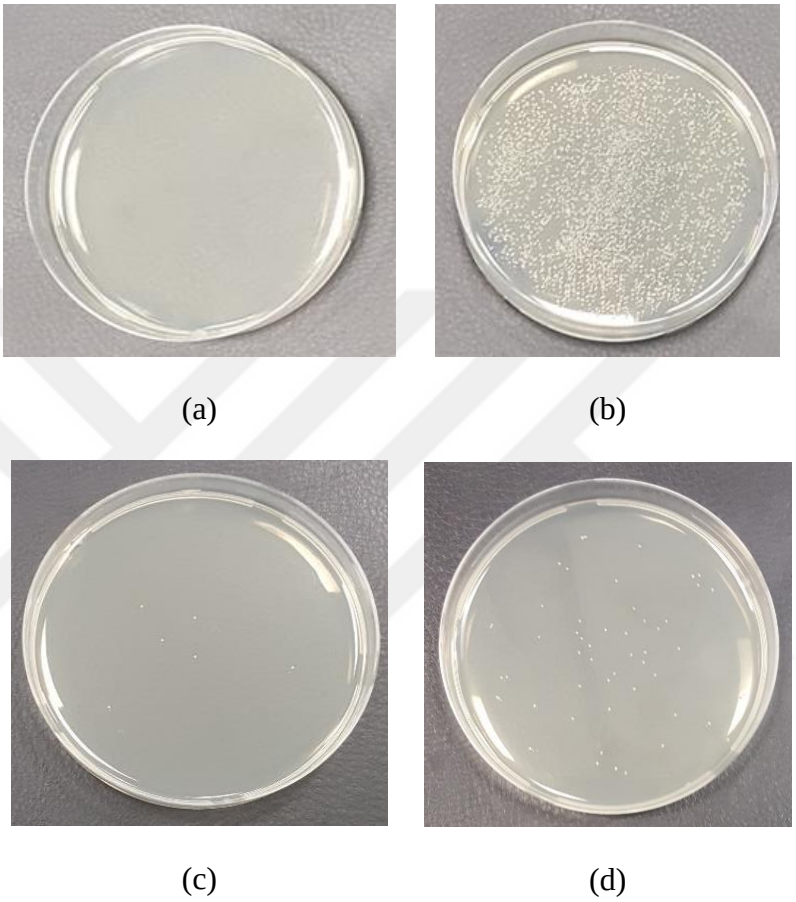

Figure 5.3: JIS Z 2801 assay to test contact inhibition of coated surfaces against gram negative (*E.coli*) and gram positive (*S.epidermidis*) bacteria. *E.coli* grown on PEOX5K-AgNP/TA (a) and PEOX5K/TA film coated surfaces (b). S.epidermidis grown on PEOX5K-AgNP/TA (c) and PEOX5K/TA film coated surfaces (d).

For an ideal antimicrobial coating design, material should demonstrate ability for inactivation of microbes either through the release of an antimicrobial agent or through a direct contact killing mechanism. AgNPs containing PEOX/TA H-bonded self-assembled

coatings on silicon substrates demonstrated significant contact killing property. The colonies were counted (in CFU/mL) and the activity values were expressed as a reduction in viability % by calculating surviving fraction (ratio between the viable cells on bare silicon as control and the films) as tabulated in Table 5.2.

Table 5.2: JIS Z 2801 Antibacterial activity test results of 12 BL PEOX-AgNP/TA and PEOX/TA films against gram negative (*E. coli*) and gram-positive (*S.epidermidis*) bacteria.

	E.coli		*S.epidermidis*	
Coatings	CFU ml^{-1}	Reduction in viability (%)	CFU ml^{-1}	Reduction in viability (%)
PEOX5K/TA	1.37×10^7	21.71	1.74×10^5	98.63
PEOX5K-AgNP/TA	0	> 99.99	0.2×10^5	99.84
PEOX50K/TA	1.50×10^7	14.29	1.67×10^5	98.68
PEOX50K-AgNP/TA	0	> 99.99	0.1×10^5	99.92
PEOX200K/TA	1.40×10^7	20.00	1.60×10^5	98.74
PEOX200K-AgNP/TA	0	> 99.99	0.1×10^5	99.92
PEOX500K/TA	1.73×10^7	1.14	1.54×10^5	98.79
PEOX500K-AgNP/TA	1.33×10^4	99.92	0	> 99.99
Bare Silicon surface	1.75×10^7	0	1.27×10^7	0

These results indicate that the prepared coatings strongly inhibit bacterial growth on their surfaces in contact with more than 99.9% reduction in viability of *E. coli*. Additionally, JIS Z 2801 assay was performed to understand the antimicrobial activity of the same coted surfaces against gram-positive *S. epidermidis*. As shown in Figure 5.3 and Table 5.1 all H-bonded self-assembled coatings on silicon substrates demonstrated contact killing property against *S. epidermidis*. It is shown in Table 5.1 that AgNPs are effective antimicrobial agents against *E. coli* and PEOX/TA films can be used as control samples. However, remarkable growth inhibition of *S. epidermidis* was observed for both PEOX-AgNP/TA and PEOX/TA films according to JIS Z 2801 assay. In any case, it is important to note that the silver-containing coatings showed significantly higher anti-microbial activity when compared to their control samples.

To confirm our antibacterial test results, electrochemical measurements were done. No measurable Ag^+ ion release was observed from PEOX(AgNP)/TA films at pH 7.4. Oxidation of metallic silver and Ag^+ ion release was provided by two different methods: i) reduction of pH by acid addition, ii) electrochemical oxidation (polarization). As a result of systematic experiments, it was determined that Ag^+ ions could pass through H-bonded PEOX / TA layer-layer films, PEOX did not affect Ag^+ ion release, but TA had two different mechanisms to effect Ag^+ ion release. The TA molecules in the environment decreased the pH at short time intervals and increased the Ag^+ ion release, but in the following times, TA's acting as reducing agent for Ag^+ ions prevented the spread of Ag^+ ions into the solution. These two mechanisms, which balance each other, enabled the Ag^+ concentration to be effective only near the film surface.[Demirel 2017]

5.2.3 In vitro cytotoxicity assessment of coated films on U2OS cell line

The contribution of PEOX stabilized AgNPs deposited in multilayer films to the toxicity of Human Bone Osteosarcoma Epithelial Cells U2OS was investigated. The viability of U2OS cultured on coated surfaces were determined by assessing the metabolic activity by

MTT. Although, PEOX-AgNP/TA films showed slightly lower biocompatibility than PEOX/TA films, the addition of AgNPs to PEOX/TA films did not decrease cell viability significantly (Figure 5.4).

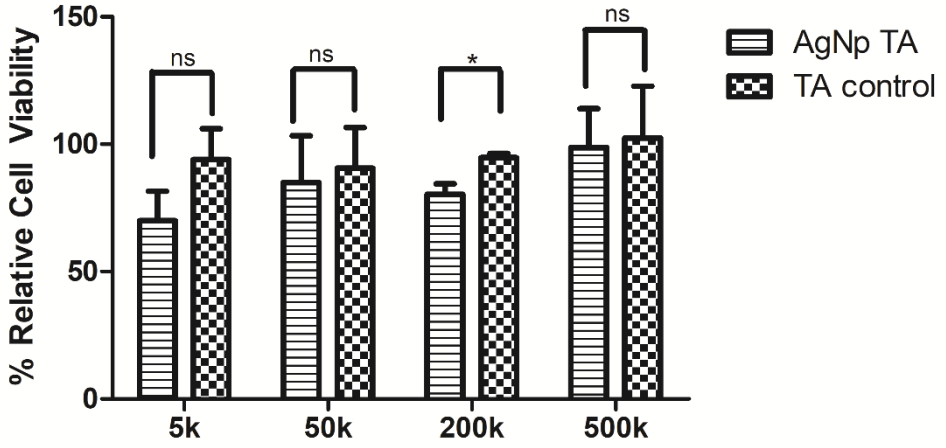

Figure 5.4: Relative U2OS cell viability grown on PEOX-AgNP/TA (horizontal lines) and PEOX/TA (square patterns) films. Relative biocompatibility of films was investigated by assessing the metabolic activity of U2OS cells grown on films with MTT. Data were presented in a grouped column graph plotting the mean with the standard error of the mean. The experiment was performed as triplicates and repeated at least three times (n=3). Two-tailed, an unpaired t-test was performed to test the significance of differences. *$p > 0.05$ was considered as statistically significant, and non-significant differences were presented as 'ns'.

5.2.4 Lifetime and Contact-Killing Ability of Multilayers in Physiological pH and Temperature

The study of the morphology change of multilayers in physiological pH and temperature was needed to follow the evolution of the film in a medium containing ions of a physiological salt solution. This allows us to understand the stability of our coatings on medical implants. 12 BL PEOX500K(AgNP)/TA coated Ti substrates were incubated in PBS pH7.4 for four months at 37^0C. PEOX 500K/TA samples were also examined as control samples. Each month one sample was removed from the solution, washed twice, and dried with nitrogen gas before characterization by FESEM. Electron microscopy was used to see whether the films are stable in PBS or removed from surfaces, also the antibacterial activity of the films were studied by JIS Z 2801 test.

Figure 5.5 and Figure 5.6 shows the morphology change of PEOX/TA and PEOX(AgNP)/TA samples after each month respectfully. The surface image of the coated sample before exposure to PBS is also shown in Figure 5.5 a-b and 5.6 a-d.

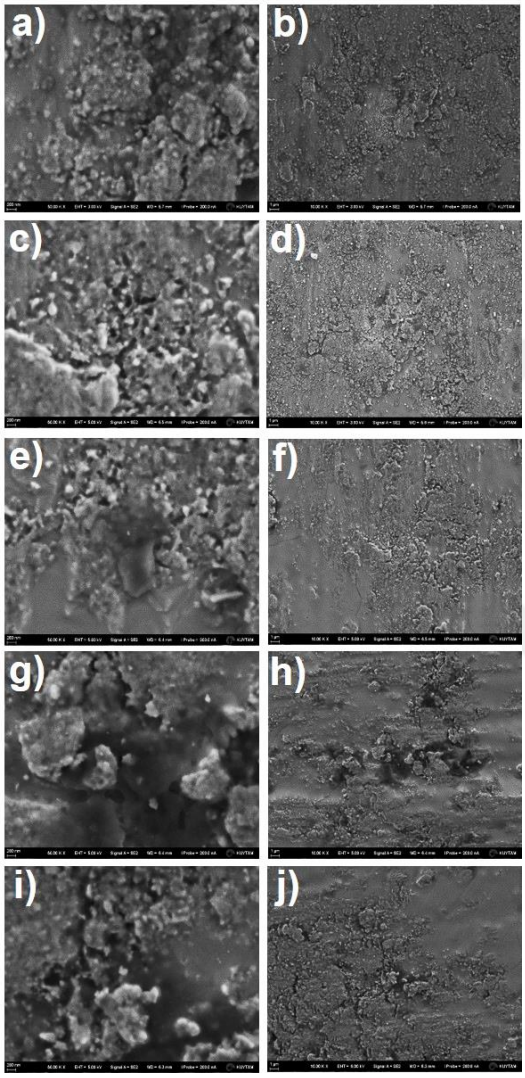

Figure 5.5: Morphology change of PEOX500K/TA coated Ti substrate in PBS pH7.4 at 37^0C. Before immersion in PBS (a: ×50.000K, b: ×10.000K), after one month immersion in PBS (c: ×50.000K, d: ×10.000K), after two months immersion in PBS (e: ×50.000K, f: ×10.000K), after three months immersion in PBS (g: ×50.000K, h: ×10.000K), after four months immersion in PBS (i: ×50.000K, j: ×10.000K).

In both cases of PEOX/TA and PEOX(AgNP)/TA films, the incubation of multilayers in PBS shows that the multilayers are stable on Ti surface and in time only some loosely bonded polymers and aggregates are removed, which cause AgNP to become more apparent in FESEM images. (can be seen better in 200K X magnified images) In these images, it is clear that the AgNPs on the surfaces are shrinking and the lumps are not observed in the film held in PBS for 4 months and the surface is smoother. These results indicate that PEOX-AgNP/TA LbL films remain stable for more than 3 months on Ti.

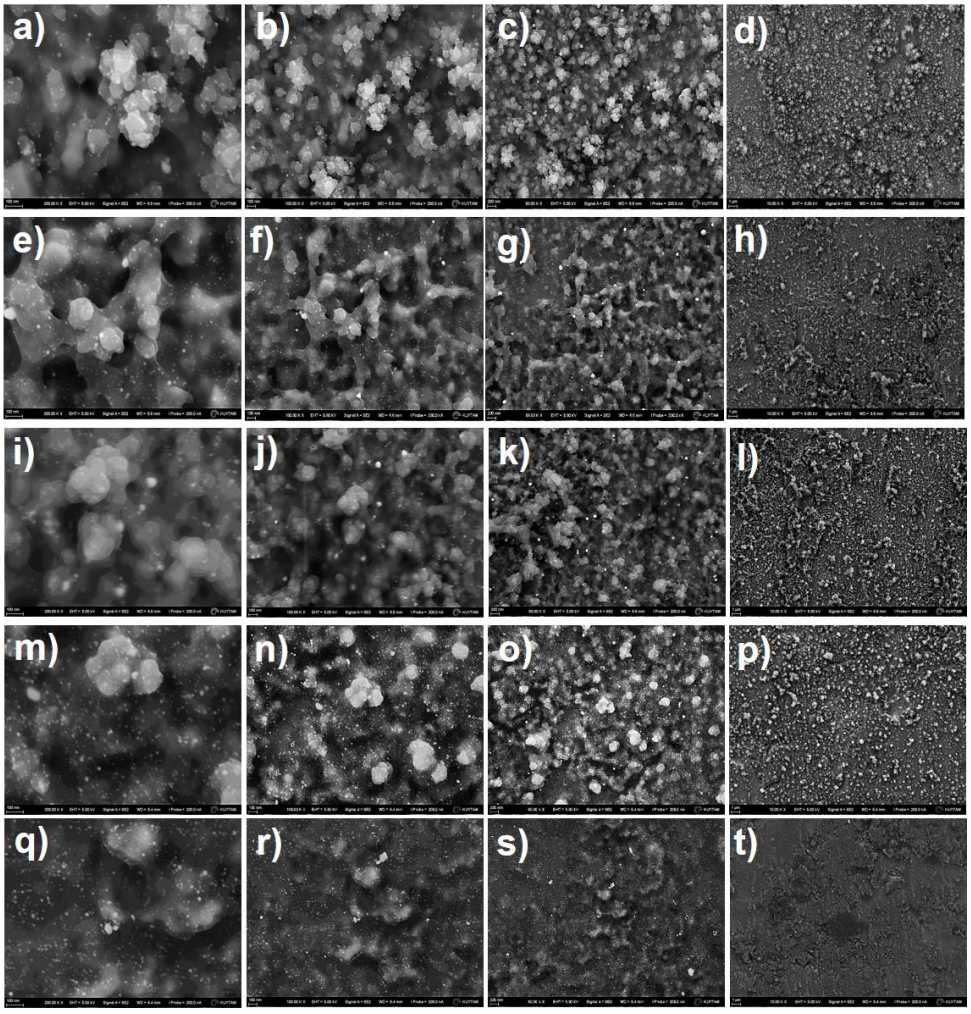

Figure 5.6: Morphology change of PEOX500K-AgNP/TA coated Ti substrate in PBS pH7.4 at 37^{0}C. Before immersion in PBS (a: ×200.000K, b: ×100.000K, c: ×50.000K, d: ×10.000K), after one month immersion in PBS (e: ×200.000K, f: ×100.000K, g: ×50.000K, h: ×10.000K), after two months immersion in PBS (i: ×200.000K, j: ×100.000K, k: ×50.000K, l: ×10.000K), after three months immersion in PBS (m: ×200.000K, n: ×100.000K, o: ×50.000K, p: ×10.000K), after four months immersion in PBS (q: ×200.000K, r: ×100.000K, s: ×50.000K, t: ×10.000K).

JIS Z 2801 test has been used to show the contact killing activity of the coatings incubated in PBS pH7.4 at 37^0C in time for four months. After overnight incubation of samples, surviving microorganisms were counted to evaluate the antimicrobial activity of the test material and the log of the difference between the two counts is determined to give a measurement of antimicrobial activity. The colonies were counted (in CFU/mL) and the activity values were expressed as a reduction in viability % by calculating surviving fraction (ratio between the viable cells on bare silicon as control and the films) as tabulated in table 5.3.

Table 5.3: Contact-killing results of 12 BL PEOX-AgNP/TA and PEOX/TA coatings on titanium substrate (incubated in PBS pH7.4 at 37^0C) against gram negative *E. coli* in time for four months.

Sample	Result of contact killing test	CFU/ml	% reduction
PEOX500K / TA		1.6x109	
PEOX500K(AgNP) / TA (after 1month)		2.87x107	98.6
PEOX500K / TA (after 1month)		$2.07x10^9$	

PEOX500K(AgNP) / TA (after 2months)		$2.63x10^7$	98.6
PEOX500K / TA (after 2months)		$1.87x10^9$	
PEOX500K(AgNP) / TA (after 3months)		$3.2x10^7$	98
PEOX500K / TA (after 3months)		$1.63x10^9$	

PEOX500K(AgNP) / TA (after 4months)		$2.83x10^8$	83.7
PEOX500K / TA (after 4months)		$1.73x10^9$	

These results indicate that prepared coatings strongly inhibit bacterial growth on their surfaces in contact with a 98.6% reduction in viability. JIS Z 2801 employed for the same coatings after immersion in PBS pH7.4 shows up to three months samples are showing almost the same amount of reduction in viability, and after four months, a small decrease inviability reduction to 83.7% was observed which is compatible with electron microscopy images in Figure 4.32. It is observed that silver nanoparticle on the surface has decreased in time in PBS solution. This may be due to the very slow Ag^+ ion release, as well as the removal of PEOX and TA from the surface over time, which may lead to the passage of AgNPs into the solution. These results show that the contact-killing ability of AgNP containing coatings is superior compared to their control samples even after four months incubation in pH7.4.

5.3 Conclusions

PEOX stabilized AgNPs were immobilized on silicon surfaces with TA via H-bonding LbL assembly. Normally, antibacterial activity of AgNPs containing materials are mediated through either mainly silver ion release from nanoparticle surfaces due to oxidation of nanoparticles and formation of reactive oxygen species or through direct contact with AgNPs immobilized on surfaces or release as colloids. Two release-based antibacterial methods were done; agar disk diffusion method and soft agar assay. No clear inhibition zones were observed indicating the antibacterial activity against gram-negative *E. coli* for the coatings in agar diffusion assays. This behavior was attributed to the difficulty in the diffusion of AgNPs and ions into agar medium. Also, no bacteria inhibition zone was observed in soft agar assay against *E. coli*. These results pointed out that the release of silver from multilayers as colloids or as silver cations are prevented. AgNPs were wrapped with PEOX and immobilized with H-bonding with TA via layer-by-layer assembly which may cause inhibition of release of silver as colloids from the surfaces. Also, PEOX is considered as tertiary polyamide and it is very well known that amides have a strong affinity to silver ions and AgNPs. These highly polar amide groups may capture the released silver cations from the AgNP surfaces easily and prevent Ag^+ release. Independent of PEOX molecular weight, all coatings exhibited significant antibacterial activity against gram-negative *E. coli* and gram-positive *S. epidermidis* by acting predominantly via contact-killing mechanism according to JIS Z 2801 standard test. Immobilization of AgNPs and prevention of silver ion release via capturing through amide groups indicate that toxicity of the films towards mammalian cells was minimized. To confirm our results, the release of Ag+ from multilayers were measured by electrochemical methods. Results showed thatAg^+ ions do not spread out from the surface due to the reducing effect of TA. Cytotoxicity of the films was investigated with human bone epithelial, U2OS cells and addition of AgNPs into PEOX/TA films did not decrease the cell viabilities significantly. The SEM images of the multilayers immersed in

PBS pH7.4 showed that only aggregates removed from the surface in 4 months. Also, contact-killing test showed that AgNP loaded films strongly inhibit bacterial growth on their surfaces in contact with 98.6% reduction in viability in the first three months, and in forth month the reduction viability decreased to 83.7%.

Chapter 6: Hollow Microcapsules of Hydrogen-Bonded Multilayers

Overview

Surface-mediated LbL deposition results in high control over the properties of the resulting films and allows a wide range of materials to be incorporated within films. The LbL deposition method has been used for the formation of multilayer capsules in the last twenty years [61, 189]. This system includes LbL shell, micro/nano-particles as a sacrificial template and one or several functional molecules such as drugs, nanoparticles, enzymes, or fluorescent probes. Generally, the sacrificial template is removed by dissolution or calcination [226, 227]. The removal process of the template is a critical step and it should not damage the loaded material. Thus, the template and loading method should be chosen based on the molecules that are going to be entrapped into the capsules. Different methods have been reported to load the molecules in LbL capsules. The cargo molecules can be directly loaded during formation of the capsule (pre-loading method), or after capsule formation (post-loading method) [202]. The cargo molecules can be loaded in the hollow capsule, into multilayers or on the external surface of the capsule.

The hollow capsules can be loaded with cargo molecules by diffusion into the capsule cavity. Depending on the multilayer composition, the permeability of hollow capsule can be switched from closed to open state by variation of pH [202], ionic strength[147], temperature [225, 401], and solvent polarity [402]. Change in these parameters causes the change in the surface morphology and structure of the capsules and results in the release of loaded active molecules.

The driving force for LbL assembly can be electrostatic interaction [40], Van der Waals interaction [403] or Hydrogen bonding (H-bonding) [225]. Most common LbL assemblies are based on electrostatic interaction, but due to cytotoxicity of polycations, these systems are not favored in biological applications. In this chapter, the preparation of H-bonded LbL capsules is presented. H-bonded multilayers offer many different paths for the development of responsive films and capsules. H-bonded LbL assemblies show reversible responses to different stimuli like pH, ionic strength, temperature, external stress, and electrical field [7, 8, 177, 178]. Paramasivam et al. [225] reported the temperature responsive H-bonded capsules based on tannic acid and poly(2-n-propyl-2-oxazoline) with the ability to capture and release of loaded fluorescent molecules at a physiological temperature of 37 ^{0}C. Switching of temperature results in the collapse of polymer chains and as a result of morphological changes, the capsules release the loaded molecules. More examples from the literature will be given in section 1.2.2.1. The versatility of H-bonded multilayers has allowed the development of materials with a range of properties tailored to biomedical applications. These include the potential for controllable disassembly, the capability to respond to stimuli such as pH and temperature, and the ability to load and release cargo specifically.

To prepare H-bonded thin film with LbL assembly, a polymer pair, one H-bond donor and the other H-bond acceptor, is needed. H-bonded multilayers based on water-soluble neutral polymers and polycarboxylic acids are mostly prepared at an acidic pH, at which polyacids are completely protonated [7, 8]. Above the critical pH, H-bonds are disrupted due to ionization of the polyacid, therefore the LbL film is disintegrated [7, 8, 179, 184]. Herein, to prepare H-bonded LbL capsule, PEOX and TA were used as H-acceptor and H-donor, respectively. TA has a unique functional structure with numerous terminal hydroxyl groups, (Figure 1.6a) thus it is able to form multiple H-bonding. Moreover, TA has been shown to exhibit high biological activity including antioxidant, antimicrobial, anti-carcinogenic, anti-mutagenic and antibacterial properties [265–267]. PEOX is a member of poly(2-alkyl-2-

oxazoline)s (PAOX) family and a nonionic, non-toxic and biocompatible polymer (Figure 1.6b) showing lower critical solution temperature (LCST) of ~ 60^0C [271–274]. H-bonds are primarily formed between the carbonyl groups of PEOX and hydroxyl groups of TA [275].

In Chapter 4, we reported the pH-responsive LbL films of PEOX and TA. Also, in Chapter 5, we introduced H-bonded LbL films of PEOX stabilized silver nanoparticle/TA as antibacterial coatings. Kempe et al [228], reported the hollow capsules prepared by the LbL assembly of PEOX and poly (methacrylic acid) (PMA). Later, they also reported the LbL assembly of thiol-containing poly(2-ethyl-2-oxazoline) (PEOX SH) brushes and PMA multilayers onto silica (SiO_2) particle templates, wherein the layers are stabilized by cross-linking them through disulfide bond formation [229].

In this chapter, we report on the formation of pH responsive hollow capsules of PEOX and TA. Calcium carbonate ($CaCO_3$) particles have been synthesized and used as a template. $CaCO_3$ particles are very useful micro particles, because of the low synthesis costs, simple synthesis method, the porosity that leads to easy loading, the biocompatibility, the low toxicity and the mild decomposition conditions [404, 405]. H-bonded PEOX/TA capsules have not been reported previously. Rhodamine 6G is used as a model cargo molecule to study the loading and release properties of the PEOX/TA capsules. It is predicted that these capsules may be used to load nanoparticles and macromolecules into them, yielding loaded capsules for versatile applications as micro-carriers in fields of drug delivery and controlled release.

6.1 Experimental

6.1.1 Preparation of $CaCO_3$ particles as capsule templates

Spherical polystyrene sulfonate (PSS) doped $CaCO_3$ particles with a diameter of 5-8 μm were prepared by colloidal aggregation of Na_2CO_3 and $CaCl_2$, and used as a sacrificial template. The process was started by rapid mixing of equal volumes of $CaCl_2$ and Na_2CO_3

solutions. The PSS was completely dissolved in Na_2CO_3 solution prior to mixing and final concentration was maintained at 2 mg mL^{-1}. Negatively charged PSS was adsorbed on the surface of nanoparticles constituting the porous $CaCO_3$ microparticles and prevented the recrystallization into rhombohedral calcite form (Figure 6.1). 0.3 M Na_2CO_3 solution was rapidly poured into an equal volume of 0.3 M solution of $CaCl_2$ at room temperature under vigorous stirring, and after intense agitation on a magnetic stirrer, the precipitate was filtered off with a cellulose filter having pore size of 0.45 µm, thoroughly washed with pure water twice to remove residual salts, and then dried in air.

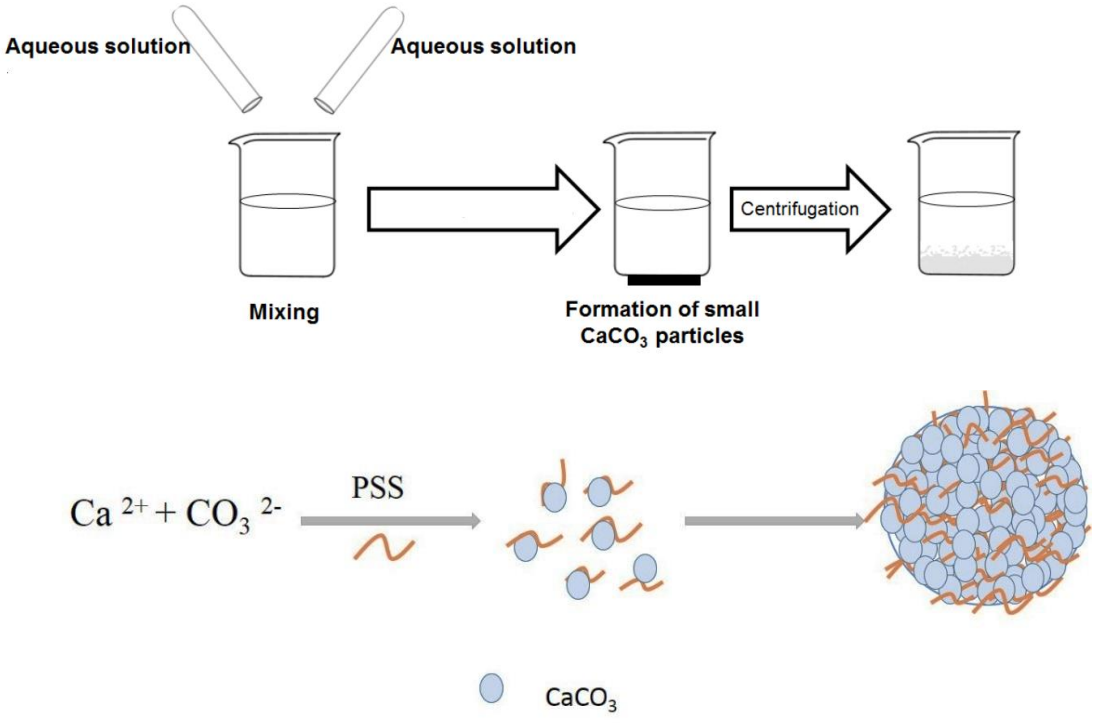

Figure 6.1 Schematic of the $CaCO_3$ microparticle preparation process.

6.1.2 LbL coating and capsule preparation

Microcapsules of PEOX/TA were prepared by LbL assembly using $CaCO_3$ particles as sacrificial templates. As the $CaCO_3$ particles possess a negatively charged surface, the first layer was BPEI (5.0 mg mL^{-1} aqueous solution for 30 min), which is a polycation, to form a precursor layer for LbL self-assembly initiation. Excess BPEI was centrifuged and rinsed off by distilled water. PEOX and TA solutions were prepared at a concentration of 1 $mgmL^{-1}$ with DI water at pH 4.5. For LbL assembly, 15 ml of each PEOX solution was added to a centrifuge tube containing ~1% w/w microparticle suspension. After 15 min of deposition, PEOX coated particles were separated by centrifugation at 8000 rpm for 2 min. The coated particles were triple washed with pH adjusted water by centrifugation cycles to remove residual unabsorbed and loosely adsorbed PEOX chains. This process of adsorption and washing was repeated for TA as well. The process was repeated until the desired number of bilayers of PEOX/TA films were obtained. After each bilayer, the coated microparticles were dispersed with ultrasound for 15 s to avoid aggregation. After achieving 8 bilayers, the $CaCO_3$ core was dissolved with 0.2 M EDTA solution at pH 6.0 (adjusted by HCl) to dissolve the calcium carbonate core. After 30 min of agitation, the capsules were centrifuged, the supernatant was removed, and the capsules were resuspended in fresh EDTA. After triple washing with water, the prepared capsules were stored in a closed container at 4 ^{0}C and used for further experiments.

6.1.3 Rhodamine 6G loading and release experiments

To encapsulate the Rhodamine 6G into the PEOX/TA capsules, capsules were mixed with Rhodamine 6G solution (0.02 mg mL^{-1}, pH 1.7) and incubated in a dark room for 1 h. After the encapsulation process, the capsule suspension was washed twice with DI water to remove the excess amount of Rhodamine 6G in the supernatant. To investigate the release of Rhodamine 6G from capsules at physiological pH, the Rhodamine 6G loaded capsule

suspension was then incubated in an incubator shaker at 37 ^{0}C in HCl solution at pH 1.5, acetate buffer solution at pH 4.5, and phosphate buffer solution at pH 7.4. The reason that these three pHs have been chosen is the range of pH values in the gastrointestinal track. The pH of saliva ranges from 6.5 to 7.5. After swallowing, the food reaches the stomach where upper and lower parts of the stomach have different pH values. The upper part has a pH of 4.0−6.5, while the lower part is highly acidic with a pH of 1.5−4.0. It then enters the intestine which is slightly alkaline, with a pH of 7.0−8.5. Thus, the choice of pH 1.5, 4.5, and 7.4 represent the wide range of pH in the gastrointestinal track.

6.1.4 Atomic force microscopy (AFM) and scanning electron microscopy (SEM) characterizations

The morphology changes of the H-bonded capsules were observed by AFM and SEM. AFM measurements were performed with Bruker Dimension Atomic Force Microscope in tapping mode. AFM samples were prepared by depositing a droplet of the capsule suspension on a silicon wafer and allowing it to dry. SEM images of Carbon sputtered samples dried on a silicon wafer were obtained with Zeiss Ultra Plus field emission scanning electron microscope (FESEM).

6.1.5 Confocal laser scanning microscopy (CLSM)

CLSM was used to study the loading and the effect of pH on shell permeability and morphology of microcapsules. For CLSM imaging, 2 mL of the capsule suspension was placed on a microscopic slide and imaged.

6.1.6 Fluorescence spectroscopy

Fluorescence spectra were recorded to show the release of loaded Rhodamine 6G at pH 1.5 HCl solution, an acetate buffer solution pH 4.5 and phosphate buffer solution pH 7.4. The excitation wavelength was chosen to be 532 nm. To study the release process as a function of incubation time, the Rhodamine 6G loaded capsule suspension was incubated at

37 ^{0}C. At specific points of time, 1 mL of sample was withdrawn from the suspension and centrifuged at 8000 rpm to remove the supernatant. Supernatant fluorescence spectrum was measured to determine the released amount. Solid sample and 1 mL of fresh solution were added back into the incubated sample. The fluorescence spectrum of the supernatant was acquired as a function of incubation time.

6.2 Results and discussion

Spherical $CaCO_3$ microparticles were used as the templates for capsule preparation. $CaCO_3$ particles recently gained increasing interest as templates because of complete removal of the core without leaving any residues during dissolution by chelating agent or acid, and also because of its non-toxicity. PSS-doped $CaCO_3$ microparticles (Figure 6.2) were prepared through colloidal crystallization of $CaCl_2$ and Na_2CO_3 in the presence of PSS. PSS, negatively charged polymer, is adsorbed on the surface of nanoparticles constituting the porous $CaCO_3$ microparticles (Figure 6.1) and prevents the recrystallization into rhombohedral calcite form. Both OM and FESEM images (Figure 6.2) showed that uniform and spherical $CaCO_3$ microparticles were obtained. The diameter of $CaCO_3$ microparticles was measured by FESEM in the size range of 5 to 8 μm. The inserted image in Figure 6.2b shows that microparticles have a porous structure. Porosity is an important feature, since it increases the effective surface area of the $CaCO_3$ microparticles, and it is a great advantage for layer by layer adsorption. These empty pores were formed among tiny crystals of $CaCO_3$ during crystallization resulting in a connected network of LbL film after core removal. Thus, networks could be loaded by cargo molecules.

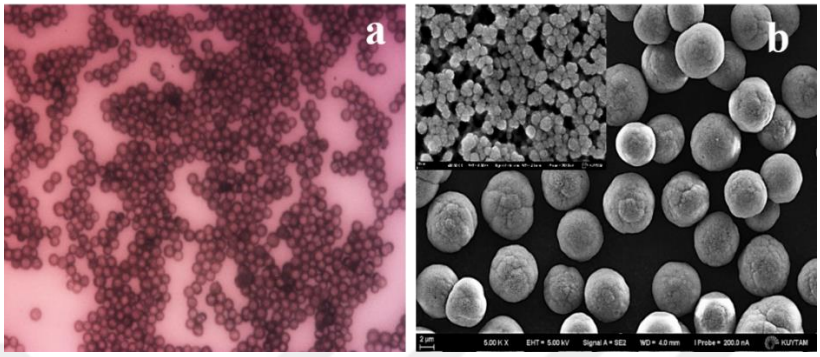

Figure 6.2: a) OM, and b) FESEM (scale bar = 2 μm) images of PSS-doped $CaCO_3$ microparticles. The insert shows the higher magnification (400.00K X) of these microcapsules.

These $CaCO_3$ microparticles were used as a sacrificial template for capsule fabrication using LbL method with PEOX and TA. After formation of 8 bilayers on $CaCO_3$ particles, the template was dissolved by addition of EDTA and hollow capsules were obtained. The coating permeability allows small molecules, such as EDTA, inorganic ions and dyes, to freely enter and leave the capsule interior. The pre-loaded negatively charged PSS molecules enable the hollow capsules to spontaneously load with positively charged drug molecules by electrostatic interactions [406]. The scheme illustrating the capsule preparation is depicted in Figure 6.3.

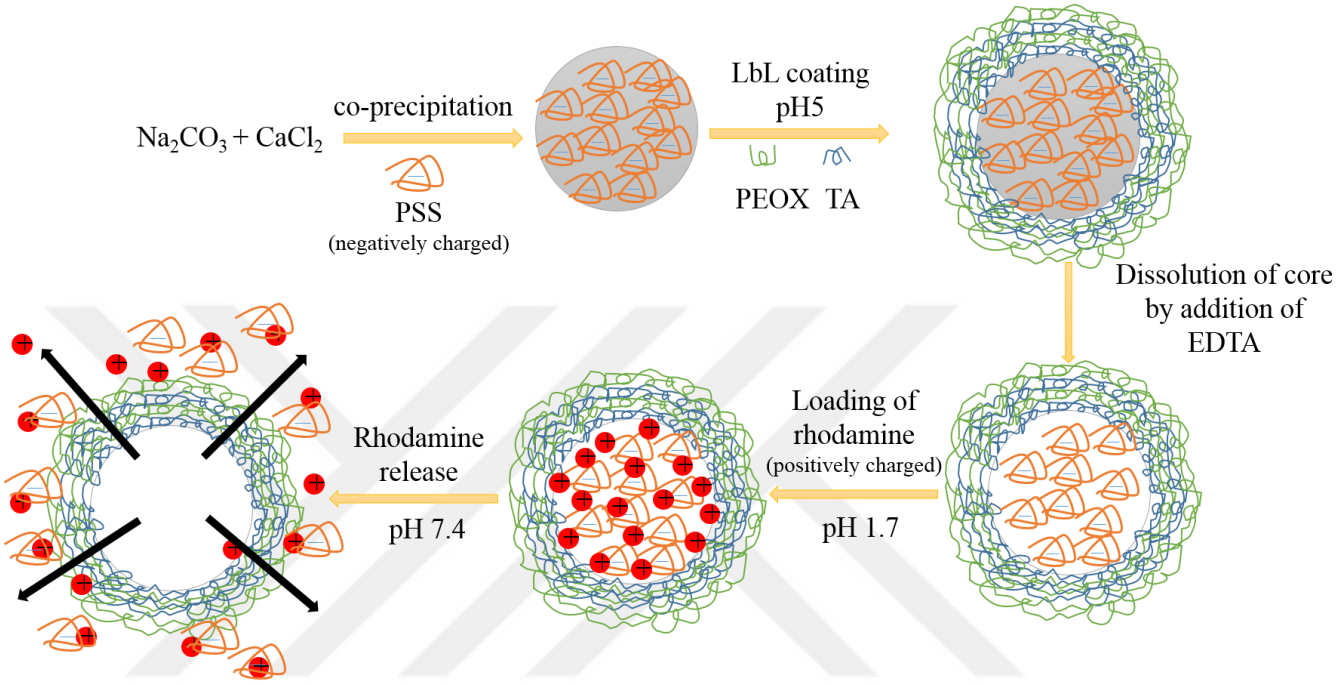

Figure 6.3: Scheme of microcapsules preparation, loading and release steps of Rhodamine 6G loaded into the hollow capsules.

6.2.1. Loading of Rhodamine 6G into PEOX/TA capsules

The permeability and loading capability of capsules are especially important for drug loading and release in drug delivery applications. The loaded hollow capsules were observed by CLSM using Rhodamine 6G as a model molecule. CLSM image of unloaded and Rhodamine 6G loaded PEOX/TA capsule is shown in Figure 6.4. CLSM investigations showed that the capsules were permeable for Rhodamine 6G at pH 1.7 as shown in Figure 6.4b. CLSM was also used for washed Rhodamine 6G loaded capsules, and it was observed that Rhodamine 6G moleculeswere successfully loaded into the capsules showing that both

the capsule wall structure and the presence of PSS inside the capsules are important in driving the Rhodamine 6G molecules from the bulk to the interior of the capsules. The driving force for spontaneous loading of Rhodamine 6G is the electrostatic interactions between Rhodamine 6G and preloaded PSS molecules in the capsules. Tong et al., reported that the free PSS formed during the dissolution of template for poly(allylamine hydrochloride) (PAH)/PSS capsule fabrication facilitate the loading of the positively charged water-soluble substances based on electrostatic interaction [406]**.** Gao and co-workers also reported that positively charged molecules such as Rhodamine 6G and TRITC-Dextran can be spontaneously loaded inside the PSS/PAH capsules when melamine formaldehyde (MF) particles were used as the template [406, 407]**.**

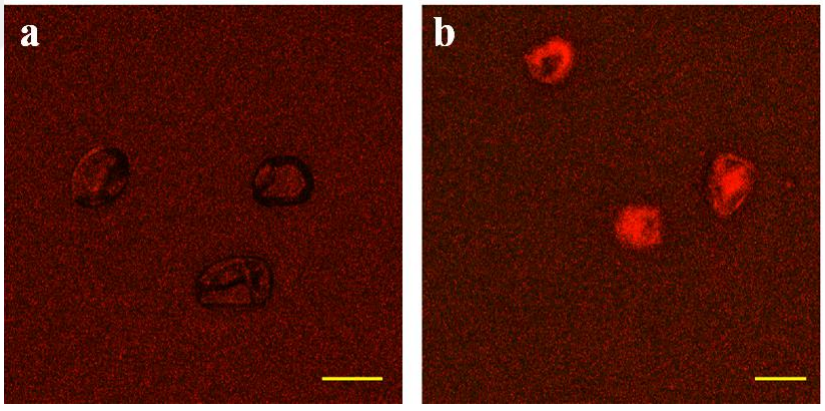

Figure 6.4: CLSM image of a) unloaded, b) Rhodamine 6G loaded microcapsules.

The morphological changes of PEOX/TA capsules prior to and after loading with Rhodamine 6G were monitored by AFM (Figure 6.5) and SEM investigations (Figure 6.6). AFM and SEM images of hollow PEOX/TA capsules showed collapsed structure as a result of core removal as shown in Figure 6.5a and Figure 6.6a. The AFM images of empty and loaded capsules showed different collapsed morphologies. The hollow capsules were completely flat and collapsed (Figure 6.5a) whereas the loaded capsules (Figure 6.5b) showed a swollen structure with much higher average vertical height. The height of an unloaded control capsule was 140 nm which increased to an average height of 2.22 µm after loading with Rhodamine 6G.

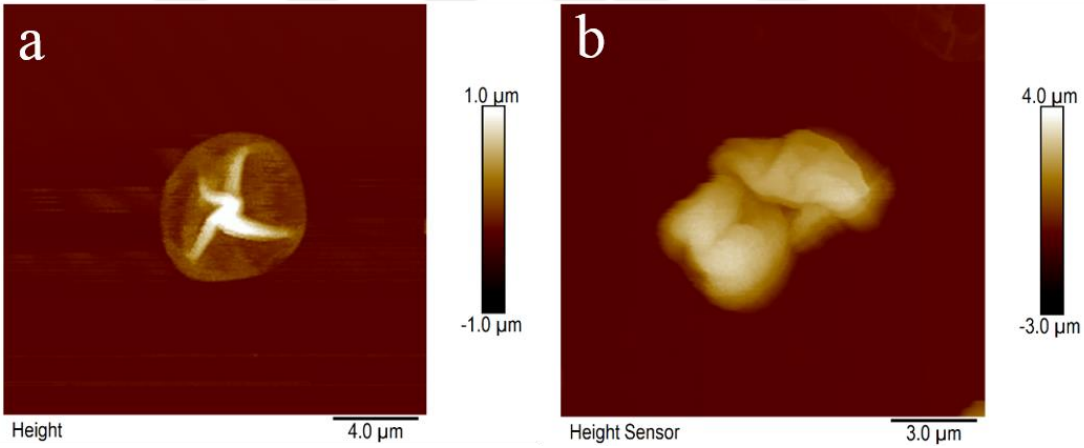

Figure 6.5: AFM images of hollow and loaded capsules and their height profiles. a) Hollow PEOX/TA capsules; b) Rhodamine 6G loaded capsules.

This increase in thickness is attributed to swollen structure and loaded Rhodamine 6G, which was observed by SEM as well (Figure 6.6). The collapsed structure of the hollow

capsules with SEM (Figure 6.6a) was similar to the AFM images shown in Figure 6a, and the loaded capsules demonstrated a swollen structure (Figure 6.6b).

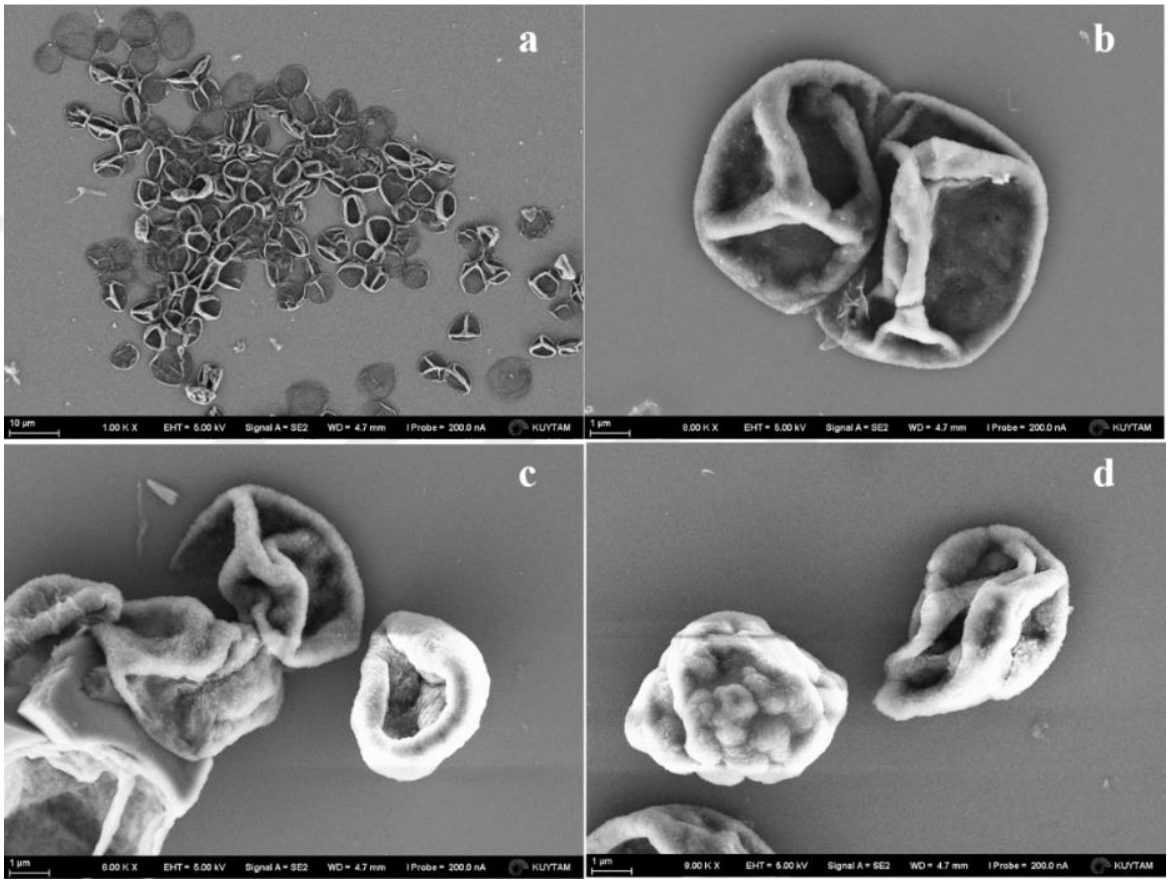

Figure 6.6: a) SEM image of hollow capsules with 1.00k magnification, b) 8.00K magnification, c) SEM image of loaded capsule 1.00K, b) 8.00K

6.2.2. The release of Loaded Rhodamine 6G Molecules from PEOX/TA Microcapsules

The release of loaded Rhodamine 6G from PEOX/TA microcapsules was studied at pH 1.5, 4.5, and 7.4. Figure 6.7 shows the cumulative release of Rhodamine 6G as a function of time.

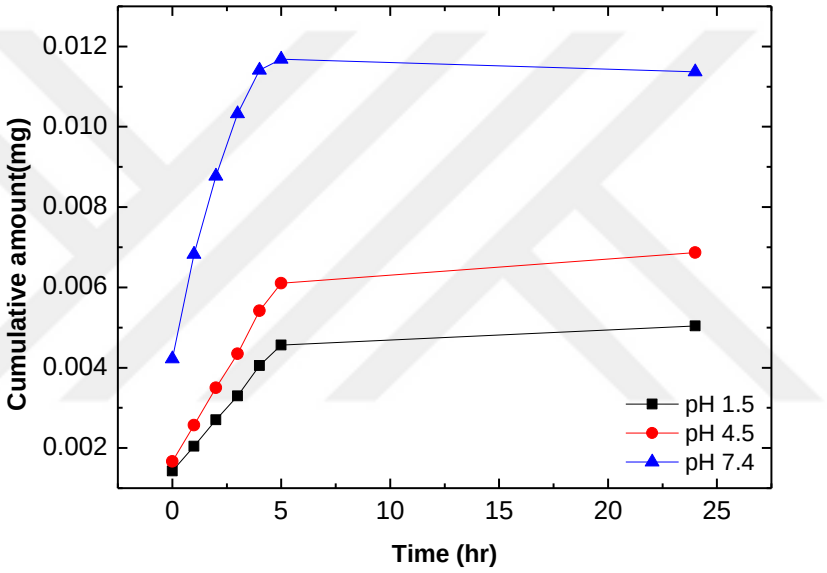

Figure 6.7: Release profile from Rhodamine 6G loaded capsules at pH 1.5, 4.5, and 7.4.

The release profile of Rhodamine 6G from the capsules shows a fast release in the first 5h at all pH values studied. A cumulative release of 100% in PBS is obtained at the end of 24 h for pH 7.4 and no further release was observed after 24 h in pH 7.4. At low pH values, TA is in a state of protonation and form H-bonds with the carbonyl groups of PEOX to hold the initial capsule structure. At high pH values, TA becomes partially deprotonated which leads to the breakage of H-bonding and separation of the polymer chains. By increasing pH, TA

becomes partially deprotonated and leading to weaker intermolecular interaction between PEOX and TA and result in increasing permeability of capsule wall and releasing the loaded molecules.

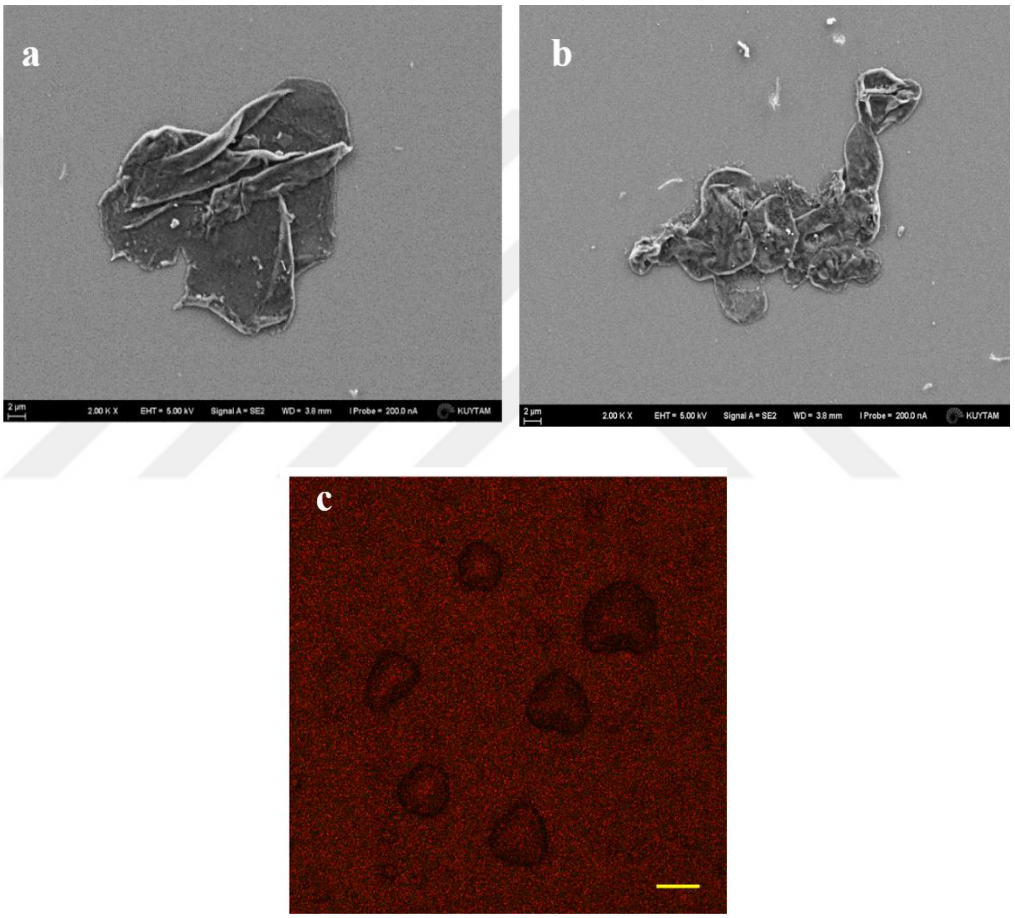

Figure 6.8: a,b) SEM (magnification 2.00K, scale bar = 2 µm), and c) CLSM images of Rhodamine 6G loaded capsules after 24hr incubation in PBS pH7.4, at 37 ^{0}C.

Finally, SEM (Figure 6.8a,b) and CLSM (Figure 6.8c) were used to observe the morphology of capsules after release at pH 7.4. Both investigations showed that the capsules appeared empty with a change in the structure. This observation indicates that pH treatment changes the permeability of the capsules, possibly related to morphological changes of the capsule wall. The capsule size apparently increasing by increasing pH and eventually leads to the disintegration of them by increasing pH. This can be explained as a result of the loss of H-bonding and the charge repulsion between the deprotonated $-COO^-$ groups, as it has been previously reported for polyelectrolyte multilayer microcapsules [408]. These observations show that pH-induced morphological changes of microcapsules could be effectively exploited for encapsulation and release of molecules at a physiological pH of 37 ^0C.

6.3 Conclusions

Capsules formed from H-bonded multilayers would have a number of advantages over polyelectrolyte capsules. H-bonded films tend to be more biocompatible than their cytotoxic counterparts. In addition, the pH-responsive nature of H-bonded films causes increased permeability and film dissolution with increasing pH. This allows triggered dissolution at a well-defined pH value.

In this chapter, a hollow H-bonded microcapsule system based on biocompatible PEOX and TA which is able to capture molecules and release at physiological conditions was reported. Switching pH to 7.4 resulted in a morphological change of the capsules leading to the release of the loaded Rhodamine 6G molecules.

$CaCO_3$ microparticles containing PSS, as morphology control reagent, have been successfully synthesized. FESEM showed that these microparticles had diameters in the range of 5-8 μm. $CaCO_3$ microparticles have been used as template for preparation of H-bonded multilayer microcapsules by LbL technique. After sacrificing $CaCO_3$ with EDTA,

hollow H-bonded microcapsules was fabricated. Their hollow nature was confirmed by FESEM, AFM, and CLSM. Rhodamine 6G has been used as a model cationic molecule to study the loading and release ability of microcapsules. AFM, CLSM and FESEM images showed that Rhodamine 6G molecules are successfully loaded into microcapsules. Loaded Rhodamine 6G at low pH yields a swollen structure. Release study showed that the capsules were able to release loaded molecules at physiological pH which was close to pKa value of TA (~8.5). By increasing pH, deprotonation of TA occurs, leading to the breakage of H-bonding and repulsion between the polymer chains and increasing the permeability, and eventually result in releasing of loaded Rhodamine 6G. It is likely that this special swelling-disintegration technique may be used to load nanoparticles and macromolecules into the preformed microcapsules, resulting loaded capsules for versatile applications as micro-carriers in fields of drug delivery and controlling the release of therapeutically relevant molecules for in vivo applications.

Chapter 7: Conclusions

Surface modification by using LbL assembly technique results in precise control over the coating properties and allows a broad range of materials to be incorporated within multilayers. LbL coatings can be deposited on a substrate in any shape and size. However, polyelectrolyte LbL films have not been the choice for biological applications because of the cytoxicity of polycations [231, 246, 409]. Thus, H-bonding has attracted great interest as driving force for LbL film formation due to the ability to use biocompatible and neutral components. In considering the potential uses of H-bonded LbL films, it is important to understand the current applications of them.

The focus of this thesis is on the H-bonded LbL assembly of PEOX and TA. It has been shown that H-bonded multilayers of PEOX and TA can be assembled as 2D and 3D materials, such as thin films and hollow capsules, with unique response properties to environmental stimuli (pH). To functionalize PEOX/TA multilayers, AgNP was introduced as the antimicrobial agent, and LbL films of PEOX stabilized AgNP/TA with long-lasting contact-killing antibacterial activity was produced on solid substrates.

During this study, a novel AgNP loaded multilayers with the contact-killing property was designed. In general, the mode of the antibacterial mechanism of AgNPs is attributed to the release of silver ions. Our non-release antibacterial coating design is important since it can prevent the reservoir exhaustion issue of release-based antibacterial coatings. To the best of our knowledge, the method that has been used here, stabilizing AgNPs with PEOX and incorporation of them in H-bonded LbL film with TA, has not been reported before. In addition to contact-killing property, these multilayers are pH-responsive which make them attractive due to their stability at

physiological pH and release AgNPs only above the critical pH upon the disintegration of the multilayers by breakage of H-bonds. These features make this multilayer of particular interest for antimicrobial coatings and surfaces in biomedical applications, especially in surgical devices and implants. Hence, the study of the pH-responsive multilayers with contact-killing property appears rewarding.

For incorporation of AgNPs into LbL matrices, stabilization of AgNPs by PEOX was studied in detail. PEOX is a biocompatible and non-toxic polymer. PEOX has an amide group linking the backbone and the side chain which is expected to contribute to better stabilization of AgNPs. AgNPs were synthesized in aqueous solutions using $AgNO_3$ and $NaBH_4$ as a reducing agent in the presence of PEOX as a stabilizer. The effect of PEOX molar mass, PEOX concentration, pH and time on the temporal stability of AgNP dispersions was investigated. The particle sizes were measured by DLS. DLS analysis showed the bimodal distribution for all PEOX stabilized AgNP. Smaller size corresponded to individual PEOX(AgNPs) and the larger size was attributed to agglomerates, which consisted of individual AgNPs in the mesh of bridging PEOX chains. The particle sizes determined by SEM analysis were also compatible with DLS. Moreover, DLS results showed that the stability of AgNP dispersions and the particle size depended on PEOX molar mass. The stability of AgNPs in aqueous solutions over time and at different pHs was also investigated. Control AgNPs (no PEOX) were not stable. PEOX5K or PEOX50K stabilized AgNPs were stable up to 6 days. The PEOX500K showed the most effective stabilizing effect for AgNPs up to 2 weeks. With increasing PEOX concentration, the amount of AgNPs in the dispersion increased. By decreasing the pH of as-prepared dispersion from 9.9 to 4.5, the individual AgNP size increased from 10 nm to 16 nm. All PEOX stabilized dispersions were stable up to 8 days at pH values below 9.9.

After successful stabilization of AgNP dispersion by PEOX, PEOX(AgNPs) were used as H-accepting component and TA as H-donating component in the preparation of H-bond

driven LbL films. PEOX/TA films also prepared as control samples. Because of physiologically relevant pH stability of TA based films, most studies have so far focused on biomedical applications.

AgNPs coated with either of the four different molecular weight PEOX was used to form multilayers on solid surfaces via H-bonds with TA. The growth behavior, morphologies, and pH stability of these films were studied. The growth profiles and the pH-induced disintegration of PEOX(AgNPs)/TA multilayers were similar to PEOX/TA multilayers. All films grew linearly up to 12 bilayers and were stable up to pH 8.5 as determined by ellipsometry and UV–visible spectroscopy. Disintegration started at pH 8.5, as expected, due to the deprotonation of TA. UV–visible spectra showed the faster release of TA at the critical disintegration pH compared to PEOX stabilized AgNPs. After pH–stability study the morphology of the surfaces was checked with AFM. AFM images indicate that the film remains stable at pH 8.5. Above this pH, the film is removed in large areas over the substrate. Although some AgNPs still appear on the surface, their amount is much less than the amount after preparation. These observations confirm the ellipsometry and the UV-Visible spectrometry results.

The loading capacity of AgNPs in 12 bilayers of PEOX(AgNP)/TA films was determined by XPS. Small PEOX molar masses (5K and 50K) coated AgNPs were incorporated more (~ 7-9 atomic %) into multilayers compared to 200K and 500K PEOX stabilized AgNPs (~ 3-4 atomic %). The main reason for this difference is that the smaller polymer chains are more likely to bring nanoparticles closer by bridging.

Antibacterial tests based on release (agar disk diffusion test and soft top agar test) were done. No growth inhibition zones were observed. On the other hand, to prove that coatings have Ag^+ on the top surface and able to kill bacteria upon contact, JIS Z 2801 tests were carried out against two gram negative and gram-positive bacteria. All multilayers showed significant antibacterial activity against both grams negative and gram positive bacteria by

acting predominantly via contact-killing mechanism. Electrochemical measurements of Ag^+ ion release confirmed antibacterial tests and no measurable ion release could be observed from PEOX-AgNP/TA films at pH 7.4. It was concluded that TA acts as a reducing agent for the Ag^+ ions and prevent the diffusion of Ag^+ ions away from the multilayers.

To investigate the adhesion of multilayers and their stability and antibacterial activity on possible implant coatings, PEOX/TA and PEOX-AgNP/TA multilayers have been prepared on titanium substrates**.** The coatings prepared on titanium substrates were maintained in PBS solution at pH 7.4, which was used as simulated body fluid, for a period of up to 4 months to determine their stability and antibacterial activity. All coatings were shown to remain stable for 3 months on titanium surfaces and retain their antibacterial activity. AgNP loaded LbL coatings with a minimum of 3 months of antibacterial activity is important to prevent infection on the implant surfaces in the first few months and to eliminate the need to replace the implant. Considering that life expectancy is prolonged, the economic widespread effect of preventing infection in implants becomes even more important.

Although LbL films have mainly been prepared on flat substrates, coating solid nano- and micro-particles with multilayers is attracting growing interest as an effective method to encapsulate a large number of materials for controlled release applications. In Chapter 6, the preparation of H-bonded LbL hollow capsules of PEOX and TA was reported. Capsules formed from H-bonded multilayers of PEOX/TA would have a number of advantages over polyelectrolyte capsules. As mentioned before, H-bonded films tend to be more biocompatible than their cytotoxic counterparts. Additionally, the pH-responsive nature of H-bonded films causes the film dissolution with increasing pH. This allows for triggerable dissolution at a well-defined pH value.

For capsule preparation, PEOX and TA were sequentially deposited onto a template particle ($CaCO_3$ microparticles), and after obtaining the desired number of bilayers, the sacrificial core template was dissolved, leading to the formation of hollow capsules. The

attractive property of these hollow capsules is that the interior volume can be filled with functional cargo molecules with no electrostatic charge within the LbL materials, and release at high pH values which are an attractive feature for drug release. Results suggested that these hollow capsules containing negatively charged PSS have the potential to be loaded with positively charged molecules. Loading of capsules with Rhodamine 6G, which is a cationic dye, as a model molecule and the subsequent release were studied. Microscopy analysis showed that these capsules can be loaded with Rhodamine 6G molecules successfully. Release study has shown that these capsules are able to release loaded Rhodamine 6G at physiological pH 7.4 which is close to pKa value of TA. At this pH, TA is partially ionized and leads to H-bond weakening between TA and PEOX and as a result morphology change of microcapsule and release of loaded material. The change in morphology is confirmed by microscopic analysis. In the future, the application of these microcapsules can be studied and optimized for controlling the release of therapeutically relevant molecules for in vivo applications.

Bibliography

1. Decher G (1997) Fuzzy nanoassemblies: Toward layered polymeric multicomposites. Science (80-) 277:1232–1237. doi: 10.1126/science.277.5330.1232

2. Decher G, Hong JD, Schmitt J (1992) Buildup of ultrathin multilayer films by a self-assembly process: III. Consecutively alternating adsorption of anionic and cationic polyelectrolytes on charged surfaces. Thin Solid Films 210–211:831–835. doi: 10.1016/0040-6090(92)90417-A

3. Caruso F, Caruso RA, Möhwald H (1998) Nanoengineering of inorganic and hybrid hollow spheres by colloidal templating. Science (80-) 282:1111–1114. doi: 10.1126/science.282.5391.1111

4. Hou S, Harrell CC, Trofin L, et al (2004) Layer-by-Layer Nanotube Template Synthesis. J Am Chem Soc 126:5674–5675. doi: 10.1021/ja049537t

5. Stockton WB, Rubner MF (1997) Molecular-level processing of conjugated polymers. 4. Layer-by-layer manipulation of polyaniline via hydrogen-bonding interactions. Macromolecules 30:2717–2725. doi: 10.1021/ma9700486

6. Wang L, Wang Z, Zhang X, et al (1997) A new approach for the fabrication of an alternating multilayer film of poly(4-vinylpyridine) and poly(acrylic acid) based on hydrogen bonding. Macromol Rapid Commun 18:509–514. doi: 10.1002/marc.1997.030180609

7. Sukhishvili SA, Granick S (2002) Layered, erasable polymer multilayers formed by hydrogen-bonded sequential self-assembly. Macromolecules 35:301–310. doi: 10.1021/ma011346c

8. Sukhishvili SA, Granick S (2000) Layered, Erasable, Ultrathin Polymer Films. J Am Chem Soc 122:9550–9551. doi: 10.1021/ja002410t

9. Delongchamp DM, Hammond PT (2004) Highly ion conductive poly(ethylene oxide)-based solid polymer electrolytes from hydrogen bonding layer-by-layer assembly. Langmuir 20:5403–5411. doi: 10.1021/la049777m

10. Ono SS, Decher G (2006) Preparation of ultrathin self-standing polyelectrolyte

multilayer membranes at physiological conditions using pH-responsive film segments as sacrificial layers. Nano Lett 6:592–598. doi: 10.1021/nl0515504

11. Mehrotra S, Lee I, Chan C (2009) Multilayer mediated forward and patterned siRNA transfection using linear-PEI at extended N/P ratios. Acta Biomater 5:1474–1488. doi: 10.1016/j.actbio.2009.01.004

12. Kharlampieva E, Koziovskaya V, Sukhishvili SA (2009) Layer-by-layer hydrogen-bonded polymer films: From fundamentals to applications. Adv Mater 21:3053–3065. doi: 10.1002/adma.200803653

13. Lee D, Cohen RE, Rubner MF (2005) Antibacterial properties of Ag nanoparticle loaded multilayers and formation of magnetically directed antibacterial microparticles. Langmuir 21:9651–9659. doi: 10.1021/la0513306

14. Ulman A (1996) Formation and structure of self-assembled monolayers. Chem Rev 96:1533–1554. doi: 10.1021/cr9502357

15. Nuzzo RG, Allara DL (1983) Adsorption of Bifunctional Organic Disulfides on Gold Surfaces. J Am Chem Soc 105:4481–4483. doi: 10.1021/ja00351a063

16. Bain CD, Whitesides GM (1989) Formation of monolayers by the coadsorption of thiols on gold: Variation in the length of the alkyl chain. J Am Chem Soc 111:7164–7175. doi: 10.1021/ja00200a040

17. Stafford CM, Harrison C, Beers KL, et al (2004) A buckling-based metrology for measuring the elastic moduli of polymeric thin films. Nat Mater 3:545–550. doi: 10.1038/nmat1175

18. Ozaydin-Ince G, Coclite AM, Gleason KK (2012) CVD of polymeric thin films: Applications in sensors, biotechnology, microelectronics/organic electronics, microfluidics, MEMS, composites and membranes. Reports Prog Phys. doi: 10.1088/0034-4885/75/1/016501

19. Malik MA, Afzaal M, O'Brien P (2010) Precursor chemistry for main group elements in semiconducting materials. Chem Rev 110:4417–4446. doi: 10.1021/cr900406f

20. Uyama Y, Kato K, Ikada Y (1998) Surface Modification of Polymers by Grafting. In: Grafting/Characterization Tech. Model. Springer Berlin Heidelberg, Berlin, Heidelberg, pp 1–39

21. Lavanant L, Paripovic D, Schu N, et al (2009) Polymer Brushes via Surface-Initiated Controlled Radical Polymerization : Synthesis , Characterization , Properties , and Applications. 5437–5527. doi: 10.1021/cr900045a

22. Edmondson S, Osborne VL, Huck WTS (2004) Polymer brushes via surface-initiated polymerizations. Chem Soc Rev 33:14–22. doi: 10.1039/b210143m

23. Milner ST (1991) Polymer brushes. Science (80-) 251:905–914. doi: 10.1126/science.251.4996.905

24. Peterson IR (1990) Langmuir-Blodgett-Films. Phys D-Applied Phys 23:379–395.

25. Borges J, Mano JF (2014) Molecular interactions driving the layer-by-layer assembly of multilayers. Chem Rev 114:8883–8942. doi: 10.1021/cr400531v

26. Matharu Z, Bandodkar AJ, Gupta V, Malhotra BD (2012) Fundamentals and application of ordered molecular assemblies to affinity biosensing. Chem Soc Rev 41:1363–1402. doi: 10.1039/c1cs15145b

27. Hammond PT (2004) Form and function in multilayer assembly: New applications at the nanoscale. Adv Mater 16:1271–1293. doi: 10.1002/adma.200400760

28. Bertrand P, Jonas A, Laschewsky A, Legras R (2000) Ultrathin polymer coatings by complexation of polyelectrolytes at interfaces: Suitable materials, structure and properties. Macromol Rapid Commun 21:319–348. doi: 10.1002/(SICI)1521-3927(20000401)21:7<319::AID-MARC319>3.0.CO;2-7

29. Knoll W (1996) Self-assembled microstructures at interfaces. Curr Opin Colloid Interface Sci 1:137–143. doi: 10.1016/S1359-0294(96)80054-9

30. Fendler JH (1996) Self-assembled nanostructured materials. Chem Mater 8:1616–1624. doi: 10.1021/cm960116n

31. Love JC, Estroff LA, Kriebel JK, et al (2005) Self-assembled monolayers of thiolates on metals as a form of nanotechnology. Chem Rev. doi: 10.1021/cr0300789

32. Iler RK (1966) Multilayers of colloidal particles. J Colloid Interface Sci 21:569–594. doi: 10.1016/0095-8522(66)90018-3

33. Kirkland JJ (1965) Porous Thin-Layer Modified Glass Bead Supports for Gas Liquid Chromatography. Anal Chem 37:1458–1461. doi: 10.1021/ac60231a004

34. ILER RK (1964) Adsorption of Colloidal Silica on Alumina and of Colloidal Alumina on Silica. J Am Ceram Soc 47:194–198. doi: 10.1111/j.1151-2916.1964.tb14391.x

35. Decher G, Hong JD (1991) Buildup of Ultrathin Multilayer Films by a Self-Assembly Process: II. Consecutive Adsorption of Anionic and Cationic Bipolar Amphiphiles and Polyelectrolytes on Charged Surfaces. Berichte der Bunsengesellschaft für Phys Chemie 95:1430–1434. doi: 10.1002/bbpc.19910951122

36. Lvov Y, Decher G, Mohwald M (1993) Assembly, Structural Characterization, and Thermal Behavior of Layer-by-Layer Deposited Ultrathin Films of Poly(vinyl sulfate) and Poly(allylamine). Langmuir 9:481–486. doi: 10.1021/la00026a020

37. Decher G, Hong JD (1991) Buildup of Ultrathin Multilayer Films by a Self-Assembly Process: II. Consecutive Adsorption of Anionic and Cationic Bipolar Amphiphiles and Polyelectrolytes on Charged Surfaces. Berichte der Bunsengesellschaft für Phys Chemie 95:1430–1434. doi: 10.1002/bbpc.19910951122

38. Decher G, Hong J -D (1991) Buildup of ultrathin multilayer films by a self-assembly process, 1 consecutive adsorption of anionic and cationic bipolar amphiphiles on charged surfaces. Makromol Chemie Macromol Symp 46:321–327. doi: 10.1002/masy.19910460145

39. Rogach AL, Koktysh DS, Harrison M, Kotov NA (2000) Layer-by-layer assembled films of HgTe nanocrystals with strong infrared emission. Chem Mater 12:1526–1528. doi: 10.1021/cm0000649

40. Caruso F, Caruso F (2000) Hollow capsule possessing through colloidal templating and self assembly. Chem Eur J 6:413–419.

41. Shchukin DG, Patel AA, Sukhorukov GB, Lvov YM (2004) Nanoassembly of Biodegradable Microcapsules for DNA Encasing. J Am Chem Soc 126:3374–3375. doi: 10.1021/ja036952x

42. Sultan Y, Derosa MC (2011) Target binding influences permeability in aptamer-polyelectrolyte microcapsules. Small 7:1219–1226. doi: 10.1002/smll.201001829

43. Lvov Y, Haas H, Decher G, et al (1994) Successive Deposition of Alternate Layers of Polyelectrolytes and a Charged Virus. Langmuir 10:4232–4236. doi: 10.1021/la00023a052

44. Sun Y, Zhang X, Sun C, et al (1996) Supramolecular assembly of alternating

porphyrin and phthalocyanine layers based on electrostatic interactions. Chem Commun 2379–2380. doi: 10.1039/cc9960002379

45. Kleinfeld ER, Ferguson GS (1994) Stepwise formation of multilayered nanostructural films from macromolecular precursors. Science (80-) 265:370–373. doi: 10.1126/science.265.5170.370

46. Fu Y, Xu H, Bai S, et al (2002) 张希-2002-Au.pdf. 256–259.

47. Huo F, Xu H, Zhang L, et al (2003) Hydrogen-bonding based multilayer assemblies by self-deposition of dendrimer. Chem Commun 3:874–875. doi: 10.1039/b300405h

48. Zhang H, Fu Y, Wang D, et al (2003) Hydrogen-bonding-directed layer-by-layer assembly of dendrimer and poly(4-vinylpyridine) and micropore formation by post-base treatment. Langmuir 19:8497–8502. doi: 10.1021/la035036u

49. Olek M, Ostrander J, Jurga S, et al (2004) Layer-by-layer assembled composites from multiwall carbon nanotubes with different morphologies. Nano Lett 4:1889–1895. doi: 10.1021/nl048950w

50. Correa-Duarte MA, Kosiorek A, Kandulski W, et al (2005) Layer-by-layer assembly of multiwall carbon nanotubes on spherical colloids. Chem Mater 17:3268–3272. doi: 10.1021/cm047710e

51. Sun J, Sun Y, Wang Z, et al (2001) Ionic self-assembly of glucose oxidase with polycation bearing Os complex. Macromol Chem Phys 202:111–116. doi: 10.1002/1521-3935(20010101)202:1<111::AID-MACP111>3.0.CO;2-D

52. An Z, Lu G, M??hwald H, Li J (2004) Self-assembly of human serum albumin (HSA) and L-??- dimyristoylphosphatidic acid (DMPA) microcapsules for controlled drug release. Chem - A Eur J 10:5848–5852. doi: 10.1002/chem.200400090

53. Lvov Y, Decher G, Sukhorukov G (1993) Assembly of Thin Films by Means of Successive Deposition of Alternate Layers of DNA and Poly(allylamine). Macromolecules 26:5396–5399. doi: 10.1021/ma00072a016

54. Peiffer DG, Nielsen LE (1979) Preparation and mechanical properties of thick interlayer composites. J Appl Polym Sci 23:2253–2264. doi: 10.1002/app.1979.070230804

55. Iler RK (1966) Multilayers of colloidal particles. J Colloid Interface Sci 21:569–594. doi: 10.1016/0095-8522(66)90018-3

56. Peiffer DG (1979) Impact strength of thick-interlayer composites. J Appl Polym Sci 24:1451–1455. doi: 10.1002/app.1979.070240606

57. Peiffre DG, Corley TJ, Halpern GM, Brinker BA (1981) Utilization of polymeric materials in laser fusion target fabrication. Polymer (Guildf) 22:450–460. doi: 10.1016/0032-3861(81)90159-2

58. Donath E, Walther D, Shilov VN, et al (1997) Nonlinear Hairy Layer Theory of Electrophoretic Fingerprinting Applied to Consecutive Layer by Layer Polyelectrolyte Adsorption onto Charged Polystyrene Latex Particles. Langmuir 13:5294–5305. doi: 10.1021/la970090u

59. Caruso F, Lichtenfeld H, Giersig M, Mohwald H (1998) Electrostatic self-assembly of silica nanoparticle-polyelectrolyte multilayers on polystyrene latex particles [4]. J Am Chem Soc 120:8523–8524. doi: 10.1021/ja9815024

60. Sukhorukov GB, Donath E, Davis S, et al (1998) Stepwise polyelectrolyte assembly on particle surfaces: A novel approach to colloid design. Polym Adv Technol 9:759–767. doi: 10.1002/(SICI)1099-1581(1998100)9:10/11<759::AID-PAT846>3.0.CO;2-Q

61. Donath E, Sukhorukov GB, Caruso F, et al (1998) Novel Hollow Polymer Shells by Colloid-Templated Assembly of Polyelectrolytes. Angew Chemie Int Ed 37:2201–2205. doi: 10.1002/(SICI)1521-3773(19980904)37:16<2201::AID-ANIE2201>3.0.CO;2-E

62. Thomas IM (1987) Single-layer TiO_2 and multilayer TiO_2–SiO_2 optical coatings prepared from colloidal suspensions. Appl Opt 26:4688. doi: 10.1364/AO.26.004688

63. Lee SS, Hong JD, Kim CH, et al (2001) Layer-by-layer deposited multilayer assemblies of ionene-type polyelectrolytes based on the spin-coating method [2]. Macromolecules 34:5358–5360. doi: 10.1021/ma0022304

64. Zhuk A, Selin V, Zhuk I, et al (2015) Chain conformation and dynamics in spin-assisted weak polyelectrolyte multilayers. Langmuir 31:3889–3896. doi: 10.1021/acs.langmuir.5b00401

65. Campbell VE, Chiarelli PA, Kaur S, Johal MS (2005) Coadsorption of a polyanion

and an azobenzene dye in self-assembled and spin-assembled polyelectrolyte multilayers. Chem Mater 17:186–190. doi: 10.1021/cm048905p

66. Cho J, Char K, Hong JD, Lee KB (2001) Fabrication of highly ordered multilayer films using a spin self-assembly method. Adv Mater 13:1076–1078. doi: 10.1002/1521-4095(200107)13:14<1076::AID-ADMA1076>3.0.CO;2-M

67. Johal MS, Casson JL, Chiarelli PA, et al (2003) Polyelectrolyte Trilayer Combinations Using Spin-Assembly and Ionic Self-Assembly. Langmuir 19:8876–8881. doi: 10.1021/la034788l

68. Kharlampieva E, Kozlovskaya V, Chan J, et al (2009) Spin-assisted layer-by-layer assembly: Variation of stratification as studied with neutron reflectivity. Langmuir 25:14017–14024. doi: 10.1021/la9014042

69. Schmitt J, Decker G, Dressick WJ, et al (1997) Metal nanoparticle/polymer superlattice films: Fabrication and control of layer structure. Adv Mater 9:61–65. doi: 10.1002/adma.19970090114

70. Schlenoff JB, Dubas ST, Farhat T (2000) Sprayed polyelectrolyte multilayers. Langmuir 16:9968–9969. doi: 10.1021/la001312i

71. Izquierdo A, Ono SS, Voegel JC, et al (2005) Dipping versus spraying: Exploring the deposition conditions for speeding up layer-by-layer assembly. Langmuir 21:7558–7567. doi: 10.1021/la047407s

72. Mulhearn WD, Kim DD, Gu Y, Lee D (2012) Facilitated transport enhances spray layer-by-layer assembly of oppositely charged nanoparticles. Soft Matter 8:10419–10427. doi: 10.1039/c2sm26456k

73. Merrill MH, Sun CT (2009) Fast, simple and efficient assembly of nanolayered materials and devices. Nanotechnology. doi: 10.1088/0957-4484/20/7/075606

74. Kyung KH, Shiratori S (2011) Nanoscale texture control of polyelectrolyte multilayer using spray layer-by-layer method. Jpn J Appl Phys. doi: 10.1143/JJAP.50.025602

75. Félix O, Zheng Z, Cousin F, Decher G (2009) Are sprayed LbL-films stratified? A first assessment of the nanostructure of spray-assembled multilayers by neutron reflectometry. Comptes Rendus Chim 12:225–234. doi: 10.1016/j.crci.2008.09.009

76. Krogman KC, Lowery JL, Zacharia NS, et al (2009) Spraying asymmetry into

functional membranes layer-by-layer. Nat Mater 8:512–518. doi: 10.1038/nmat2430

77. Gittleson FS, Hwang D, Ryu WH, et al (2015) Ultrathin Nanotube/Nanowire Electrodes by Spin-Spray Layer-by-Layer Assembly: A Concept for Transparent Energy Storage. ACS Nano 9:10005–10017. doi: 10.1021/acsnano.5b03578

78. Krogman KC, Zacharia NS, Schroeder S, Hammond PT (2007) Automated process for improved uniformity and versatility of layer-by-layer deposition. Langmuir 23:3137–3141. doi: 10.1021/la063085b

79. Gittleson FS, Kohn DJ, Li X, Taylor AD (2012) Improving the assembly speed, quality, and tunability of thin conductive multilayers. ACS Nano 6:3703–3711. doi: 10.1021/nn204384f

80. Lefort M, Popa G, Seyrek E, et al (2010) Spray-on organic/inorganic films: A general method for the formation of functional nano- to microscale coatings. Angew Chemie - Int Ed 49:10110–10113. doi: 10.1002/anie.201002729

81. Wertz CF, Santore MM (2002) Adsorption and reorientation kinetics of lysozyme on hydrophobic surfaces. Langmuir 18:1190–1199. doi: 10.1021/la0108813

82. Dubas ST, Schlenoff JB (2001) Swelling and smoothing of polyelectrolyte multilayers by salt. Langmuir 17:7725–7727. doi: 10.1021/la0112099

83. Decher G, Lvov Y, Schmitt J (1994) Proof of multilayer structural organization in self-assembled polycation-polyanion molecular films. Thin Solid Films 244:772–777. doi: 10.1016/0040-6090(94)90569-X

84. Shen L, Hu N (2005) Electrostatic adsorption of heme proteins alternated with polyamidoamine dendrimers for layer-by-layer assembly of electroactive films. Biomacromolecules 6:1475–1483. doi: 10.1021/bm049248x

85. Silva JM, Duarte ARC, Custódio CA, et al (2014) Nanostructured Hollow Tubes Based on Chitosan and Alginate Multilayers. Adv Healthc Mater 3:433–440. doi: 10.1002/adhm.201300265

86. Hyder MN, Lee SW, Cebeci FÇ, et al (2011) Layer-by-layer assembled polyaniline nanofiber/multiwall carbon nanotube thin film electrodes for high-power and high-energy storage applications. ACS Nano 5:8552–8561. doi: 10.1021/nn2029617

87. Wang HL, Sun Q, Chen M, et al (2011) Layer-by-layer assembly and characterization

of multilayers of a manganese porphyrin linked poly(4-vinylpyridinium) derivative and poly(styrenesulfonic acid-o-maleic) acid. Langmuir 27:9880–9889. doi: 10.1021/la2022165

88. Kim JY, DeRocher JP, Mao P, et al (2010) Formation of nanoparticle-containing multilayers in nanochannels via layer-by-layer assembly. Chem Mater 22:6409–6415. doi: 10.1021/cm1025816

89. Chen L, Bromberg L, Lee JA, et al (2010) Multifunctional electrospun fabrics via layer-by-layer electrostatic assembly for chemical and biological protection. Chem Mater 22:1429–1436. doi: 10.1021/cm902834a

90. Zhu Y, Tour JM (2010) Graphene nanoribbon thin films using layer-by-layer assembly. Nano Lett 10:4356–4362. doi: 10.1021/nl101695g

91. Kim J, Lee SW, Hammond PT, Shao-Horn Y (2009) Electrostatic layer-by-layer assembled au nanoparticle/MWNT thin films: Microstructure, optical property, and electrocatalytic activity for methanol oxidation. Chem Mater 21:2993–3001. doi: 10.1021/cm900688r

92. Shen J, Hu Y, Li C, et al (2009) Layer-by-layer self-assembly of graphene nanoplatelets. Langmuir 25:6122–6128. doi: 10.1021/la900126g

93. Crouzier T, Picart C (2009) Containing Polysaccharides. Society 433–442.

94. Lee SW, Kim BS, Chen S, et al (2009) Layer-by-layer assembly of all carbon nanotube ultrathin films for electrochemical applications. J Am Chem Soc 131:671–679. doi: 10.1021/ja807059k

95. Wågberg L, Decher G, Norgren M, et al (2008) The build-up of polyelectrolyte multilayers of microfibrillated cellulose and cationic polyelectrolytes. Langmuir 24:784–795. doi: 10.1021/la702481v

96. Findenig G, Kargl R, Stana-Kleinschek K, Ribitsch V (2013) Interaction and structure in polyelectrolyte/clay multilayers: A QCM-D study. Langmuir 29:8544–8553. doi: 10.1021/la400880a

97. Kharlampieva E, Izumrudov VA, Sukhishvili SA (2007) Electrostatic layer-by-layer self-assembly of poly(carboxybetaine)s: Role of zwitterions in film growth. Macromolecules 40:3663–3668. doi: 10.1021/ma062811e

98. Xing Q, Eadula SR, Lvov YM (2007) Cellulose fiber-enzyme composites fabricated through layer-by-layer nanoassembly. Biomacromolecules 8:1987–1991. doi: 10.1021/bm070125x

99. Stricker JT, Gudmundsdóttir AD, Smith AP, et al (2007) Fabrication of Organic Thin-Film Transistors Using Layer-by-Layer Assembly. J Phys Chem B 111:6322–6326. doi: 10.1021/jp0688862

100. Matsumura S, Hlil AR, Lepiller C, et al (2008) Ionomers for proton exchange membrane fuel cells with sulfonic acid groups on the end-groups: Novel branched poly(ether-ketone)s. Am Chem Soc Polym Prepr Div Polym Chem 49:511–512. doi: 10.1002/pola

101. Croll TI, O'Connor AJ, Stevens GW, Cooper-White JJ (2006) A blank slate? Layer-by-layer deposition of hyaluronic acid and chitosan onto various surfaces. Biomacromolecules 7:1610–1622. doi: 10.1021/bm060044l

102. Paloniemi H, Lukkarinen M, Ääritalo T, et al (2006) Layer-by-layer electrostatic self-assembly of single-wall carbon nanotube polyelectrolytes. Langmuir 22:74–83. doi: 10.1021/la051736i

103. Liu H, Hu N (2006) Interaction between myoglobin and hyaluronic acid in their layer-by-layer assembly: Quartz crystal microbalance and cyclic voltammetry studies. J Phys Chem B 110:14494–14502. doi: 10.1021/jp061271k

104. Zhang H, Lu H, Hu N (2006) Fabrication of electroactive layer-by-layer films of myoglobin with gold nanoparticles of different sizes. J Phys Chem B 110:2171–2179. doi: 10.1021/jp055301f

105. Serizawa T, Matsukuma D, Akashi M (2005) Loading and release of charged dyes using ultrathin hydrogels. Langmuir 21:7739–7742. doi: 10.1021/la0505263

106. He P, Hu N (2004) Interactions between heme proteins and dextran sulfate in layer-by-layer assembly films. J Phys Chem B 108:13144–13152. doi: 10.1021/jp049974u

107. Jin H, Choi S, Velu R, et al (2012) Preparation of multilayered cdse quantum dot sensitizers by electrostatic layer-by-layer assembly and a series of post-treatments toward efficient quantum dot-sensitized mesoporous TiO2solar cells. Langmuir 28:5417–5426. doi: 10.1021/la202892h

108. Artyukhin AB, Bakajin O, Stroeve P, Noy A (2004) Layer-by-Layer Electrostatic

Self-Assembly of Polyelectrolyte Nanoshells on Individual Carbon Nanotube Templates. Langmuir 20:1442–1448. doi: 10.1021/la035699b

109. Serizawa T, Kawanishi N, Akashi M (2003) Layer-by-layer assembly between poly(vinylamine hydrochloride-co-N-vinylformamide) with variable primary amine content and poly(sodium styrenesulfonate). Macromolecules 36:1967–1974. doi: 10.1021/ma020734r

110. Constantine CA, Mello S V., Dupont A, et al (2003) Layer-by-layer self-assembled chitosan/poly(thiophene-3-acetic acid) and organophosphorus hydrolase multilayers. J Am Chem Soc 125:1805–1809. doi: 10.1021/ja028691h

111. Khopade AJ, Caruso F (2002) Investigation of the factors influencing the formation of dendrimer/polyanion multilayer films. Langmuir 18:7669–7676. doi: 10.1021/la020251g

112. Shi X, Cassagneau T, Caruso F (2002) Electrostatic interactions between polyelectrolytes and a titania precursor: Thin film and solution studies. Langmuir 18:904–910. doi: 10.1021/la011310d

113. Ai H, Fang M, Jones SA, Lvov YM (2002) Electrostatic layer-by-layer nanoassembly on biological microtemplates: Platelets. Biomacromolecules 3:560–564. doi: 10.1021/bm015659r

114. He P, Hu N, Zhou G (2002) Assembly of electroactive layer-by-layer films of hemoglobin and polycationic poly(diallyldimethylammonium). Biomacromolecules 3:139–146. doi: 10.1021/bm015599p

115. Sasaki T, Ebina Y, Tanaka T, et al (2001) Layer-by-layer assembly of titania nanosheet/polycation composite films. Chem Mater 13:4661–4667. doi: 10.1021/cm010478h

116. Anzai JI, Hoshi T, Nakamura N (2000) Construction of multilayer thin films containing avidin by a layer-by-layer deposition of avidin and poly(anion)s. Langmuir 16:6306–6311. doi: 10.1021/la000353b

117. Ladam G, Gergely C, Senger B, et al (2000) Protein interactions with polyelectrolyte multilayers: Interactions between human serum albumin and polystyrene sulfonate/polyallylamine multilayers. Biomacromolecules 1:674–687. doi: 10.1021/bm005572q

118. Komatsu T (2012) Protein-based nanotubes for biomedical applications. Nanoscale 4:1910–1918. doi: 10.1039/c1nr11224d

119. Kurth DG, Caruso F, Schüler C (1999) Giant self-contained metallosupramolecular entities. Chem Commun 16:1579–1580. doi: 10.1039/a905115e

120. He J, Samuelson L, Li L, et al (1998) Oriented Bacteriorhodopsin / Polycation Multilayers by Electrostatic Layer-by-Layer Assembly. J Phys Chem B 102:7067–7072. doi: 10.1021/la971336y

121. Lvov Y, Ariga K, Onda M, et al (1997) Alternate Assembly of Ordered Multilayers of SiO_2 and Other Nanoparticles and Polyions. Langmuir 13:6195–6203. doi: 10.1021/la970517x

122. Ariga K, Lvov Y, Kunitake T (1997) Assembling alternate dye-polyion molecular films by electrostatic layer-by-layer adsorption. J Am Chem Soc 119:2224–2231. doi: 10.1021/ja963442c

123. Torkkeli A (2003) Droplet microfluidics on a planar surface. VTT Publ 57:3–194. doi: 10.1002/aic

124. Tettey KE, Ho JWC, Lee D (2011) Modulating Layer-by-layer assembly of oppositely charged nanoparticles using a short amphiphilic molecule. J Phys Chem C 115:6297–6304. doi: 10.1021/jp112386n

125. Mulligan K, Jakubek ZJ, Johnston LJ (2011) Supported lipid bilayers on biocompatible polysaccharide multilayers. Langmuir 27:14352–14359. doi: 10.1021/la203207p

126. Dey S, Pal AJ (2011) Layer-by-layer electrostatic assembly with a control over orientation of molecules: Anisotropy of electrical conductivity and dielectric properties. Langmuir 27:8687–8693. doi: 10.1021/la201471f

127. Martins G V., Mano JF, Alves NM (2011) Dual responsive nanostructured surfaces for biomedical applications. Langmuir 27:8415–8423. doi: 10.1021/la200832n

128. Schoeler B, Kumaraswamy G, Caruso F (2002) Investigation of the influence of polyelectrolyte charge density on the growth of multilayer thin films prepared by the layer-by-layer technique. Macromolecules 35:889–897. doi: 10.1021/ma011349p

129. Hoogeveen NG, Cohen Stuart MA, Fleer GJ, Böhmer MR (1996) Formation and

Stability of Multilayers of Polyelectrolytes. Langmuir 12:3675–3681. doi: 10.1021/la951574y

130. Kolarik L, Furlong DN, Joy H, et al (1999) Building assemblies from high molecular weight polyelectrolytes. Langmuir 15:8265–8275. doi: 10.1021/la990413h

131. Schoeler B, Sharpe S, Hatton TA, Caruso F (2004) Polyelectrolyte multilayer films of different charge density copolymers with synergistic nonelectrostatic interactions prepared by the layer-by-layer technique. Langmuir 20:2730–2738. doi: 10.1021/la035909k

132. Cochin D, Passmann M, Wilbert G, et al (1997) Layered nanostructures with LC-polymers, polyelectrolytes, and inorganics. Macromolecules 30:4775–4779. doi: 10.1021/ma970162o

133. Chung AJ, Rubner MF (2002) Methods of loading and releasing low molecular weight cationic molecules in weak polyelectrolyte multilayer films. Langmuir 18:1176–1183. doi: 10.1021/la010873m

134. Wood KC, Boedicker JQ, Lynn DM, Hammond PT (2005) Tunable drug release from hydrolytically degradable layer-by-layer thin films. Langmuir 21:1603–1609. doi: 10.1021/la0476480

135. Lynn DM (2007) Peeling back the layers: Controlled erosion and triggered disassembly of multilayered polyelectrolyte thin films. Adv Mater 19:4118–4130. doi: 10.1002/adma.200701748

136. Jiang S, Chen X, Liu M (2004) The pH stimulated reversible loading and release of a cationic dye in a layer-by-layer assembled DNA/PAH film. J Colloid Interface Sci 277:396–403. doi: 10.1016/j.jcis.2004.04.008

137. Burke SE, Barrett CJ (2004) pH-dependent loading and release behavior of small hydrophilic molecules in weak polyelectrolyte multilayer films. Macromolecules 37:5375–5384. doi: 10.1021/ma049445o

138. Müller M, Kessler B, Adler HJ, Lunkwitz K (2004) Reversible switching of protein uptake and release at polyelectrolyte multilayers detected by ATR-FTIR spectroscopy. Macromol Symp 210:157–164. doi: 10.1002/masy.200450618

139. Vázquez E, Dewitt DM, Hammond PT, Lynn DM (2002) Construction of hydrolytically-degradable thin films via layer-by-layer deposition of degradable

polyelectrolytes. J Am Chem Soc 124:13992–13993. doi: 10.1021/ja026405w

140. Dubas ST, Farhat TR, Schlenoff JB (2001) Multiple Membranes from Polyelectrolyte Multilayers. J Am Chem Soc 123:5368–5369. doi: 10.1021/ja015774+

141. Mendelsohn JD, Barrett CJ, Chan V V., et al (2000) Fabrication of microporous thin films from polyelectrolyte multilayers. Langmuir 16:5017–5023. doi: 10.1021/la000075g

142. Delcea M, Möhwald H, Skirtach AG (2011) Stimuli-responsive LbL capsules and nanoshells for drug delivery. Adv Drug Deliv Rev 63:730–747. doi: 10.1016/j.addr.2011.03.010

143. Schwarz B, Schönhoff M (2002) Surface potential driven swelling of polyelectrolyte multilayers. Langmuir 18:2964–2966. doi: 10.1021/la015636y

144. Dubas ST, Schlenoff JB (2001) Polyelectrolyte multilayers containing a weak polyacid: Construction and deconstruction. Macromolecules 34:3736–3740. doi: 10.1021/ma001720t

145. Büscher K, Graf K, Ahrens H, Helm CA (2002) Influence of adsorption conditions on the structure of polyelectrolyte multilayers. Langmuir 18:3585–3591. doi: 10.1021/la011682m

146. Schüler C, Caruso F (2001) Decomposable hollow biopolymer-based capsules. Biomacromolecules 2:921–926. doi: 10.1021/bm010052w

147. Ibarz G, Dähne L, Donath E, Möhwald H (2001) Smart micro- and nanocontainers for storage, transport, and release. Adv Mater 13:1324–1327. doi: 10.1002/1521-4095(200109)13:17<1324::AID-ADMA1324>3.0.CO;2-L

148. Kovacevic D, Van der Burgh S, De Keizer A, Cohen Stuart MA (2002) Kinetics of formation and dissolution of weak polyelectrolyte multilayers: Role of salt and free polyions. Langmuir 18:5607–5612. doi: 10.1021/la025639q

149. Antipov AA, Sukhorukov GB, Möhwald H (2003) Influence of the ionic strength on the polyelectrolyte multilayers' permeability. Langmuir 19:2444–2448. doi: 10.1021/la026101n

150. Gao M, Sun J, Dulkeith E, et al (2002) Lateral patterning of CdTe nanocrystal films by the electric field directed layer-by-layer assembly method. Langmuir 18:4098–

4102. doi: 10.1021/la015599a

151. Cho C, Jeon JW, Lutkenhaus J, Zacharia NS (2013) Electric field induced morphological transitions in polyelectrolyte multilayers. ACS Appl Mater Interfaces 5:4930–4936. doi: 10.1021/am400667y

152. Ko YH, Kim YH, Park J, et al (2011) Electric-field-assisted layer-by-layer assembly of weakly charged polyelectrolyte multilayers. Macromolecules 44:2866–2872. doi: 10.1021/ma102112a

153. Zhang G, Dai L, Zhang L, Ji S (2011) Effects of external electric field on film growth, morphology, and nanostructure of polyelectrolyte and nanohybrid multilayers onto insulating substrates. Langmuir 27:2093–2098. doi: 10.1021/la104120b

154. Schmidt DJ, Moskowitz JS, Hammond PT (2010) Electrically triggered release of a small molecule drug from a polyelectrolyte multilayer coating. Chem Mater 22:6416–6425. doi: 10.1021/cm102578j

155. Boulmedais F, Tang CS, Keller B, Vörös J (2006) Controlled electrodissolution of polyelectrolyte multilayers: A platform technology towards the surface-initiated delivery of drugs. Adv Funct Mater 16:63–70. doi: 10.1002/adfm.200400406

156. Yamauchi F, Kato K, Iwata H (2005) Layer-by-layer assembly of poly(ethyleneimine) and plasmid DNA onto transparent indium-tin oxide electrodes for temporally and spatially specific gene transfer. Langmuir 21:8360–8367. doi: 10.1021/la0505059

157. Shi L, Lu Y, Sun J, et al (2003) Site-selective lateral multilayer assembly of bienzyme with polyelectrolyte on ITO electrode based on electric field-induced directly layer-by-layer deposition. Biomacromolecules 4:1161–1167. doi: 10.1021/bm030003e

158. Sun J, Gao M, Zhu M, et al (2002) Layer-by-layer depositions of polyelectrolyte/CdTe nanocrystal films controlled by electric fields. J Mater Chem 12:1775–1778. doi: 10.1039/b111013f

159. Skirtach AG, Antipov AA, Shchukin DG, Sukhorukov GB (2004) Remote activation of capsules containing Ag nanoparticles and IR dye by laser light. Langmuir 20:6988–6992. doi: 10.1021/la048873k

160. Angelatos AS, Radt B, Caruso F (2005) Light-responsive polyelectrolyte/gold nanoparticle microcapsules. J Phys Chem B 109:3071–3076. doi: 10.1021/jp045070x

161. Katagiri K, Matsuda A, Caruso F (2006) Effect of UV-irradiation on polyelectrolyte multilayered films and hollow capsules prepared by layer-by-layer assembly. Macromolecules 39:8067–8074. doi: 10.1021/ma0615598

162. Nagaoka Y, Shiratori S, Einaga Y (2008) Photo-control of adhesion properties by detachment of the outermost layer in layer-by-layer assembled multilayer films of Preyssler-type polyozometalate and polyethyleneimine. Chem Mater 20:4004–4010. doi: 10.1021/cm800370f

163. Wang Y, Han P, Wu G, et al (2010) Selectively erasable multilayer thin film by photoinduced disassembly. Langmuir 26:9736–9741. doi: 10.1021/la1004648

164. Bédard MF, De Geest BG, Skirtach AG, et al (2010) Polymeric microcapsules with light responsive properties for encapsulation and release. Adv Colloid Interface Sci 158:2–14. doi: 10.1016/j.cis.2009.07.007

165. Pennakalathil J, Hong JD (2011) Self-standing polyelectrolyte multilayer films based on light-triggered disassembly of a sacrificial layer. ACS Nano 5:9232–9237. doi: 10.1021/nn203490q

166. Tan HL, McMurdo MJ, Pan G, Van Patten PG (2003) Temperature Dependence of Polyelectrolyte Multilayer Assembly. Langmuir 19:9311–9314. doi: 10.1021/la035094f

167. Mertz D, Hemmerlé J, Mutterer J, et al (2007) Mechanically responding nanovalves based on polyelectrolyte multilayers. Nano Lett 7:657–662. doi: 10.1021/nl062657+

168. Mertz D, Hemmerlé J, Boulmedais F, et al (2007) Polyelectrolyte multilayer films under mechanical stretch. Soft Matter 3:1413. doi: 10.1039/b710305k

169. Han L, Wang L, Chia KK, et al (2011) Geometrically controlled mechanically responsive polyelectrolyte tube arrays. Adv Mater 23:4667–4673. doi: 10.1002/adma.201102917

170. Mertz D, Vogt C, Hemmerlé J, et al (2009) Mechanotransductive surfaces for reversible biocatalysis activation. Nat Mater 8:731–735. doi: 10.1038/nmat2504

171. Serizawa T, Yamaguchi M, Akashi M (2003) Time-controlled desorption of ultrathin polymer films triggered by enzymatic degradation. Angew Chemie - Int Ed 42:1115–1118. doi: 10.1002/anie.200390293

172. Picart C, Schneider A, Etienne O, et al (2005) Controlled degradability of polysaccharide multilayer films in vitro and in vivo. Adv Funct Mater 15:1771–1780. doi: 10.1002/adfm.200400588

173. Abdelkebir K, Gaudière F, Morin-Grognet S, et al (2011) Protein-triggered instant disassembly of biomimetic layer-by-layer films. Langmuir 27:14370–14379. doi: 10.1021/la2033109

174. Becker AL, Johnston APR, Caruso F (2010) Peptide Nucleic Acid Films and Capsules: Assembly and Enzymatic Degradation. Macromol Biosci n/a-n/a. doi: 10.1002/mabi.200900347

175. Ren K, Ji J, Shen J (2006) Construction and enzymatic degradation of multilayered poly-L-lysine/DNA films. Biomaterials 27:1152–1159. doi: 10.1016/j.biomaterials.2005.07.021

176. Rahim MA, Choi WS, Lee HJ, Jeon IC (2010) Ionic surfactant-triggered renewal of the structures and properties of polyelectrolyte multilayer films. Langmuir 26:4680–4686. doi: 10.1021/la9035634

177. Ochs CJ, Such GK, Yan Y, et al (2010) Biodegradable click capsules with engineered drug-loaded multilayers. ACS Nano 4:1653–1663. doi: 10.1021/nn9014278

178. Zhang Y, Guan Y, Yang S, et al (2003) Fabrication of hollow capsules based on hydrogen bonding. Adv Mater 15:832–835. doi: 10.1002/adma.200304315

179. Kharlampieva E, Sukhishvili SA (2006) Hydrogen-bonded layer-by-layer polymer films. Polym Rev 46:377–395. doi: 10.1080/15583720600945386

180. Decher G, Schlenoff JB (2012) Multilayer Thin Films: Sequential Assembly of Nanocomposite Materials: Second Edition. Multilayer Thin Film Seq Assem Nanocomposite Mater Second Ed. doi: 10.1002/9783527646746

181. Guan Y, Yang S, Zhang Y, et al (2006) Fabry-perot fringes and their application to study the film growth, chain rearrangement, and erosion of hydrogen-bonded PVPON/PAA films. J Phys Chem B 110:13484–13490. doi: 10.1021/jp061548g

182. Quinn JF, Caruso F (2005) Thermoresponsive nanoassemblies: Layer-by-layer assembly of hydrophilic-hydrophobic alternating copolymers. Macromolecules 38:3414–3419. doi: 10.1021/ma047414n

183. Quinn JF, Caruso F (2004) Facile Tailoring of Film Morphology and Release Properties Using Layer-by-Layer Assembly of Thermoresponsive Materials. Langmuir 20:20–22. doi: 10.1021/la0360310

184. Zhuk A, Pavlukhina S, Sukhishvili SA (2009) Hydrogen-bonded layer-by-layer temperature-triggered release films. Langmuir 25:14025–14029. doi: 10.1021/la901478v

185. Chu LY, Li Y, Zhu JH, Chen WM (2005) Negatively thermoresponsive membranes with functional gates driven by zipper-type hydrogen-bonding interactions. Angew Chemie - Int Ed 44:2124–2127. doi: 10.1002/anie.200462687

186. Yang S, Zhang Y, Guan Y, et al (2006) Water uptake behavior of hydrogen-bonded PVPON-PAA LBL film. Soft Matter 2:699–704. doi: 10.1039/b606923a

187. Seo J, Lutkenhaus JL, Kim J, et al (2008) Effect of the layer-by-layer (LbL) deposition method on the surface morphology and wetting behavior of hydrophobically modified PEO and PAA LbL films. Langmuir 24:7995–8000. doi: 10.1021/la800906x

188. Caruso F, Schüler C, Kurth DG (1999) Core-shell particles and hollow shells containing metallo-supramolecular components. Chem Mater 11:3394–3399. doi: 10.1021/cm9911058

189. Caruso F, Caruso RA, Möhwald H (1998) Nanoengineering of inorganic and hybrid hollow spheres by colloidal templating. Science (80-) 282:1111–1114. doi: 10.1126/science.282.5391.1111

190. Becker AL, Johnston APR, Caruso F (2010) Layer-by-layer-assembled capsules and films for therapeutic delivery. Small 6:1836–1852. doi: 10.1002/smll.201000379

191. Lee D, Rubner MF, Cohen RE (2005) Formation of nanoparticle-loaded microcapsules based on hydrogen-bonded multilayers. Chem Mater 17:1099–1105. doi: 10.1021/cm048441v

192. Schuetz P, Caruso F (2003) Copper-Assisted Weak Polyelectrolyte Multilayer Formation on Microspheres and Subsequent Film Crosslinking. Adv Funct Mater 13:929–937. doi: 10.1002/adfm.200304483

193. Yu A, Wang Y, Barlow E, Caruso F (2005) Mesoporous silica particles as templates for preparing enzyme-loaded biocompatible microcapsules. Adv Mater 17:1737–1741. doi: 10.1002/adma.200402045

194. Volodkin D V., Larionova NI, Sukhorukov GB (2004) Protein encapsulation via porous CaCO3 microparticles templating. Biomacromolecules 5:1962–1972. doi: 10.1021/bm049669e

195. Antipov AA, Shchukin D, Fedutik Y, et al (2003) Carbonate microparticles for hollow polyelectrolyte capsules fabrication. Colloids Surfaces A Physicochem Eng Asp 224:175–183. doi: 10.1016/S0927-7757(03)00195-X

196. Gaponik N, Radtchenko IL, Gerstenberger MR, et al (2003) Labeling of biocompatible polymer microcapsules with near-infrared emitting nanocrystals. Nano Lett 3:369–372. doi: 10.1021/nl0259333

197. Donath E, Moya S, Neu B, et al (2002) Hollow polymer shells from biological templates: Fabrication and potential applications. Chem - A Eur J 8:5481–5485. doi: 10.1002/1521-3765(20021202)8:23<5481::AID-CHEM5481>3.0.CO;2-8

198. Shenoy DB, Antipov AA, Sukhorukov GB, M??hwald H (2003) Layer-by-layer engineering of biocompatible, decomposable core-shell structures. Biomacromolecules 4:265–272. doi: 10.1021/bm025661y

199. Priest C, Quinn A, Postma A, et al (2008) Microfluidic polymer multilayer adsorption on liquid crystal droplets for microcapsule synthesis. Lab Chip 8:2182–2187. doi: 10.1039/b808826h

200. Tjipto E, Cadwell KD, Quinn JF, et al (2006) Tailoring the interfaces between nematic liquid crystal emulsions and aqueous phases via layer-by-layer assembly. Nano Lett 6:2243–2248. doi: 10.1021/nl061604p

201. Shchukin DG, Köhler K, Möhwald H, Sukhorukov GB (2005) Gas-filled polyelectrolyte capsules. Angew Chemie - Int Ed 44:3310–3314. doi: 10.1002/anie.200462889

202. Sukhorukov GB, Volodkin D V., Günther AM, et al (2004) Porous calcium carbonate microparticles as templates for encapsulation of bioactive compounds. J Mater Chem 14:2073–2081. doi: 10.1039/b402617a

203. Quinn JF, Johnston APR, Such GK, et al (2007) Next generation, sequentially assembled ultrathin films: Beyond electrostatics. Chem Soc Rev 36:707–718. doi: 10.1039/b610778h

204. Kozlovskaya V, Ok S, Sousa A, et al (2003) Hydrogen-bonded polymer capsules

formed by layer-by-layer self-assembly. Macromolecules 36:8590–8592. doi: 10.1021/ma035084l

205. Such GK, Johnston APR, Caruso F (2011) Engineered hydrogen-bonded polymer multilayers: From assembly to biomedical applications. Chem Soc Rev 40:19–29. doi: 10.1039/c0cs00001a

206. Bergbreiter DE, Liao KS (2009) Covalent layer-by-layer assembly - An effective, forgiving way to construct functional robust ultrathin films and nanocomposites. Soft Matter 5:23–28. doi: 10.1039/b810852h

207. Johnston APR, Caruso F (2007) Exploiting the directionality of DNA: Controlled shrinkage of engineered oligonucleotide capsules. Angew Chemie - Int Ed 46:2677–2680. doi: 10.1002/anie.200605135

208. Cavalieri F, Ng SL, Mazzuca C, et al (2011) Thin multilayer films and microcapsules containing DNA quadruplex motifs. Small 7:101–111. doi: 10.1002/smll.201001246

209. Johnston APR, Caruso F (2008) Stabilization of DNA multilayer films through oligonucleotide crosslinking. Small 4:612–618. doi: 10.1002/smll.200700813

210. Johnston APR, Lee L, Wang Y, Caruso F (2009) Controlled degradation of dna capsules with engineered restriction-enzyme cut sites. Small 5:1418–1421. doi: 10.1002/smll.200900075

211. Johnston APR, Mitomo H, Read ES, Caruso F (2006) Compositional and Structural Engineering of DNA Multilayer Films. Langmuir 22:3251–3258. doi: 10.1021/la052581h

212. Johnston APR, Read ES, Caruso F (2005) DNA multilayer films on planar and colloidal supports: Sequential assembly of like-charged polyelectrolytes. Nano Lett 5:953–956. doi: 10.1021/nl050608b

213. Kida T, Mouri M, Akashi M (2006) Fabrication of hollow capsules composed of poly(methyl methacrylate) stereocomplex films. Angew Chemie - Int Ed 45:7534–7536. doi: 10.1002/anie.200602116

214. Serizawa T, Hamada K, Akashi M (2004) Polymerization within a molecular- scale stereoregular template. Nature 429:52–55. doi: 10.1038/nature02495.1.

215. Shchepelina O, Drachuk I, Gupta MK, et al (2011) Silk-on-silk layer-by-layer

microcapsules. Adv Mater 23:4655–4660. doi: 10.1002/adma.201102234

216. Li C, Luo GF, Wang HY, et al (2011) Host-guest assembly of pH-responsive degradable microcapsules with controlled drug release behavior. J Phys Chem C 115:17651–17659. doi: 10.1021/jp203940s

217. Xiao W, Chen WH, Zhang J, et al (2011) Design of a photoswitchable hollow microcapsular drug delivery system by using a supramolecular drug-loading approach. J Phys Chem B 115:13796–13802. doi: 10.1021/jp208692c

218. Wang Z, Feng Z, Gao C (2008) Stepwise assembly of the same poly electrolytes using host-guest interaction to obtain microcapsules with multiresponsive properties. Chem Mater 20:4194–4199. doi: 10.1021/cm8003358

219. Zhang Y, Guan Y, Yang S, et al (2003) Fabrication of hollow capsules based on hydrogen bonding. Adv Mater 15:832–835. doi: 10.1002/adma.200304315

220. Feng Z, Wang Z, Gao C, Shen J (2007) Template polymerization to fabricate hydrogen-bonded poly(acrylic acid)/poly(vinylpyrrolidone) hollow microcapsules with a pH-mediated swelling-deswelling property. Chem Mater 19:4648–4657. doi: 10.1021/cm070042n

221. Yang SY, Lee D, Cohen RE, Rubner MF (2004) Bioinert solution-cross-linked hydrogen-bonded multilayers on colloidal particles. Langmuir 20:5978–5981. doi: 10.1021/la0490442

222. Guan Y, Zhang Y, Zhou T, Zhou S (2009) Stability of hydrogen-bonded hydroxypropylcellulose/poly(acrylic acid) microcapsules in aqueous solutions. Soft Matter 5:842–849. doi: 10.1039/b815913k

223. Kozlovskaya V, Shamaev A, Sukhishvili SA (2008) Tuning swelling pH and permeability of hydrogel multilayer capsules. Soft Matter 4:1499–1507. doi: 10.1039/b719952j

224. Kharlampieva E, Kozlovskaya V, Tyutina J, Sukhishvili SA (2005) Hydrogen-bonded multilayers of thermoresponsive polymers. Macromolecules 38:10523–10531. doi: 10.1021/ma0516891

225. Paramasivam G, Vergaelen M, Ganesh MR, et al (2017) Hydrogen bonded capsules by layer-by-layer assembly of tannic acid and poly(2-: N -propyl-2-oxazoline) for encapsulation and release of macromolecules. J Mater Chem B 5:8967–8974. doi:

10.1039/c7tb02284k

226. Skirtach AG, De Geest BG, Mamedov A, et al (2007) Ultrasound stimulated release and catalysis using polyelectrolyte multilayer capsules. J Mater Chem 17:1050–1054. doi: 10.1039/b609934c

227. Caruso F, Spasova M, Susha A, et al (2001) Magnetic nanocomposite particles and hollow spheres constructed by a sequential layering approach. Chem Mater 13:109–116. doi: 10.1021/cm001164h

228. Kempe K, Ng SL, Noi KF, et al (2013) Clickable poly(2-oxazoline) architectures for the fabrication of low-fouling polymer capsules. ACS Macro Lett 2:1069–1072. doi: 10.1021/mz400522e

229. Kempe K, Ng SL, Gunawan ST, et al (2014) Intracellularly degradable hydrogen-bonded polymer capsules. Adv Funct Mater 24:6187–6194. doi: 10.1002/adfm.201401397

230. Kim BS, Park SW, Hammond PT (2008) Hydrogen-bonding layer-by-layer-assembled biodegradable polymeric micelles as drug delivery vehicles from surfaces. ACS Nano 2:386–392. doi: 10.1021/nn700408z

231. Stadler B, Chandrawati R, Price AD, et al (2009) A microreactor with thousands of subcompartments: Enzyme-loaded liposomes within polymer capsules. Angew Chemie - Int Ed 48:4359–4362. doi: 10.1002/anie.200900386

232. Hosta-Rigau L, Stadler B, Yan, et al (2010) Capsosomes with multilayered subcompartments: Assembly and loading with hydrophobic Cargo. Adv Funct Mater 20:59–66. doi: 10.1002/adfm.200901297

233. Wang A, Tao C, Cui Y, et al (2009) Assembly of environmental sensitive microcapsules of PNIPAAm and alginate acid and their application in drug release. J Colloid Interface Sci 332:271–279. doi: 10.1016/j.jcis.2008.12.032

234. Sivakumar S, Bansal V, Cortez C, et al (2009) Degradable, surfactant-free, monodisperse polymer-encapsulated emulsions as anticancer drug carriers. Adv Mater 21:1820–1824. doi: 10.1002/adma.200802475

235. Zelikin AN, Becker AL, Johnston APR, et al (2007) A general approach for DNA encapsulation in degradable polymer microcapsules. ACS Nano 1:63–69. doi: 10.1021/nn700063w

236. Sexton A, Whitney PG, Chong S, et al (2009) ARTICLE A Protective Vaccine Delivery System for. 3:3391–3400.

237. Caruso F, Trau D, Möhwald H, Renneberg R (2000) Enzyme encapsulation in layer-by-layer engineered polymer multilayer capsules. Langmuir 16:1485–1488. doi: 10.1021/la991161n

238. Erel-Unal I, Sukhishvili SA (2008) Hydrogen-bonded multilayers of a neutral polymer and a polyphenol. Macromolecules 41:3962–3970. doi: 10.1021/ma800186q

239. Erel-Unal I, Sukhishvili SA (2008) Hydrogen-bonded hybrid multilayers: Film architecture controls release of macromolecules. Macromolecules 41:8737–8744. doi: 10.1021/ma8013564

240. Lynam D, Maloney R, Pawelec KM, et al (2010) NIH Public Access. 20:247–258. doi: 10.1002/adfm.200901172.Time

241. Kim B, Park SW, Hammond PT Surfaces. 2:386–392.

242. Erel I, Karahan HE, Tuncer C, et al (2012) Hydrogen-bonded multilayers of micelles of a dually responsive dicationic block copolymer. Soft Matter 8:827–836. doi: 10.1039/c1sm06248d

243. Zou X, Zhao X, Ye L (2015) Synthesis of cationic chitosan hydrogel and its controlled glucose-responsive drug release behavior. Chem Eng J 273:92–100. doi: 10.1016/j.cej.2015.03.075

244. Zhu Z, Sukhishvili SA (2009) Temperature-induced swelling and small molecule release with hydrogen- bonded multilayers of block copolymer micelles. ACS Nano 3:3595–3605. doi: 10.1021/nn900655z

245. Becker AL, Zelikin AN, Johnston APR, Caruso F (2009) Tuning the formation and degradation of layer-by-layer assembled polymer hydrogel microcapsules. Langmuir 25:14079–14085. doi: 10.1021/la901687a

246. Jiang J, Zhu L, Zhu L, et al (2013) Antifouling and antimicrobial polymer membranes based on bioinspired polydopamine and strong hydrogen-bonded poly(n -vinyl pyrrolidone). ACS Appl Mater Interfaces 5:12895–12904. doi: 10.1021/am403405c

247. Lemire JA, Harrison JJ, Turner RJ (2013) Antimicrobial activity of metals: Mechanisms, molecular targets and applications. Nat Rev Microbiol 11:371–384. doi:

10.1038/nrmicro3028

248. Kohanski MA, Dwyer DJ, Collins JJ (2010) How antibiotics kill bacteria: From targets to networks. Nat Rev Microbiol 8:423–435. doi: 10.1038/nrmicro2333

249. Carmona-Ribeiro AM, de Melo Carrasco LD (2013) Cationic antimicrobial polymers and their assemblies. Int J Mol Sci 14:9906–9946. doi: 10.3390/ijms14059906

250. Science B EFFICACY OF ANTIMICROBIAL-IMPREGNATED SILICONE. 4295:303–307.

251. Chung D, Papadakis SE, Yam KL (2003) Evaluation of a polymer coating containing triclosan as the antimicrobial layer for packaging materials. Int J Food Sci Technol 38:165–169. doi: 10.1046/j.1365-2621.2003.00657.x

252. Klueh U, Wagner V, Kelly S, et al (2000) Efficacy of silver-coated fabric to prevent bacterial colonization and subsequent device-based biofilm formation. J Biomed Mater Res 53:621–631. doi: 10.1002/1097-4636(2000)53:6<621::AID-JBM2>3.0.CO;2-Q

253. Johnson JR, Roberts PL, Olsen RJ, et al (1990) Prevention of catheter-associated urinary tract infection with a silver oxide-coated urinary catheter: Clinical and microbiologic correlates. J Infect Dis 162:1145–1150. doi: 10.1093/infdis/162.5.1145

254. Etienne O, Picart C, Taddei C, et al (2004) Multilayer polyelectrolyte films functionalized by insertion of defensin: A new approach to protection of implants from bacterial colonization. Antimicrob Agents Chemother 48:3662–3669. doi: 10.1128/AAC.48.10.3662-3669.2004

255. Danese PN (2002) Antibiofilm Approaches: Prevention of Catheter Colonization. Chem Biol 9:873–880. doi: 10.1016/S1074-5521(02)00192-8

256. Lichter JA, Rubner MF (2009) Polyelectrolyte multilayers with intrinsic antimicrobial functionality: The importance of mobile polycations. Langmuir 25:7686–7694. doi: 10.1021/la900349c

257. Illergård J, Wågberg L, Ek M (2011) Bacterial-growth inhibiting properties of multilayers formed with modified polyvinylamine. Colloids Surfaces B Biointerfaces 88:115–120. doi: 10.1016/j.colsurfb.2011.06.023

258. Graisuwan W, Wiarachai O, Ananthanawat C, et al (2012) Multilayer film assembled

from charged derivatives of chitosan: Physical characteristics and biological responses. J Colloid Interface Sci 376:177–188. doi: 10.1016/j.jcis.2012.02.039

259. Cerkez I, Kocer HB, Worley SD, et al (2011) N-halamine biocidal coatings via a layer-by-layer assembly technique. Langmuir 27:4091–4097. doi: 10.1021/la104923x

260. Faure E, Lecomte P, Lenoir S, et al (2011) Sustainable and bio-inspired chemistry for robust antibacterial activity of stainless steel. J Mater Chem 21:7901–7904. doi: 10.1039/c1jm11380a

261. Aslan S, Deneufchatel M, Hashmi S, et al (2012) Carbon nanotube-based antimicrobial biomaterials formed via layer-by-layer assembly with polypeptides. J Colloid Interface Sci 388:268–273. doi: 10.1016/j.jcis.2012.08.025

262. Aslan S, Määttä J, Haznedaroglu BZ, et al (2013) Carbon nanotube bundling: Influence on layer-by-layer assembly and antimicrobial activity. Soft Matter 9:2136–2144. doi: 10.1039/c2sm27444b

263. Kharlampieva E, Sukhishvili SA (2006) Hydrogen-bonded layer-by-layer polymer films. Polym Rev 46:377–395. doi: 10.1080/15583720600945386

264. Meng F, Zhong Z, Feijen J (2009) Stimuli-responsive polymersomes for programmed drug delivery. Biomacromolecules 10:197–209. doi: 10.1021/bm801127d

265. Lopes GKB, Schulman HM, Hermes-Lima M (1999) Polyphenol tannic acid inhibits hydroxyl radical formation from Fenton reaction by complexing ferrous ions. Biochim Biophys Acta - Gen Subj 1472:142–152. doi: 10.1016/S0304-4165(99)00117-8

266. Riedl KM, Hagerman AE (2001) Tannin-protein complexes as radical scavengers and radical sinks. J Agric Food Chem 49:4917–4923. doi: 10.1021/jf010683h

267. Shutava TG, Balkundi SS, Vangala P, et al (2009) Layer-by-layer-coated gelatin nanoparticles as a vehicle for delivery of natural polyphenols. ACS Nano 3:1877–1885. doi: 10.1021/nn900451a

268. Kozlovskaya V, Kharlampieva E, Drachuk I, et al (2010) Responsive microcapsule reactors based on hydrogen-bonded tannic acid layer-by-layer assemblies. Soft Matter 6:3596–3608. doi: 10.1039/b927369g

269. Erel-Unal I, Sukhishvili SA (2008) Hydrogen-bonded multilayers of a neutral polymer and a polyphenol. Macromolecules 41:3962–3970. doi: 10.1021/ma800186q

270. Erel-Unal I, Sukhishvili SA (2008) Hydrogen-bonded hybrid multilayers: Film architecture controls release of macromolecules. Macromolecules 41:8737–8744. doi: 10.1021/ma8013564

271. Schlaad H, Diehl C, Gress A, et al (2010) Poly(2-oxazoline)s as smart bioinspired polymers. Macromol Rapid Commun 31:511–525. doi: 10.1002/marc.200900683

272. Güner PT, Mikó A, Schweinberger FF, Demirel AL (2012) Self-assembled poly(2-ethyl-2-oxazoline) fibers in aqueous solutions. Polym Chem 3:322–324. doi: 10.1039/c1py00463h

273. Hoogenboom R (2009) Poly(2-oxazoline)s: A polymer class with numerous potential applications. Angew Chemie - Int Ed 48:7978–7994. doi: 10.1002/anie.200901607

274. Tatar Güner P, Demirel AL (2012) Effect of anions on the cloud point temperature of aqueous poly(2-ethyl-2-oxazoline) solutions. J Phys Chem B 116:14510–14514. doi: 10.1021/jp310648d

275. Erel I, Schlaad H, Demirel AL (2011) Effect of structural isomerism and polymer end group on the pH-stability of hydrogen-bonded multilayers. J Colloid Interface Sci 361:477–482. doi: 10.1016/j.jcis.2011.05.033

276. Sundaramurthy A, Vergaelen M, Maji S, et al (2014) Hydrogen Bonded Multilayer Films Based on Poly(2-oxazoline)s and Tannic Acid. Adv Healthc Mater 3:2040–2047. doi: 10.1002/adhm.201400377

277. Costerton JW, Stewart PS, Greenberg EP (1999) Bacterial biofilms: A common cause of persistent infections. Science (80-) 284:1318–1322. doi: 10.1126/science.284.5418.1318

278. Trandafilović L V., Božanić DK, Dimitrijević-Branković S, et al (2012) Fabrication and antibacterial properties of ZnO-alginate nanocomposites. Carbohydr Polym 88:263–269. doi: 10.1016/j.carbpol.2011.12.005

279. Kavitha K, Sutha S, Prabhu M, et al (2013) In situ synthesized novel biocompatible titania-chitosan nanocomposites with high surface area and antibacterial activity. Carbohydr Polym 93:731–739. doi: 10.1016/j.carbpol.2012.12.031

280. Cady NC, Behnke JL, Strickland AD (2011) Copper-based nanostructured coatings on natural cellulose: Nanocomposites exhibiting rapid and efficient inhibition of a multi-drug resistant wound pathogen, A. baumannii, and mammalian cell

biocompatibility in vitro. Adv Funct Mater 21:2506–2514. doi: 10.1002/adfm.201100123

281. Dallas P, Sharma VK, Zboril R (2011) Silver polymeric nanocomposites as advanced antimicrobial agents: Classification, synthetic paths, applications, and perspectives. Adv Colloid Interface Sci 166:119–135. doi: 10.1016/j.cis.2011.05.008

282. Azam A, Ahmed AS, Oves M, et al (2012) Antimicrobial activity of metal oxide nanoparticles against Gram-positive and Gram-negative bacteria: A comparative study. Int J Nanomedicine 7:6003–6009. doi: 10.2147/IJN.S35347

283. Marambio-Jones C, Hoek EMV (2010) A review of the antibacterial effects of silver nanomaterials and potential implications for human health and the environment. J Nanoparticle Res 12:1531–1551. doi: 10.1007/s11051-010-9900-y

284. Berger TJ, Spadaro JA, Chapin SE, Becker RO (1976) Electrically generated silver ions: quantitative effects on bacterial and mammalian cells. Antimicrob Agents Chemother 9:357–358. doi: 10.1128/AAC.9.2.357

285. Kim JS, Kuk E, Yu KN, et al (2007) Antimicrobial effects of silver nanoparticles. Nanomedicine Nanotechnology, Biol Med 3:95–101. doi: 10.1016/j.nano.2006.12.001

286. Shahverdi AR, Fakhimi A, Shahverdi HR, Minaian S (2007) Synthesis and effect of silver nanoparticles on the antibacterial activity of different antibiotics against Staphylococcus aureus and Escherichia coli. Nanomedicine Nanotechnology, Biol Med 3:168–171. doi: 10.1016/j.nano.2007.02.001

287. Martinez-Castanon GA, Niño-Martínez N, Martínez-Gutierrez F, et al (2008) Synthesis and antibacterial activity of silver nanoparticles with different sizes. J Nanoparticle Res 10:1343–1348. doi: 10.1007/s11051-008-9428-6

288. Bhui DK, Bar H, Sarkar P, et al (2009) Synthesis and UV-vis spectroscopic study of silver nanoparticles in aqueous SDS solution. J Mol Liq 145:33–37. doi: 10.1016/j.molliq.2008.11.014

289. Kapoor S (1998) Preparation, Characterization, and Surface Modification of Silver Particles. Langmuir 14:1021–1025. doi: 10.1021/la9705827

290. Munro CH, Smith WE, Garner M, et al (1995) Characterization of the Surface of a Citrate-Reduced Colloid Optimized for use as a Substrate for Surface-Enhanced

Resonance Raman Scattering. Langmuir 11:3712–3720. doi: 10.1021/la00010a021

291. Sun L, Song Y, Wang L, et al (2008) Ethanol-induced formation of silver nanoparticle aggregates for highly active SERS substrates and application in DNA detection. J Phys Chem C 112:1415–1422. doi: 10.1021/jp075550z

292. Seo D, Yoon W, Park S, et al (2008) The preparation of hydrophobic silver nanoparticles via solvent exchange method. Colloids Surfaces A Physicochem Eng Asp 313–314:158–161. doi: 10.1016/j.colsurfa.2007.04.086

293. Dubas ST, Pimpan V (2008) Humic acid assisted synthesis of silver nanoparticles and its application to herbicide detection. Mater Lett 62:2661–2663. doi: 10.1016/j.matlet.2008.01.033

294. Chen M, Ding W, Kong Y, Diao GW (2008) Conversion of the surface property of oleic acid stabilized silver nanoparticles from hydrophobic to hydrophilic based on host-guest binding interaction. Langmuir 24:3471–3478. doi: 10.1021/la704020j

295. Bauer CA, Stellacci F, Perry JW (2008) Relationship between structure and solubility of thiol-protected silver nanoparticles and assemblies. Top Catal 47:32–41. doi: 10.1007/s11244-007-9032-5

296. Wei H, Li J, Wang Y, Wang E (2007) Silver nanoparticles coated with adenine: Preparation, self-assembly and application in surface-enhanced Raman scattering. Nanotechnology. doi: 10.1088/0957-4484/18/17/175610

297. Raveendran P, Fu J, Wallen SL (2003) Completely “Green” Synthesis and Stabilization of Metal Nanoparticles. J Am Chem Soc 125:13940–13941. doi: 10.1021/ja029267j

298. Mandal S, Gole A, Lala N, et al (2001) Studies on the reversible aggregation of cysteine-capped colloidal silver particles interconnected via hydrogen bonds. Langmuir 17:6262–6268. doi: 10.1021/la010536d

299. Tan S, Erol M, Attygalle A, et al (2007) Synthesis of positively charged silver nanoparticles via photoreduction of AgNO3in branched polyethyleneimine/HEPES solutions. Langmuir 23:9836–9843. doi: 10.1021/la701236v

300. Mafuné, F, Kohno J, Takeda Y, et al (2000) Structure and Stability of Silver Nanoparticles in Aqueous Solution Produced by Laser Ablation. J Phys Chem B 104:8333–8337. doi: 10.1021/jp001803b

301. Morones JR, Elechiguerra JL, Camacho A, et al (2005) The bactericidal effect of silver nanoparticles. Nanotechnology 16:2346–2353. doi: 10.1088/0957-4484/16/10/059

302. Pal S, Tak YK, Song JM (2015) Does the antibacterial activity of silver nanoparticles depend on the shape of the nanoparticle? A study of the gram-negative bacterium Escherichia coli. J Biol Chem 290:1712–1720. doi: 10.1128/AEM.02218-06

303. El Badawy AM, Luxton TP, Silva RG, et al (2010) Impact of environmental conditions (pH, ionic strength, and electrolyte type) on the surface charge and aggregation of silver nanoparticles suspensions. Environ Sci Technol 44:1260–1266. doi: 10.1021/es902240k

304. Fabrega J, Renshaw JC, Lead JR (2009) Interactions of Silver Nanoparticles with. Environ Sci Technol 43:9004–9009.

305. Xiu Z-M, Ma J, Alvarez PJJ (2011) Differential Effect of Common Ligands and Molecular Oxygen on Antimicrobial Activity of Silver Nanoparticles versus Silver Ions. Environ Sci Technol 45:9003–9008. doi: 10.1021/es201918f

306. Choi O, Yu CP, Esteban Fernández G, Hu Z (2010) Interactions of nanosilver with Escherichia coli cells in planktonic and biofilm cultures. Water Res 44:6095–6103. doi: 10.1016/j.watres.2010.06.069

307. Periasamy S, Joo H-S, Duong AC, et al (2012) How Staphylococcus aureus biofilms develop their characteristic structure. Proc Natl Acad Sci 109:1281–1286. doi: 10.1073/pnas.1115006109

308. Lazar V (2011) Quorum sensing in biofilms - How to destroy the bacterial citadels or their cohesion/power? Anaerobe 17:280–285. doi: 10.1016/j.anaerobe.2011.03.023

309. Lu Z, Dai T, Huang L, et al (2011) rescues mice from fatal wound infections. 5:1525–1533. doi: 10.2217/nnm.10.98.Photodynamic

310. Rai M, Kon K, Ingle A, et al (2014) Broad-spectrum bioactivities of silver nanoparticles: The emerging trends and future prospects. Appl Microbiol Biotechnol 98:1951–1961. doi: 10.1007/s00253-013-5473-x

311. Wu D, Fan W, Kishen A, et al (2014) Evaluation of the antibacterial efficacy of silver nanoparticles against Enterococcus faecalis biofilm. J Endod 40:285–290. doi: 10.1016/j.joen.2013.08.022

312. Tamayo LA, Zapata PA, Vejar ND, et al (2014) Release of silver and copper nanoparticles from polyethylene nanocomposites and their penetration into Listeria monocytogenes. Mater Sci Eng C 40:24–31. doi: 10.1016/j.msec.2014.03.037

313. Collins TL, Markus EA, Hassett DJ, Robinson JB (2010) The effect of a cationic porphyrin on pseudomonas aeruginosa biofilms. Curr Microbiol 61:411–416. doi: 10.1007/s00284-010-9629-y

314. Kim S, Choi JE, Choi J, et al (2009) Oxidative stress-dependent toxicity of silver nanoparticles in human hepatoma cells. Toxicol Vitr 23:1076–1084. doi: 10.1016/j.tiv.2009.06.001

315. de Lima R, Seabra AB, Durán N (2012) Silver nanoparticles: A brief review of cytotoxicity and genotoxicity of chemically and biogenically synthesized nanoparticles. J Appl Toxicol 32:867–879. doi: 10.1002/jat.2780

316. Kim JS, Kuk E, Yu KN, et al (2007) Antimicrobial effects of silver nanoparticles. Nanomedicine Nanotechnology, Biol Med 3:95–101. doi: 10.1016/j.nano.2006.12.001

317. Sondi I, Salopek-Sondi B (2004) Silver nanoparticles as antimicrobial agent: A case study on E. coli as a model for Gram-negative bacteria. J Colloid Interface Sci 275:177–182. doi: 10.1016/j.jcis.2004.02.012

318. Danilczuk M, Lund A, Sadlo J, et al (2006) Conduction electron spin resonance of small silver particles. Spectrochim Acta - Part A Mol Biomol Spectrosc 63:189–191. doi: 10.1016/j.saa.2005.05.002

319. Lok C-N, Ho C-M, Chen R, et al (2007) Silver nanoparticles: partial oxidation and antibacterial activities. JBIC J Biol Inorg Chem 12:527–534. doi: 10.1007/s00775-007-0208-z

320. Dubas ST, Kumlangdudsana P, Potiyaraj P (2006) Layer-by-layer deposition of antimicrobial silver nanoparticles on textile fibers. Colloids Surfaces A Physicochem Eng Asp 289:105–109. doi: 10.1016/j.colsurfa.2006.04.012

321. Chen X, Schluesener HJ (2008) Nanosilver: A nanoproduct in medical application. Toxicol Lett 176:1–12. doi: 10.1016/j.toxlet.2007.10.004

322. Ahamed M, Karns M, Goodson M, et al (2008) DNA damage response to different surface chemistry of silver nanoparticles in mammalian cells. Toxicol Appl Pharmacol

233:404–410. doi: 10.1016/j.taap.2008.09.015

323. Nishanth RP, Jyotsna RG, Schlager JJ, et al (2011) Inflammatory responses of RAW 264.7 macrophages upon exposure to nanoparticles: Role of ROS-NFκB signaling pathway. Nanotoxicology 5:502–516. doi: 10.3109/17435390.2010.541604

324. Lee D, Rubner MF, Cohen RE (2005) Formation of nanoparticle-loaded microcapsules based on hydrogen-bonded multilayers. Chem Mater 17:1099–1105. doi: 10.1021/cm048441v

325. Oei JD, Zhao WW, Chu L, et al (2012) Antimicrobial acrylic materials with in situ generated silver nanoparticles. J Biomed Mater Res - Part B Appl Biomater 100 B:409–415. doi: 10.1002/jbm.b.31963

326. Lischer S, Körner E, Balazs DJ, et al (2011) Antibacterial burst-release from minimal Ag-containing plasma polymer coatings. J R Soc Interface 8:1019–1030. doi: 10.1098/rsif.2010.0596

327. Sur I, Cam D, Kahraman M, et al (2010) Interaction of multi-functional silver nanoparticles with living cells. Nanotechnology 21:175104. doi: 10.1088/0957-4484/21/17/175104

328. Huda S, Smoukov SK, Nakanishi H, et al (2010) Antibacterial nanoparticle monolayers prepared on chemically inert surfaces by cooperative electrostatic adsorption (CELA). ACS Appl Mater Interfaces 2:1206–1210. doi: 10.1021/am100045v

329. Eby DM, Luckarift HR, Johnson GR (2009) Hybrid antimicrobial enzyme and silver nanoparticle coatings for medical Instruments. ACS Appl Mater Interfaces 1:1553–1560. doi: 10.1021/am9002155

330. Park EJ, Bae E, Yi J, et al (2010) Repeated-dose toxicity and inflammatory responses in mice by oral administration of silver nanoparticles. Environ Toxicol Pharmacol 30:162–168. doi: 10.1016/j.etap.2010.05.004

331. Costa CS, Ronconi JVV, Daufenbach JF, et al (2010) In vitro effects of silver nanoparticles on the mitochondrial respiratory chain. Mol Cell Biochem 342:51–56. doi: 10.1007/s11010-010-0467-9

332. Asharani P V., Lianwu Y, Gong Z, Valiyaveettil S (2011) Comparison of the toxicity of silver, gold and platinum nanoparticles in developing zebrafish embryos.

Nanotoxicology 5:43–54. doi: 10.3109/17435390.2010.489207

333. Yen H-J, Hsu S, Tsai C-L (2009) Cytotoxicity and Immunological Response of Gold and Silver Nanoparticles of Different Sizes. Small 5:1553–1561. doi: 10.1002/smll.200900126

334. Eom H-J, Choi J (2010) p38 MAPK Activation, DNA Damage, Cell Cycle Arrest and Apoptosis As Mechanisms of Toxicity of Silver Nanoparticles in Jurkat T Cells. Environ Sci Technol 44:8337–8342. doi: 10.1021/es1020668

335. Lee YS, Kim DW, Lee YH, et al (2011) Silver nanoparticles induce apoptosis and G2/M arrest via PKCζ-dependent signaling in A549 lung cells. Arch Toxicol 85:1529–1540. doi: 10.1007/s00204-011-0714-1

336. Zanette C, Pelin M, Crosera M, et al (2011) Silver nanoparticles exert a long-lasting antiproliferative effect on human keratinocyte HaCaT cell line. Toxicol Vitr 25:1053–1060. doi: 10.1016/j.tiv.2011.04.005

337. Piao MJ, Kang KA, Lee IK, et al (2011) Silver nanoparticles induce oxidative cell damage in human liver cells through inhibition of reduced glutathione and induction of mitochondria-involved apoptosis. Toxicol Lett 201:92–100. doi: 10.1016/j.toxlet.2010.12.010

338. Lim DH, Jang J, Kim S, et al (2012) The effects of sub-lethal concentrations of silver nanoparticles on inflammatory and stress genes in human macrophages using cDNA microarray analysis. Biomaterials 33:4690–4699. doi: 10.1016/j.biomaterials.2012.03.006

339. Hackenberg S, Scherzed A, Kessler M, et al (2011) Silver nanoparticles: Evaluation of DNA damage, toxicity and functional impairment in human mesenchymal stem cells. Toxicol Lett 201:27–33. doi: 10.1016/j.toxlet.2010.12.001

340. Potara M, Jakab E, Damert A, et al (2011) Synergistic antibacterial activity of chitosan-silver nanocomposites on Staphylococcus aureus. Nanotechnology 22:135101. doi: 10.1088/0957-4484/22/13/135101

341. Yu L, Zhang Y, Zhang B, Liu J (2014) Enhanced antibacterial activity of silver nanoparticles/halloysite nanotubes/graphene nanocomposites with sandwich-like structure. Sci Rep 4:4551. doi: 10.1038/srep04551

342. Xu WP, Zhang LC, Li JP, et al (2011) Facile synthesis of silver@graphene oxide

nanocomposites and their enhanced antibacterial properties. J Mater Chem 21:4593–4597. doi: 10.1039/c0jm03376f

343. Shao W, Liu X, Min H, et al (2015) Preparation, Characterization, and Antibacterial Activity of Silver Nanoparticle-Decorated Graphene Oxide Nanocomposite. ACS Appl Mater Interfaces 7:6966–6973. doi: 10.1021/acsami.5b00937

344. Fortunati E, Armentano I, Zhou Q, et al (2012) Multifunctional bionanocomposite films of poly(lactic acid), cellulose nanocrystals and silver nanoparticles. Carbohydr Polym 87:1596–1605. doi: 10.1016/j.carbpol.2011.09.066

345. Ma J, Zhang J, Xiong Z, et al (2011) Preparation, characterization and antibacterial properties of silver-modified graphene oxide. J Mater Chem 21:3350–3352. doi: 10.1039/c0jm02806a

346. Mayer ABR, Johnson RW, Hausner SH, Mark JE (1999) Colloidal silver nanoparticles protected by water-soluble nonionic polymers and "soft" polyacids. J Macromol Sci - Pure Appl Chem 36 A:1427–1441. doi: 10.1081/MA-100101606

347. Yesmurzayeva NN, Nurakhmetova ZA, Tatykhanova GS, et al (2015) Catalytic Activity of Gold and Silver Nanoparticles Supported on Zinc Oxide. Supramol Catal 2:1–8. doi: 10.1515/supcat-2015-0001

348. Evanoff DD, Chumanov G (2005) Synthesis and optical properties of silver nanoparticles and arrays. ChemPhysChem 6:1221–1231. doi: 10.1002/cphc.200500113

349. Knetsch MLW, Koole LH (2011) New strategies in the development of antimicrobial coatings: The example of increasing usage of silver and silver nanoparticles. Polymers (Basel) 3:340–366. doi: 10.3390/polym3010340

350. Creighton JA, Blatchford CG, Albrecht MG (1979) Plasma resonance enhancement of Raman scattering by pyridine adsorbed on silver or gold sol particles of size comparable to the excitation wavelength. J Chem Soc Faraday Trans 2 Mol Chem Phys 75:790–798. doi: 10.1039/F29797500790

351. Merga G, Wilson R, Lynn G, et al (2007) Redox catalysis on "naked" silver nanoparticles. J Phys Chem C 111:12220–12226. doi: 10.1021/jp074257w

352. Evanoff DD, Chumanov G (2004) Size-controlled synthesis of nanoparticles. 2. Measurement of extinction, scattering, and absorption cross sections. J Phys Chem B

108:13957–13962. doi: 10.1021/jp0475640

353. Wiley B, Sun Y, Mayers B, Xia Y (2005) Shape-controlled synthesis of metal nanostructures: The case of silver. Chem - A Eur J 11:454–463. doi: 10.1002/chem.200400927

354. Oliveira MM, Ugarte D, Zanchet D, Zarbin AJG (2005) Influence of synthetic parameters on the size, structure, and stability of dodecanethiol-stabilized silver nanoparticles. J Colloid Interface Sci 292:429–435. doi: 10.1016/j.jcis.2005.05.068

355. Huang HH, Ni XP, Loy GL, et al (1996) Photochemical Formation of Silver Nanoparticles in Poly(*N* -vinylpyrrolidone). Langmuir 12:909–912. doi: 10.1021/la950435d

356. Nazeruddin GM, Prasad NR, Prasad SR, et al (2014) In-vitro bio-fabrication of silver nanoparticle using Adhathoda vasica leaf extract and its anti-microbial activity. Phys E Low-Dimensional Syst Nanostructures 61:56–61. doi: 10.1016/j.physe.2014.02.023

357. Ivanova OS, Zamborini FP (2010) Size-dependent electrochemical oxidation of silver nanoparticles. J Am Chem Soc 132:70–72. doi: 10.1021/ja908780g

358. Paramelle D, Sadovoy A, Gorelik S, et al (2014) A rapid method to estimate the concentration of citrate capped silver nanoparticles from UV-visible light spectra. Analyst 139:4855–4861. doi: 10.1039/c4an00978a

359. Hendessi S, Tatar Güner P, Miko A, Demirel AL (2017) Hydrogen bonded multilayers of poly(2-ethyl-2-oxazoline) stabilized silver nanoparticles and tannic acid. Eur Polym J 88:666–678. doi: 10.1016/j.eurpolymj.2016.10.039

360. Agnihotri S, Mukherji S, Mukherji S (2014) Size-controlled silver nanoparticles synthesized over the range 5-100 nm using the same protocol and their antibacterial efficacy. RSC Adv 4:3974–3983. doi: 10.1039/c3ra44507k

361. Tian X, Wang W, Cao G (2007) A facile aqueous-phase route for the synthesis of silver nanoplates. Mater Lett 61:130–133. doi: 10.1016/j.matlet.2006.04.021

362. Malina D, Sobczak-Kupiec A, Wzorek Z, Kowalski Z (2012) Silver nanoparticles synthesis with different concentrations of Polyvinylpyrrolidone. Dig J Nanomater Biostructures 7:1527–1534. doi: 10.1021/jp962398k

363. Mayer ABR, Johnson RW, Hausner SH, Mark JE (1999) Colloidal silver nanoparticles

protected by water-soluble nonionic polymers and “soft” polyacids. J Macromol Sci - Pure Appl Chem 36 A:1427–1441. doi: 10.1081/MA-100101606

364. Huang HH, Ni XP, Loy GL, et al (1996) Photochemical Formation of Silver Nanoparticles in Poly(*N* -vinylpyrrolidone). Langmuir 12:909–912. doi: 10.1021/la950435d

365. Ariga K, Hill JP, Ji Q (2008) Biomaterials and biofunctionality in layered macromolecular assemblies. Macromol Biosci 8:981–990. doi: 10.1002/mabi.200800102

366. Lee D, Cohen RE, Rubner MF (2005) Antibacterial properties of Ag nanoparticle loaded multilayers and formation of magnetically directed antibacterial microparticles. Langmuir 21:9651–9659. doi: 10.1021/la0513306

367. Ito K, Saito A, Fujie T, et al (2016) Development of a ubiquitously transferrable silver-nanoparticle-loaded polymer nanosheet as an antimicrobial coating. J Biomed Mater Res - Part B Appl Biomater 104:585–593. doi: 10.1002/jbm.b.33429

368. Srivastava S, Kotov NA (2008) Layer-by-layer (LBL) assembly with semiconductor nanoparticles and nanowires. Semicond Nanocrystal Quantum Dots Synth Assem Spectrosc Appl 41:197–216. doi: 10.1007/978-3-211-75237-1_7

369. Rivero PJ, Goicoechea J, Urrutia A, et al (2013) Multicolor layer-by-layer films using weak polyelectrolyte assisted synthesis of silver nanoparticles. Nanoscale Res Lett 8:1–10. doi: 10.1186/1556-276X-8-438

370. Abalde-Cela S, Ho S, Rodríguez-González B, et al (2009) Loading of exponentially grown LBL films with silver nanoparticles and their application to generalized SERS detection. Angew Chemie - Int Ed 48:5326–5329. doi: 10.1002/anie.200901807

371. Callegari A, Tonti D, Chergui M (2003) Photochemically Grown Silver Nanoparticles with Wavelength-Controlled Size and Shape. Nano Lett 3:1565–1568. doi: 10.1021/nl034757a

372. Dai J, Bruening ML (2002) Catalytic Nanoparticles Formed by Reduction of Metal Ions in Multilayered Polyelectrolyte Films. Nano Lett 2:497–501. doi: 10.1021/nl025547l

373. Machado G, Beppu MM, Feil AF, et al (2009) Silver nanoparticles obtained in PAH/PAA-based multilayers by photochemical reaction. J Phys Chem C 113:19005–

19010. doi: 10.1021/jp906018p

374. Pastoriza-Santos I, Liz-Marzán LM (1999) Formation and Stabilization of Silver Nanoparticles through Reduction by *N* , *N* -Dimethylformamide. Langmuir 15:948–951. doi: 10.1021/la980984u

375. Kvítek L, Panáček A, Soukupová J, et al (2008) Effect of surfactants and polymers on stability and antibacterial activity of silver nanoparticles (NPs). J Phys Chem C 112:5825–5834. doi: 10.1021/jp711616v

376. Karahan HE, Eyüboğlu L, Kiyilar D, Demirel AL (2014) pH-stability and pH-annealing of H-bonded multilayer films prepared by layer-by-layer spin-assembly. Eur Polym J 56:159–167. doi: 10.1016/j.eurpolymj.2014.04.015

377. Sundaramurthy A, Vergaelen M, Maji S, et al (2014) Hydrogen Bonded Multilayer Films Based on Poly(2-oxazoline)s and Tannic Acid. Adv Healthc Mater 3:2040–2047. doi: 10.1002/adhm.201400377

378. Da Fonseca Antunes AB, Dierendonck M, Vancoillie G, et al (2013) Hydrogen bonded polymeric multilayer films assembled below and above the cloud point temperature. Chem Commun 49:9663–9665. doi: 10.1039/c3cc45068f

379. Erel I, Karahan HE, Tuncer C, et al (2012) Hydrogen-bonded multilayers of micelles of a dually responsive dicationic block copolymer. Soft Matter 8:827–836. doi: 10.1039/c1sm06248d

380. Zhang W, Zhang A, Guan Y, et al (2011) Silver-loading in uncrosslinked hydrogen-bonded LBL films: Structure change and improved stability. J Mater Chem 21:548–555. doi: 10.1039/c0jm02369h

381. Keeney M, Jiang XY, Yamane M, et al (2015) Nanocoating for biomolecule delivery using layer-by-layer self-assembly. J Mater Chem B 3:8757–8770. doi: 10.1039/c5tb00450k

382. Liu J, Sonshine DA, Shervani S, Hurt RH (2010) Controlled release of biologically active silver from nanosilver surfaces. ACS Nano 4:6903–6913. doi: 10.1021/nn102272n

383. Danese PN (2002) Antibiofilm Approaches: Prevention of Catheter Colonization. Chem Biol 9:873–880. doi: 10.1016/S1074-5521(02)00192-8

384. Tiller JC, Liao C-J, Lewis K, Klibanov AM (2001) Designing surfaces that kill bacteria on contact. Proc Natl Acad Sci 98:5981–5985. doi: 10.1073/pnas.111143098

385. Lewis K, Klibanov AM (2005) Surpassing nature: Rational design of sterile-surface materials. Trends Biotechnol 23:343–348. doi: 10.1016/j.tibtech.2005.05.004

386. Green J-BD, Fulghum T, Nordhaus MA (2011) A review of immobilized antimicrobial agents and methods for testing. Biointerphases 6:MR13-MR28. doi: 10.1116/1.3645195

387. Dunne WM (2002) Bacterial adhesion: Seen any good biofilms lately? Clin Microbiol Rev 15:155–166. doi: 10.1128/CMR.15.2.155-166.2002

388. Hasan J, Crawford RJ, Ivanova EP (2013) Antibacterial surfaces: the quest for a new generation of biomaterials. Trends Biotechnol 31:295–304. doi: 10.1016/j.tibtech.2013.01.017

389. Friedlander RS, Vlamakis H, Kim P, et al (2013) Bacterial flagella explore microscale hummocks and hollows to increase adhesion. Proc Natl Acad Sci 110:5624–5629. doi: 10.1073/pnas.1219662110

390. Variola F, Francis-Zalzal S, Leduc A, et al (2014) Oxidative nanopatterning of titanium generates mesoporous surfaces with antimicrobial properties. Int J Nanomedicine 2319. doi: 10.2147/IJN.S61333

391. Zhu X, Jańczewski D, Guo S, et al (2015) Polyion multilayers with precise surface charge control for antifouling. ACS Appl Mater Interfaces 7:852–861. doi: 10.1021/am507371a

392. Morones JR, Elechiguerra JL, Camacho A, et al (2005) The bactericidal effect of silver nanoparticles. Nanotechnology 16:2346–2353. doi: 10.1088/0957-4484/16/10/059

393. Kumar A, Vemula PK, Ajayan PM, John G (2008) Silver-nanoparticle-embedded antimicrobial paints based on vegetable oil. Nat Mater 7:236–241. doi: 10.1038/nmat2099

394. Gunawan P, Guan C, Song X, et al (2011) Hollow fiber membrane decorated with Ag/MWNTs: Toward effective water disinfection and biofouling control. ACS Nano 5:10033–10040. doi: 10.1021/nn2038725

395. Fu J, Ji J, Yuan W, Shen J (2005) Construction of anti-adhesive and antibacterial

multilayer films via layer-by-layer assembly of heparin and chitosan. Biomaterials 26:6684–6692. doi: 10.1016/j.biomaterials.2005.04.034

396. Yu H, Xu X, Chen X, et al (2007) Preparation and antibacterial effects of PVA-PVP hydrogels containing silver nanoparticles. J Appl Polym Sci 103:125–133. doi: 10.1002/app.24835

397. Woodyard LL, Bowersock TL, Turek JJ, et al (1996) A comparison of the effects of several silver-treated intravenous catheters on the survival of staphylococci in suspension and their adhesion to the catheter surface. J Control Release 40:23–30. doi: 10.1016/0168-3659(95)00135-2

398. Ranoszek-Soliwoda K, Tomaszewska E, Socha E, et al (2017) The role of tannic acid and sodium citrate in the synthesis of silver nanoparticles. J Nanoparticle Res. doi: 10.1007/s11051-017-3973-9

399. Chung KT, Wong TY, Wei CI, et al (1998) Tannins and human health: A review. Crit Rev Food Sci Nutr 38:421–464. doi: 10.1080/10408699891274273

400. DemİrelPAL (2017) Implant kaplamalarda uzun ömürlü antibakteriyel etkinlik için tabaka-tabaka filmlerden kontrollü Ag + iyonu salımı Program Kodu : 2515 COST İşbirliği Proje No : 214Z165 Proje Yürütücüsü :

401. Köhler K, Sukhorukov GB (2007) Heat treatment of polyelectrolyte multilayer capsules: A versatile method for encapsulation. Adv Funct Mater 17:2053–2061. doi: 10.1002/adfm.200600593

402. Lvov Y, Antipov AA, Mamedov A, et al (2001) Urease Encapsulation in Nanoorganized Microshells. Nano Lett 1:125–128. doi: 10.1021/nl0100015

403. Such GK, Johnston APR, Caruso F (2011) Engineered hydrogen-bonded polymer multilayers: From assembly to biomedical applications. Chem Soc Rev 40:19–29. doi: 10.1039/c0cs00001a

404. Donatan S, Yashchenok A, Khan N, et al (2016) Loading Capacity versus Enzyme Activity in Anisotropic and Spherical Calcium Carbonate Microparticles. ACS Appl Mater Interfaces 8:14284–14292. doi: 10.1021/acsami.6b03492

405. Parakhonskiy B, Zyuzin M V, Yashchenok A, et al (2015) The influence of the size and aspect ratio of anisotropic, porous CaCO3 particles on their uptake by cells. J Nanobiotechnology 13:53. doi: 10.1186/s12951-015-0111-7

406. Tong W, Dong W, Gao C, Möhwald H (2005) Charge-controlled permeability of polyelectrolyte microcapsules. J Phys Chem B 109:13159–13165. doi: 10.1021/jp0511092

407. Gao C, Donath E, Möhwald H, Shen J (2002) Spontaneous deposition of water-soluble substances into microcapsules: Phenomenon, mechanism, and application. Angew Chemie - Int Ed 41:3789–3793. doi: 10.1002/1521-3773(20021018)41:20<3789::AID-ANIE3789>3.0.CO;2-D

408. Biesheuvel PM, Mauser T, Sukhorukov GB, Möhwald H (2006) Micromechanical Theory for pH-Dependent Polyelectrolyte Multilayer Capsule Swelling. Macromolecules 39:8480–8486. doi: 10.1021/ma061350u

409. De Koker S, De Geest BG, Cuvelier C, et al (2007) In vivo cellular uptake, degradation, and biocompatibility of polyelectrolyte microcapsules. Adv Funct Mater 17:3754–3763. doi: 10.1002/adfm.200700416